

UNCLASSIFIED

AD NUMBER
AD864282
NEW LIMITATION CHANGE
TO Approved for public release, distribution unlimited
FROM Distribution authorized to U.S. Gov't. agencies and their contractors; Critical Technology; OCT 1969. Other requests shall be referred to US Army Aviation Material Laboratories, Fort Eustis, VA 23604.
AUTHORITY
USAAMRL ltr, 23 Jun 1971

THIS PAGE IS UNCLASSIFIED

AD 864282

AD

USAAVLABS TECHNICAL REPORT 69-78
A FLIGHT ENVELOPE EXPANSION STUDY
FOR THE XH-51A COMPOUND HELICOPTER

By

E. S. Cruz
N. B. Gorenberg
A. W. Kerr

D D C
RECEIVED
JAN 29 1970
REGISTRY
B

October 1969

U. S. ARMY AVIATION MATERIEL LABORATORIES
FORT EUSTIS, VIRGINIA

CONTRACT DAAJ02-68-C-0033
LOCKHEED-CALIFORNIA COMPANY
TURBANK, CALIFORNIA

This document is subject to special export controls, and each transmittal to foreign governments or foreign nationals may be made only with prior approval of US Army Aviation Materiel Laboratories, Fort Eustis, Virginia 23604.



DISCLAIMERS

The findings in this report are not to be construed as an official Department of the Army position unless so designated by other authorized documents.

When Government drawings, specifications, or other data are used for any purpose other than in connection with a definitely related Government procurement operation, the United States Government thereby incurs no responsibility nor any obligation whatsoever; and the fact that the Government may have formulated, furnished, or in any way supplied the said drawings, specifications, or other data is not to be regarded by implication or otherwise as in any manner licensing the holder or any other person or corporation, or conveying any rights or permission, to manufacture, use, or sell any patented invention that may in any way be related thereto.

DISPOSITION INSTRUCTIONS

Destroy this report when no longer needed. Do not return it to the originator.

ACCESSION IN	
OFFICE	WHITE SECTION <input type="checkbox"/>
DOC	BUFF SECTION <input checked="" type="checkbox"/>
UNANNOUNCED	<input type="checkbox"/>
JUSTIFICATION	
CP	
DISTRIBUTION AVAILABILITY CODES	
INST.	AVAIL. SEC. OR SPECIAL
2	



DEPARTMENT OF THE ARMY
U. S. ARMY AVIATION MATERIEL LABORATORIES
FORT EUSTIS, VIRGINIA 23604

This report was prepared by the Lockheed-California Company under the terms of Contract DAAJ02-68-C-0033. The work reported herein was undertaken to determine the feasibility of attaining 300 knots in a slowed-rotor version of the XH-51A compound helicopter.

Analysis shows that the alleviation of compressible flow conditions, and thus speeds of 300 knots, can be achieved by slowed-rotor operation. Slowed-rotor operation also has the added benefit of reducing power requirements and of thus giving a significant increase in range and endurance characteristics. Two levels of rotor rpm, 75% and 50% of normal, were evaluated, with the rotor providing full aerodynamic control in both cases.

The conclusions and recommendations contained herein are concurred in by this Command.

Task 1F162203A14301
Contract DAAJ02-68-C-0033
USAAVLABS Technical Report 69-78
October 1969

A FLIGHT ENVELOPE EXPANSION STUDY
FOR THE XH-51A COMPOUND HELICOPTER

Final Report

Lockheed Report 21468

by

E. S. Cruz
N. B. Gorenberg
A. W. Kerr

Prepared by

Lockheed-California Company
Burbank, California

for

U. S. ARMY AVIATION MATERIEL LABORATORIES
FORT EUSTIS, VIRGINIA

This document is subject to special export controls, and each transmittal to foreign governments or foreign nationals may be made only with prior approval of US Army Aviation Materiel Laboratories, Fort Eustis, Virginia 23604.

SUMMARY

An analytical study was undertaken in support of a preliminary design effort to show the feasibility of a modified XH-51A compound helicopter achieving a speed of 300 knots by slowing the rotor in high-speed flight, while retaining good hover performance characteristics. The limitations on speed and maneuverability evident from previous flight test programs are described, and results of analysis are presented to show that these limitations can be eliminated in order to provide an increased flight envelope for compound helicopter operation.

Previous XH-51A compound helicopter flight speeds have been limited at 263 knots primarily by vibration due to compressibility effects on the advancing blade. Compressibility excites blade frequencies, causing high vibratory levels in the aircraft and high dynamic loads. Slowed-rotor operation, at speeds as low as 50% normal rpm, is explored as a method for reducing advancing tip compressibility effects to achieve the 300-knot flight speed. Two levels of rpm reduction, 25% and 50%, with some differences in design requirements and operating procedure, are evaluated. In both cases, 300-knot operation is feasible with the rotor system providing full aerodynamic control without the need for auxiliary fixed-wing control surfaces. The 75% rpm system includes modified rotor blade frequency placement, a hard-mounted transmission, and a rotor-speed control gyro. The 50% rpm system includes increased structural blade flapwise and torsional stiffness, a hard-mounted transmission, and a high-speed control gyro. With the addition of a thin-tip airfoil, increased compressibility margins at 300 knots for the 75% rpm system would result, and operation at speeds approaching 350 knots with a 50% rpm system appears to be feasible.

A test program is recommended to confirm and supplement the conclusions of the study.

FOREWORD

This report describes the results of an analytical study of a possible flight envelope expansion for the XH-51A compound helicopter by slowed-rotor operation. Analytical data are provided for a range of design parameters. This study was conducted by the Lockheed-California Company from January to April 1968 under Contract DAAJ02-68-C-0033 with the U. S. Army Aviation Materiel Laboratories. USAVLABS program direction was provided by R. C. Dumond.

Major Lockheed contributors to this report include V. Bilezikjian, I. B. Sachs, J. E. Sweers, D. H. Janda, J. A. Hoffman, and R. B. Lewis.

TABLE OF CONTENTS.

	<u>Page</u>
SUMMARY	iii
FOREWORD	v
LIST OF ILLUSTRATIONS	ix
LIST OF TABLES	xii
LIST OF SYMBOLS	xiii
INTRODUCTION	1
BACKGROUND	2
Flight Control Techniques	2
Flight Emergency Considerations	4
Prior Flight Limitations	5
Slowed-Rotor Operation	5
ROTOR DYNAMICS AND AEROELASTIC STABILITY	9
Flight Limits	9
Dynamic and Aeroelastic Stability Analysis	10
Dynamics of Flapping Motion	16
Rotor Natural Frequencies	16
1P-2P Instability	22
ROTOR CONTROL	23
Control at Reduced RPM	23
ROTOR LOADS	32
Design Loading Conditions	32
Effect of Twist, Coning Angle and Droop	36
Fatigue Analysis	50
PERFORMANCE	55
Design Point Performance at High Speed	55
Performance Comparisons	55
CONCLUSIONS AND RECOMMENDATIONS	60
Conclusions	60
Recommendations	61

TABLE OF CONTENTS (Continued)

	<u>Page</u>
REFERENCES CITED	62
APPENDIXES	64
I - Methods of Analysis	64
II - Slowed-Rotor Test Experience	69
III - Rotor Performance Charts and Sample Calculation	74
DISTRIBUTION	108

LIST OF ILLUSTRATIONS

<u>Figure</u>		<u>Page</u>
1	XH-51A Compound Helicopter in Flight	3
2	Maneuvers Attained in Flight Test with the XH-51A Compound Helicopter (Corrected to 4500 lb)	6
3	Airspeed vs. RPM Level (Power-On) Coverage Attained with the XH-51A Compound Helicopter	7
4	Stability of Rotor-Gyro Nutation Mode, Basic Configuration.	11
5	Stability of Rotor-Gyro Nutation Mode, Comparison of Basic and Recommended Configurations	13
6	Effect of Advance Ratio on Aerodynamic Spring Rate	17
7	Variation of K_{ϕ} with Tip Weight, XH-51A Rotor	18
8	Variation of XH-51A Rotor First Flapwise Frequency with Tip Weight	18
9	Main Rotor Mass and Stiffness Properties	19
10	Main Rotor Natural Frequencies	20
11	Tail Rotor Natural Frequencies	21
12	Pitch and Roll Control Sensitivity at 250 Knots	24
13	Cross Coupling at 250 Knots	25
14	Pitch and Roll Control Sensitivity at 300 Knots	26
15	Cross Coupling at 300 Knots	27
16	Pitch and Roll Control Sensitivity at 350 Knots	28
17	Cross Coupling at 350 Knots	29
18	Response to Stick Motion in Hover	31
19	Rotor Thrust Capability Diagram	33
20	Sparwise Moment Envelope, Condition 1	34
21	Measured Pitch Rate vs. Pitch Rate Computed from Load Factor and Speed	37

LIST OF ILLUSTRATIONS (Continued)

<u>Figure</u>		<u>Page</u>
22	Spanwise Moment Envelope, Condition 2	38
23	Spanwise Moment Envelope, Condition 3	39
24	Spanwise Moment Envelope, Condition 4	40
25	Spanwise Moment Envelope, Condition 5	41
26	Spanwise Moment Envelope, Condition 6	42
27	Spanwise Moment Envelope, Condition 7	43
28	Spanwise Moment Envelope, Condition 8	44
29	Spanwise Moment Envelope, Condition 9	45
30	Spanwise Moment Envelope, Condition 10	46
31	Spanwise Moment Envelope, Condition 11	47
32	Main Rotor Blade Airloads and Response, Condition 22	48
33	Effect of Twist on Cyclic Normal Bending Moments at Blade Root	49
34	Effect of Blade Twist, Condition 3	51
35	Effect of Blade Twist, Condition 7	51
36	Effect of Blade Twist, Condition 10	52
37	Effect of Blade Coning Angle and Droop, Condition 10	52
38	Fatigue Spectrum Comparison	54
39	CL-870 Model, Modified to Incorporate High-Speed Gyro, Installed in NASA-Ames 40- x 80-Foot Wind Tunnel	70
40	Results of Full-Scale Model Tests	71
41	Dynamic Model in 8- x 12-Foot Low-Speed Wind Tunnel	72
42	Summary of Dynamic Model Test Results	73
43	Rotor Hovering Performance, Effect of Twist	76

LIST OF ILLUSTRATIONS (Continued)

<u>Figure</u>		<u>Page</u>
44	Rotor Hovering Performance, Effect of Airfoil Distribution .	77
45	Rotorcraft Flight Spectrum	78
46	Rotor Performance Data for High-Speed Flight, Case 1 . . .	79
47	Rotor Performance Data for High-Speed Flight, Case 2 . . .	80
48	Rotor Performance Data for High-Speed Flight, Case 3 . . .	81
49	Rotor Performance Data for High-Speed Flight, Case 4 . . .	82
50	Rotor Performance Data for High-Speed Flight, Case 5 . . .	83
51	Rotor Performance Data for High-Speed Flight, Case 6 . . .	84
52	Rotor Performance Data for High-Speed Flight, Case 7 . . .	85
53	Rotor Performance Data for High-Speed Flight, Case 8 . . .	86
54	Rotor Performance Data for High-Speed Flight, Case 9 . . .	87
55	Rotor Performance Data for High-Speed Flight, Case 10 . . .	88
56	Rotor Performance Data for High-Speed Flight, Case 11 . . .	89
57	Rotor Performance Data for High-Speed Flight, Case 12 . . .	90
58	Rotor Performance Data for High-Speed Flight, Case 13 . . .	91
59	Rotor Performance Data for High-Speed Flight, Case 14 . . .	92
60	Rotor Performance Data for High-Speed Flight, Case 15 . . .	93
61	Rotor Performance Data for High-Speed Flight, Case 16 . . .	94
62	Rotor Performance Data for High-Speed Flight, Case 17 . . .	95
63	Rotor Performance Data for High-Speed Flight, Case 18 . . .	96
64	Rotor Performance Data for High-Speed Flight, Case 19 . . .	97
65	Rotor Performance Data for High-Speed Flight, Case 20 . . .	98
66	Tail Rotor Performance Data for High-Speed Flight, Case 21	100

LIST OF ILLUSTRATIONS (Continued)

<u>Figure</u>		<u>Page</u>
67	Correlation of Performance Data Theory and Test	101
68	Aircraft Component Angles and Relative Wind	104
69	Application of Rotor Performance Data Charts	107

LIST OF TABLES

<u>Table</u>		<u>Page</u>
I	Parameter Variations Analyzed	12
II	Summary of Loading Conditions	35
III	Effect of Twist on Loads	50
IV	Spectrum of Fatigue Loading Conditions	53
V	Design Point Performance Comparison	56
VI	Comparison of Rotor Hover Lift	57
VII	Description of Degrees of Freedom	67
VIII	Rotor Performance Data for High-Speed Flight	75

LIST OF SYMBOLS

A_{1s}	blade lateral cyclic pitch, cosine term, measured from shaft normal plane, rad
a	blade airfoil lift curve slope, per rad
a_1	blade longitudinal flapping angle with shaft normal plane and control plane parallel, deg
B_1	blade longitudinal cyclic pitch, sine term, with tip path and shaft normal plane parallel, deg
B_{1s}	blade longitudinal cyclic pitch, sine term, measured from shaft normal plane, rad
b	number of rotor blades
b_w	wing span, ft
C_{D_R}	rotor blade drag coefficient, D_p/qS_b
$C_{D_{F_R}}$	rotor blade total equivalent drag coefficient, D_{E_R}/qS_b , $C_{D_{F_R}} = C_{D_R} + C_{D_{Q_R}}$
$C_{D_{Q_R}}$	rotor blade equivalent drag coefficient resulting from rotor blade shaft power, D_{Q_R}/qS_b
C_{L_R}	rotor lift coefficient, L_R/qS_b
C_{L_w}	lift coefficient of aircraft minus blades; wing-fuselage lift coefficient, L_w/qS_w
$C_{L_{\alpha_w}}$	lift coefficient slope of aircraft minus blades; wing-fuselage lift coefficient slope, per deg
C_P	rotor power coefficient, $550 \text{ HP}_z / \pi R^2 \rho (\Omega R)^2$
C_T	rotor thrust coefficient, $T / \pi R^2 \rho \Omega^2$
$C(\psi)$	nondimensional aerodynamic damping coefficient

LIST OF SYMBOLS (Continued)

c	airfoil chord, blade chord, ft
c_d	airfoil drag coefficient
c_l	airfoil lift coefficient
c_{li}	airfoil design lift coefficient
c_m	airfoil pitching moment coefficient
D_{ER}	rotor blade total equivalent drag, lb $D_{ER} = D_R + D_{QR}$
D_{QR}	rotor blade shaft power converted to an equivalent drag force along the flight path, lb $D_{QR} = \frac{550 \text{ HP}_R}{V}$
D_L	increment of drag of aircraft minus blades associated with lift; includes fixed-wing surfaces induced drag, and elements of both fixed-wing surfaces profile drag and fuselage parasite drag above minimum, lb
D_P	drag due to minimum parasite area; includes minimum fuselage and interference drag, fixed-wing surfaces minimum profile drag (and in this treatment, tail rotor drag), lb
D_R	rotor blade drag, lb
e	Oswald's airplane efficiency factor
F_N	jet engine thrust, lb
f	parasite drag area, sq ft
$f(\phi)$	nondimensional forcing function of flapping motion
GW	gross weight, lb
g	acceleration of gravity, fps
HP_{LOSS}	sum of accessory, installation and transmission power losses for shaft drive system, hp
HP_R	rotor shaft power, hp

LIST OF SYMBOLS (Continued)

HP_{REQD}	summation of power required in shaft power system, hp
HP_{TR}	tail rotor shaft power, hp
I_1	flapping moment of inertia of one blade about axis at rotor center, slug-ft ²
i_S	rotor shaft incidence, deg
i_W	wing incidence, deg
J	polar moment of inertia of a rotor speed gyro, slug-ft ²
J_H	polar moment of inertia of a high-speed gyro, slug-ft ²
K_O	constant part of blade nondimensional stiffness, $2\left(\frac{\omega_n}{\Omega}\right)^2 / \gamma$
K_{xcs}	control moment applied to gyro per in. of longitudinal cyclic stick displacement, ft-lb/in.
K_{yCS}	control moment applied to gyro per in of lateral cyclic stick displacement, ft-lb/in.
$K(\psi)$	nondimensional blade fluctuating stiffness
L_R	rotor lift, lb
L_W	lift of aircraft minus blades, wing-fuselage lift, lb
$M_{(1)}$	blade tip Mach number in hover flight
$M_{(1,90)}$	advancing blade tip Mach number in forward flight
MA	gyro mechanical advantage
M_H	rotor hub pitching moment, ft-lb
M_N	cyclic blade root normal bending moment, ft-lb
N_G	gyro rotational speed, rpm

LIST OF SYMBOLS (Continued)

N_R	rotor rotational speed, rpm
n	flight load factor referred to a standard gross weight
n_z	vertical acceleration, ft/sec ²
p	vehicle roll rate, rad/sec
q	dynamic pressure, $\frac{\rho V^2}{2}$, psf
q'	vehicle pitch rate, rad/sec
r	distance from rotor center to radius station considered, ft
R	rotor radius, ft
S_D	rotor reference blade area, bcR, sq ft
S_W	wing area, sq ft
T	rotor thrust, lb
t	airfoil thickness, blade thickness, ft
V	flight path velocity; units are generally identified as knots, but when not identified, units are fps such as in
	$q = \frac{\rho V^2}{2}$ and in $D_{QR} = 550 \text{ HP}_R/V$
V_x	longitudinal velocity of rotor hub, fps
V_y	lateral velocity of rotor hub, fps
V_{z_0}	vertical velocity of aircraft cg, fps
W_t	blade tip weight, lb
x	rotor radius ratio, r/R
\bar{x}	longitudinal stick displacement normalized by spring constant, gyro mechanical advantage, and gyro angular momentum, sec ⁻¹

$$\bar{x} = \left[\frac{K_{xcs}}{MA(J\Omega)} \right] x_{cs}$$

LIST OF SYMBOLS (Continued)

x_c	rotor radius ratio at blade root cutout station
x_{cs}	longitudinal stick displacement, in.
\bar{y}	lateral stick displacement normalized by spring constant, gyro mechanical advantage, and gyro angular momentum, sec ⁻¹
	$\bar{y} = \left[\frac{k_{y_{cs}}}{MA(J\Omega)} \right] y_{cs}$
y_{cs}	lateral stick displacement, in.
\tilde{z}_t	vertical deflection of transmission, ft
α_F	fuselage angle of attack, deg
α_{TPP}	rotor tip path plane angle of attack, deg
α_w	wing angle of attack, deg
β	blade flapping angle, rad
$\dot{\beta}$	blade flapping velocity, rad/sec
$\ddot{\beta}$	blade flapping acceleration, rad/sec ²
$\tilde{\beta}$	collective component of rotor flapwise deflection, rad
γ	blade lock number, $\rho acR^4/I_1$
ϵ	rotor downwash angle at wing-fuselage, deg
ϵ_x	sine term of rotor in-plane cyclic deflection, rad
ϵ_y	cosine term of rotor in-plane cyclic deflection, rad
$\tilde{\epsilon}$	collective component of rotor in-plane deflection, rad
θ_G	cosine term of gyro displacement, rad
ϵ_R	cosine term of rotor flapwise deflection, rad
θ_f	pitch angle of fuselage, rad

LIST OF SYMBOLS (Continued)

θ_t	pitch angle of transmission, rad
θ_l	blade linear twist from rotor centerline to blade tip, deg
$\theta_{.75}$	rotor collective pitch setting at three-quarter radius, deg
μ	rotor in-plane advance ratio, $V/\Omega R$
ρ	air mass density, slugs/ft ³
σ	rotor solidity, $S_b/\pi R^2$
ϕ_G	sine term of gyro displacement, rad
ϕ_R	sine term of rotor flapwise deflection, rad
ϕ_f	roll angle of fuselage
ϕ_t	roll angle of transmission
ψ	blade azimuth location in rotor plane, measured from downwind position in sense of rotation, deg or rad
Ω	rotor rotational speed, and gyro rotational speed in 1:1 gyro-rotor speed system, rad/sec
Ω_H	gyro rotational speed of a high-speed gyro, rad/sec
$\bar{\Omega}$	ratio of operating rotational speed to normal rotational speed, where the latter has a reference value of 37.1 rad/sec corresponding to 355 rpm
ω_n	undamped natural flapping frequency of rotating blade, rad/sec

INTRODUCTION

This report presents the results of an analytical study performed to determine the feasibility of expanding the flight envelope of the XH-51A compound helicopter to include a 300-knot speed objective through substantially slowed rotor operation in high-speed flight, and to provide data to support preliminary design of such an aircraft. The phenomena associated with the speed limits observed in prior flight programs are identified and analyzed, and methods for their elimination are presented to show that the flight envelope may be expanded. Also, the effects of various rotor system design parameters on both high speed, at a range of tip speeds, and hover operating characteristics are considered to identify those parameters which are most critical to the design, and to provide a basis for the selection of the best rotor design for the slowed-rotor XH-51A compound helicopter. Four rotor operation problem areas are identified and treated separately:

- Rotor dynamics and aeroelastic stability
- Control phase shift and control power at low rpm
- Rotor loads
- Performance

Test-based analytical methods, outlined in Appendix I, Methods of Analysis, are applied to develop data in these areas. Elements of these analyses were applied in designing the XH-51A compound for flight speeds in the proximity of 250 knots, and the analyses reflect updating and refinement based on the results of flight experience.

The scope of this study encompasses rotor speeds from 100% to 50% normal rpm. Rotor parameters for a 75% rpm and a 50% rpm system are presented. The 75% rpm rotor system allows operation at 300 knots with the same blade geometry used in the previous configuration, but with different mass characteristics. The 50% rpm rotor system allows for operation at 300 knots but also provides a maximum potential for increasing speed due to a large operating margin before encountering the onset of advancing blade compressibility.

Although the data presented have been generated for the XH-51A compound helicopter, where practical they are presented in a form applicable to a broader category of rigid-rotor helicopters.

BACKGROUND

Since this study was performed to provide preliminary design data for the XH-51A compound helicopter, a familiarity with the basic design for the vehicle is useful. The XH-51A research compound helicopter (Figure 1) has a 35-foot-diameter, four-bladed, gyro-controlled rigid rotor, wings for unloading the rotor lift at high forward speeds, a jet engine mounted close to the fuselage on the left wing for propulsion, horizontal and vertical tail surfaces, and a two-bladed teetering tail rotor for antitorque and directional control. The aircraft requires no movable fixed-wing aerodynamic control surfaces since the rigid rotor provides sufficient pitch and roll control moment through application of cyclic pitch at any rotor thrust level.

The evolution of the XH-51A aircraft as a helicopter and a compound helicopter is described in Reference 1. References 2 and 3 describe successive maneuver envelope expansions and increased speed objectives. This section presents the approach taken in designing a rigid-rotor compound helicopter to expand the maneuver envelope for high-performance rotary-wing aircraft.

FLIGHT CONTROL TECHNIQUES

The rotor of a conventional helicopter in forward flight is used to perform two distinct but related functions: (1) to provide lift and (2) to provide propulsive force to overcome aircraft drag. When sufficient power is available so that high-speed performance is not power-limited, vibrations (caused by retreating blade stall and advancing blade compressibility) limit speed through high rotor loads and decreased control margins. While operation under these conditions may be possible from structural considerations and from the pilot's standpoint, the rotor becomes less efficient.

It is desirable to substitute alternate methods for providing vehicle lift and propulsive force. Aircraft lift may be provided by a wing, which would enhance performance at moderate speeds and improve maneuver capability. However, relieving the rotor lift requirement alone does not appreciably affect maximum speed capability, since reducing rotor lift unloads it in propulsive force as well. Substantially higher speed flight of the aircraft requires a separate propulsive device such as a shaft-driven propeller or a jet engine, whether or not the rotor is unloaded in lift. The XH-51A compound helicopter combines a wing for lift and a jet engine for propulsive force. While the jet engine is not the most efficient propulsive device which could be provided for the operating range under consideration, it is well suited to a research vehicle due to simplicity of installation and control.

For high-speed flight control of a compound helicopter with a teetering or fully articulated rotor, it is necessary to maintain a substantial level

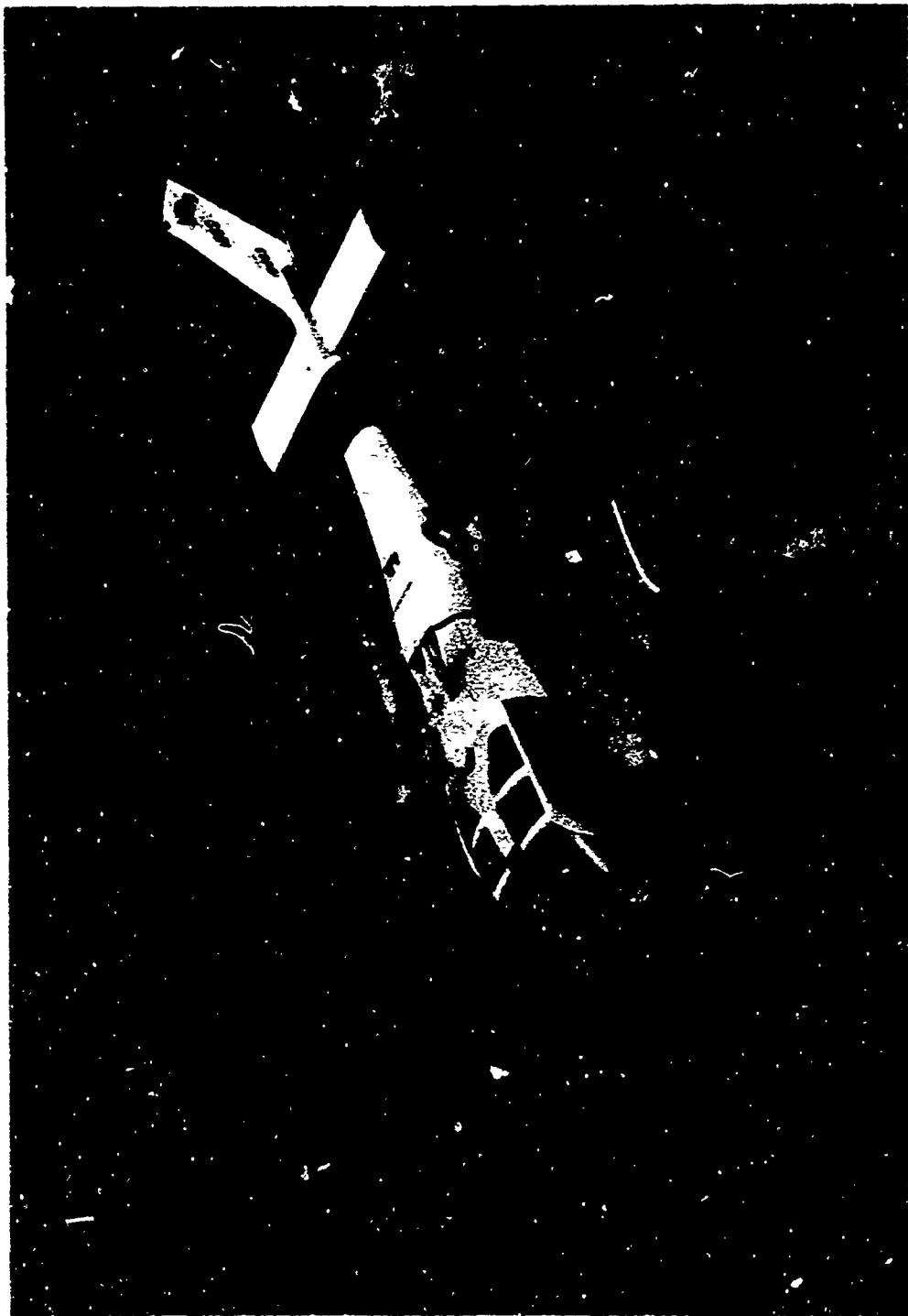


Figure 1. XH-51A Compound Helicopter in Flight.

of rotor thrust or to install airplane controls to obtain pitch and roll control. Maintaining thrust on the rotor limits speed capability, and additional controls tend to complicate the control system and add weight to the vehicle. In contrast, the XH-51A rigid rotor is capable of providing a control moment at the hub through cyclic pitch control when the rotor is completely unloaded.

The basic approach taken in the design of the XH-51A compound is to provide wing size and incidence sufficient to completely unload the rotor at the high-speed point so that maximum cyclic control power is available for maneuvering. At the high-speed point, the rotor attitude is level and the collective pitch measured at the three-quarter radius is near zero degrees. The corresponding longitudinal cyclic control setting required for trim is also near zero degrees. Further tailoring of wing parameters is a function of desired rotor/wing lift-sharing at lower speeds and vehicle attitude at the minimum speed selected for operation with the high-speed point collective pitch setting.

Flight from hover to progressively higher speeds is accomplished without a requirement for a shift in primary control systems, since all control is provided by the rotor system. In the speed regime below 80 knots, the aircraft is flown with collective and cyclic control as in any helicopter. At a speed between 80 and 120 knots, thrust on the propulsive engines is increased and the collective pitch is set at the high-speed position ($\theta_{75} = 0$). In this condition, the rotor is at a positive angle of attack and is providing most of the lift for the aircraft. As speed increases, the wing lift capability increases and the angle of attack of the aircraft is decreased, unloading the rotor. Longitudinal and lateral stick displacement provide pitch and roll control through cyclic feathering, but the aircraft is flown as an airplane without varying collective pitch. Yaw control is provided by the tail rotor.

In high-speed flight with the rotor unloaded, the effects of retreating blade stall on performance and control capability are negligible. Retreating blade stall occurs only in the reverse flow region where local velocities are low. Where a control moment must be generated with differential lift between the 90-degree and 270-degree azimuth locations, the high-velocity condition on the advancing blade easily provides the mechanism for sufficient differential lift.

FLIGHT EMERGENCY CONSIDERATIONS

In the event of a shaft engine failure while operating at high speed with the rotor unloaded, it is necessary to load the rotor to develop an autorotation condition. This cannot be accomplished merely by increasing rotor angle of attack since the wing lift increases also. To overcome this problem in the XH-51A compound helicopter, wing spoilers are installed and an emergency procedure has been established and found to be satisfactory in flight test. When a shaft engine failure is detected, the wing spoilers are deflected to unload the wing and a turn is made to increase

rotor loading more rapidly. The turn provides the necessary rotor angle of attack without extreme attitudes and a more precise control of rotor rpm through bank angle. As flight speed is reduced, the rotor lift load readily sustains autorotation.

In an operational compound where the propulsive force may be obtained through a shaft-driven propeller instead of a jet engine, the propeller drive may be geared to the power system of the main rotor. In the event of power loss, the propeller is set to absorb energy from the flight path to help slow the aircraft as well as to help keep the main rotor rotating until it can produce enough lift to sustain autorotation.

PRIOR FLIGHT LIMITATIONS

Flight tests of the XH-51A have provided extensive information useful in the study of high-speed compound rotary-wing flight. Data have been accumulated on the effects of lift-sharing between the wing and the main rotor, vehicle center-of-gravity placement and load factors. A summary of the experimentally demonstrated velocity-load factor envelope of this aircraft is shown in Figure 2. Vibration, loads and stability characteristics of the rotor and vehicle were monitored at various forward-speed and rotor-speed combinations. During the rpm-airspeed envelope exploration summarized in Figure 3, three aerodynamic-dynamic factors limiting high-speed flight were identified as follows:

1. A compressibility limit on the advancing blade was experienced in the form of high vibratory response, high oscillatory loads and a right-hand stick displacement required for trim. Repeated high-speed flights with a conventional NACA 0012 rotor blade airfoil section show that compressibility effects do not become significant until reaching an advancing tip Mach number of 0.91. Flights were conducted to a limiting Mach number of 0.942 at 95.5% rpm.
2. Decreased static stability margins limited operation at 90% rotor rpm at 185 knots and near neutral c.g. This limitation was removed by moving the c.g. forward, allowing operation up to 217 knots.
3. Rotor plane oscillations, which are possibly interrelated with the above static longitudinal stability margin, were observed at reduced rpm/high speed combinations. These oscillations had not been reported at the 90%, 185-knot test conditions.

SLOWED-ROTOR OPERATION

The primary speed limitation on the XH-51A in its previous test configuration was vibration caused by the high Mach number of the advancing blade tip. Regardless of the selection of airfoil section for the area of the

C.G. LOCATION	100% RPM	95% RPM	90% RPM
0.3 IN. FWD	△	△	△
1.2 IN. FWD	○	○	○
1.5 IN. FWD		□	□

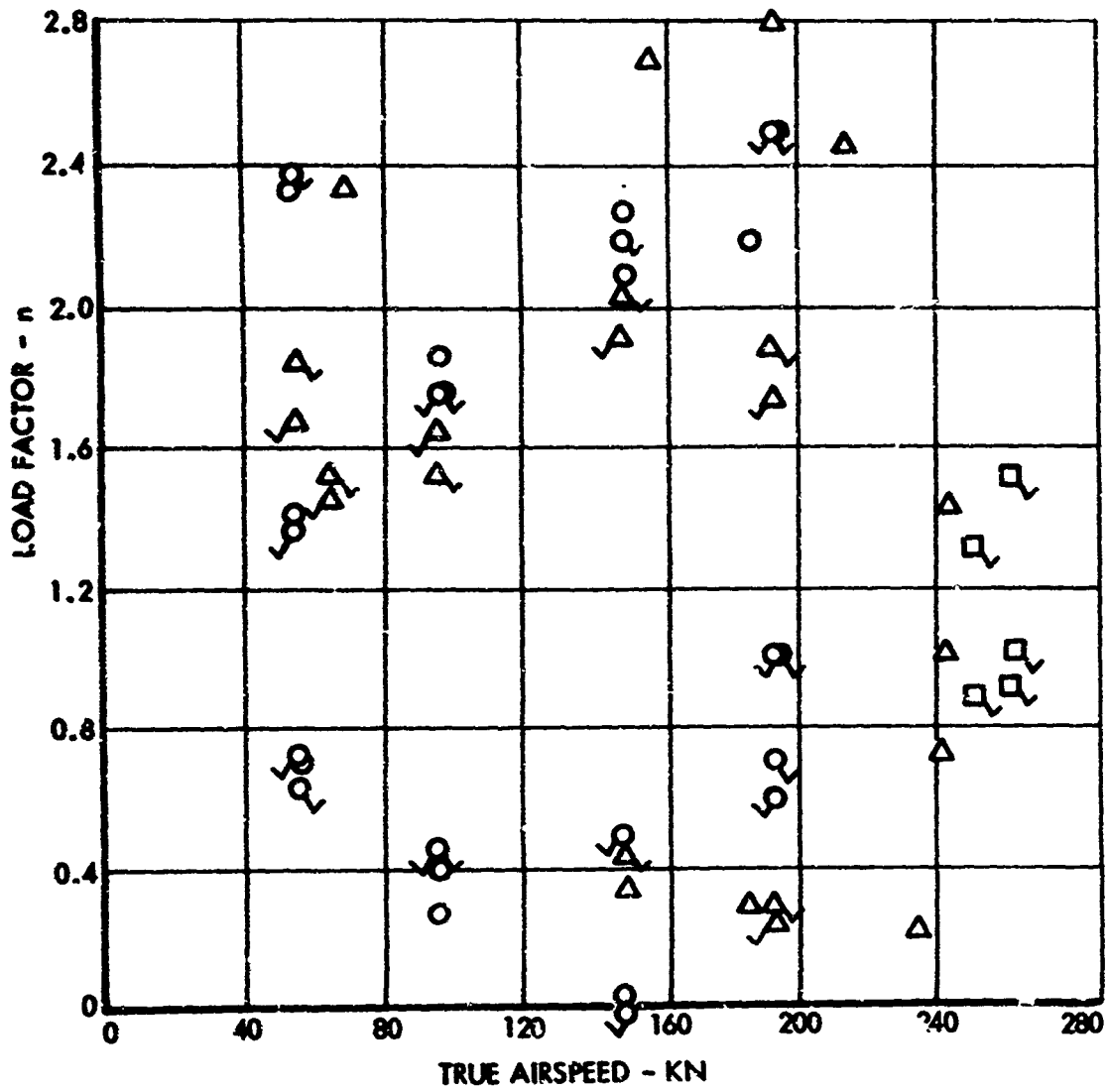


Figure 2. Maneuvers Attained in Flight Test with the XH-51A Compound Helicopter (Corrected to 4500 lb).

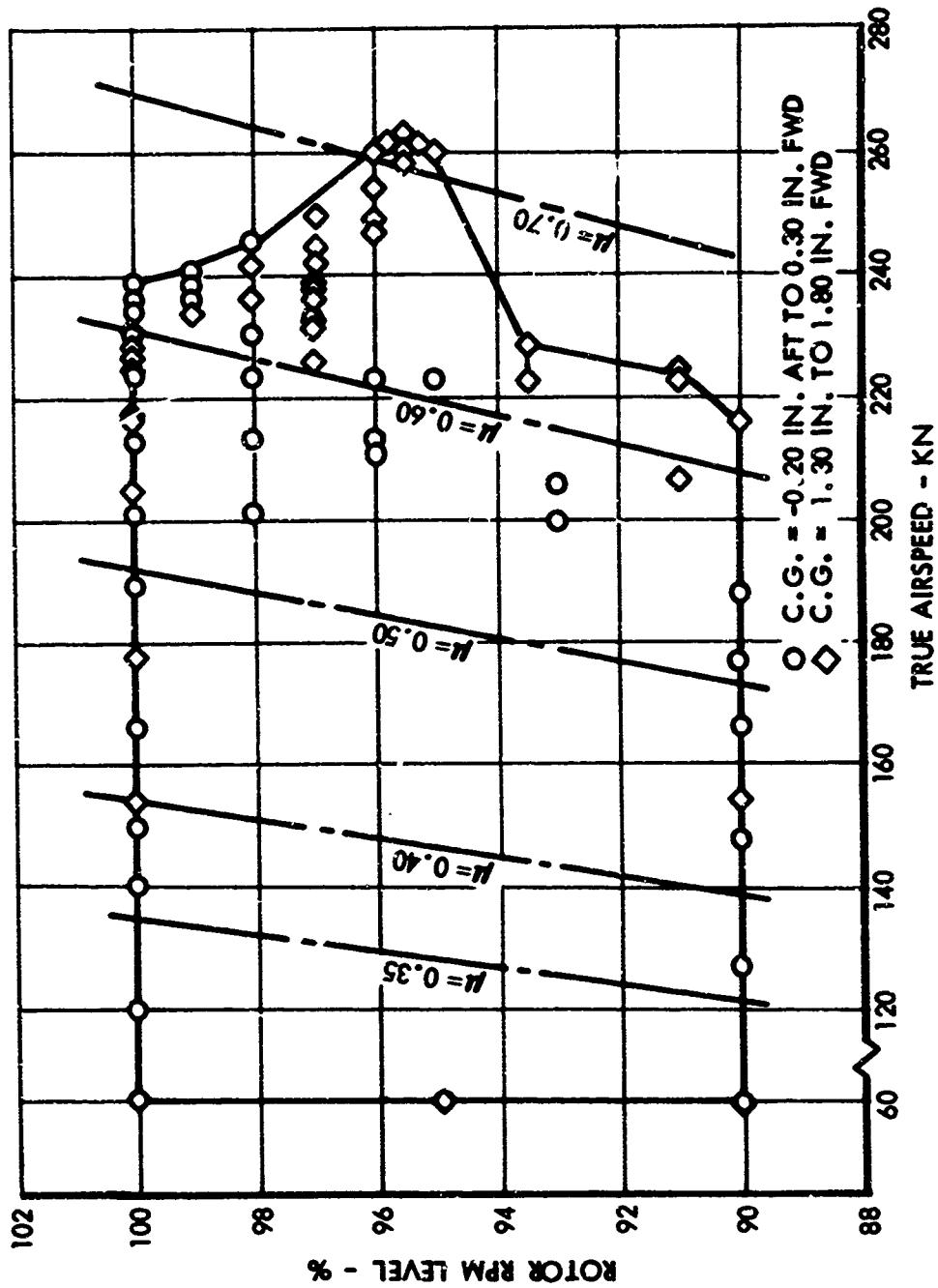


Figure 3. Airspeed vs. RPM Level (Power-On) Coverage Attained with the XH-51A Compound Helicopter.

blades near the tip, Mach number limitations will not allow a substantial increase in maximum speed at the design hover tip speed. Therefore, the next major increase in speed capability can best be attained by rotor slowing to significantly decrease the advancing blade tip Mach number to an operating range below that where compressibility effects become significant.

The purpose of this study is to evaluate the feasibility of expanding the high-speed end of the flight envelope, but it should be noted that high-speed capability is not the only benefit of slowed-rotor operation. Slowed-rotor operation has the added benefit of reducing the power requirements at moderate speeds (150 to 200 knots). This power reduction due to decreased blade profile losses produces a significant increase in range and endurance characteristics at cruise conditions.

ROTOR DYNAMICS AND AEROELASTIC STABILITY

In previous flight tests of the XH-51A, high-speed flight has been limited by vibrations induced by compressibility effects at 100% rpm, and by rotor frequency excitation at reduced rpm. In this section the flight limits experienced in these tests are discussed in detail, and results of analysis indicating the feasibility of eliminating these limits are presented.

FLIGHT LIMITS

Limitations on maximum speed experienced in previous flight tests were principally characterized by dynamic response. The primary limitation was the result of compressibility effects on the advancing blade when the tip Mach numbers from 0.91 to 0.94 produce local shock, high drag and aerodynamic center shift sufficient to excite the blade frequencies and cause a high vibratory response and oscillatory loads. The actual limiting factor was the pilot's inability to operate in a high vibratory environment (i.e., inability to read his instruments, physiological discomfort, etc.), since the level of the vibratory loads experienced in flight was well below the structural design limit. The solution to this problem is found in simply reducing rotor tip speed in high-speed flight; but in so doing, the effects of slowing the rotor on blade natural frequency, aeroelastic stability and control capability must be considered.

The second limit was experienced at 90% rotor rpm, 185 knots at neutral c.g., where two different pilots experienced what they described as a degradation in longitudinal static stability. Flight records showed that this configuration exhibited very poor longitudinal stability characteristics. By moving the c.g. forward, the speed capability was immediately increased to 217 knots.

A dynamic phenomenon observed in the flight test program at 95.5% rpm (at forward c.g.) was characterized as "hop" since it was sensed primarily as vehicle vertical acceleration. This phenomenon was encountered during an autorotation entry at 232 knots, and flight records disclosed that it involved higher than normal blade chordwise response caused by the soft-mounted transmission hitting its forward stop at the time of the initiation of autorotation. The response of the fuselage exhibited a development of pitch and roll rates and c.g. acceleration. It is believed that the impact loading as well as the nonlinear stiffness sensed by the rotor system while the stops were deflected caused the high in-plane response which produced the vehicle motions, and that the elimination of soft-mounting of the transmission will preclude the occurrence of this phenomenon.

An analytical study of the hop phenomenon, reported in Reference 4, indicates that the operation of this rotor near 93% rpm (1.5P in-plane frequency) would result in reduced rotor in-plane damping. This effect, combined with reduced longitudinal static stability margins, is believed

to have aggravated the system response which produced the observed phenomenon. It is also probable that the effect on stability of the combination of increased forward speed and reduced rotor rpm is adversely augmented by the reduction of control gyro effectivity. This condition could be alleviated by increasing gyro size. The phenomenon is dependent upon the rotor chordwise response driving the collective control system to produce the vertical accelerations. It may be eliminated by tailoring chordwise stiffness and damping and collective stiffness and damping.

DYNAMIC AND AEROELASTIC STABILITY ANALYSIS

In addition to proper placement of rotor blade frequencies, successful rotor design must feature adequate stability margins within the operational rpm excursion limits and forward speed envelope. A parametric study evaluating the necessary design changes to an XH-51A-size rotor and control system provides a high level of confidence in attaining the 300-knot speed objective. The rotor parameter variations studied are within the forward speed range of 230 to 350 knots and rotor speeds of approximately 50% to 100% rpm (where 100% rpm represents 355 rpm, 650 fps tip speed).

A brief overview of the parameters affecting the aeroelastic and dynamic stability characteristics of the gyro-controlled rigid-rotor system follows. Cyclic stability of the rotor system is achieved primarily by the selection of a control gyro size and mechanical advantage which are compatible with blade sweep and rotor power loading. Collective stability is achieved by providing adequate collective control stiffness. Advancing rotary modes of the rigid rotor are effectively stabilized by proper selection of the cant angle of the control gyro and the sweep and droop of the blade. The possibility of high-frequency blade flutter at low μ is precluded by maintaining a rotor blade chordwise center-of-gravity distribution which is virtually on the blade quarter-chord in the outboard region of the blade span. Blade flutter at high μ , in particular for the region $\psi = 225$ degrees to $\psi = 315$ degrees, is controlled by maintenance of a high blade torsional frequency. A swashplate damper is used to stabilize a 2P nutation mode.

The ranges of rotor and control system parameters studied with the 16-degree-of-freedom analytical model described in Appendix I are presented in Table I. The configuration for the current XH-51A compound helicopter rotor system is shown in this table by the underlined parameters.

The initial phase of analysis is applied to the study of the basic XH-51A compound system to provide direct comparison with flight test experience. The results of this study shown on Figure 4 indicate that the critical dynamic mode is a motion which can be characterized as rotor-gyro nutation. The airframe would develop substantial 2P vibration levels prior to reaching this limit which would easily be corrected by increasing the swashplate damping levels. When flight data from previous test programs are examined,

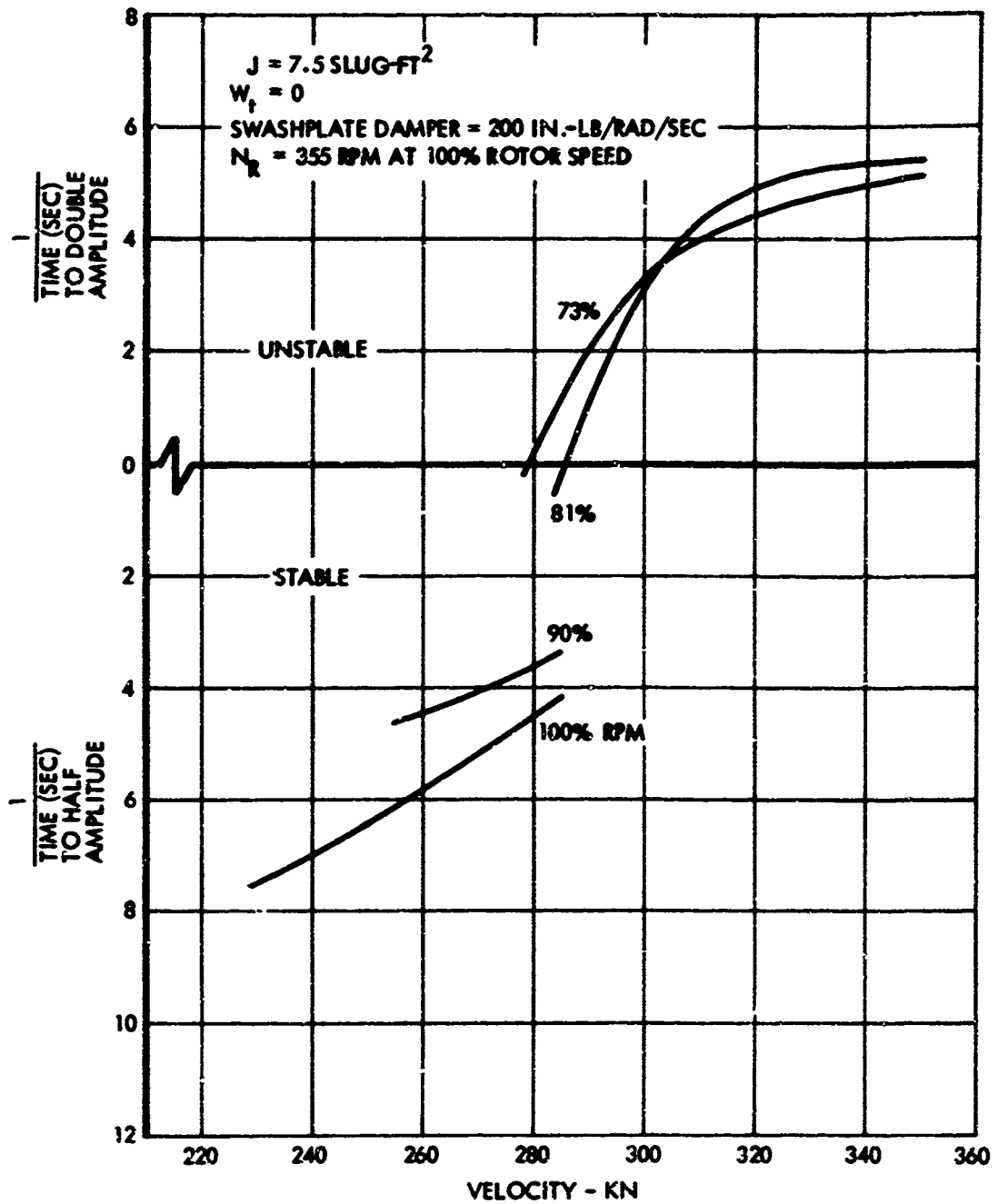


Figure 4. Stability of Rotor-Gyro Nutation Mode, Basic Configuration.

no clear evidence of damping reduction in this mode is seen within the range of operating conditions tested. However, the rpm and forward flight speeds tested did result in substantial vibration at the tip Mach number of 0.94, which may have masked this characteristic. The analysis is conservative with respect to this mode, since only the swashplate damping is accounted for and any additional damping due to control system friction provides added margins.

TABLE I. PARAMETER VARIATIONS ANALYZED

Variable	Range of Analysis	Units
Control Gyro Inertia	<u>7.5</u> , 10, 15, 25, 50	Slug-Ft ²
Blade Sweep	<u>1.18</u> , 2.36, 3.54	Deg
Gyro Cant Angle*	<u>45</u> , 60, 65	Deg
Rotor RPM	53, 73, 81, 90, 100	%
Blade Tip Weight	<u>0</u> , 10, 20	Lb
Vehicle Forward Velocity	230 to 350	Kn
Swashplate Damper	<u>200</u> , 1000, 1900	In.-Lb/Rad/Sec

*Defined as the control gyro azimuthal lead angle

The results of the analysis for a recommended configuration are shown in Figure 5. This configuration is basically an XH-51A-type rotor system which incorporates additional swashplate damping (five times the original level), a larger gyro (two times the original) and 12-pound rotor tip weights for rotor centrifugal stiffening as well as in-plane bending frequency placement at reduced rpm. All other parameters remain unchanged. Adequate operating margins down to 75% rpm are insured on the basis of the solution shown for the 73% rpm condition.

A reduction of 25% in rotor speed results in a loss in flapwise stiffness of about 40%. If the XH-51A were flown to increasingly higher forward speeds while maintaining a constant blade tip Mach number by appropriate reduction in rotor speed, the advance ratio would increase proportionately, and the retreating blades, beginning with the inboard regions, would encounter progressively more reverse flow. The result is that vertical gusts become more adversely effective inasmuch as they can produce

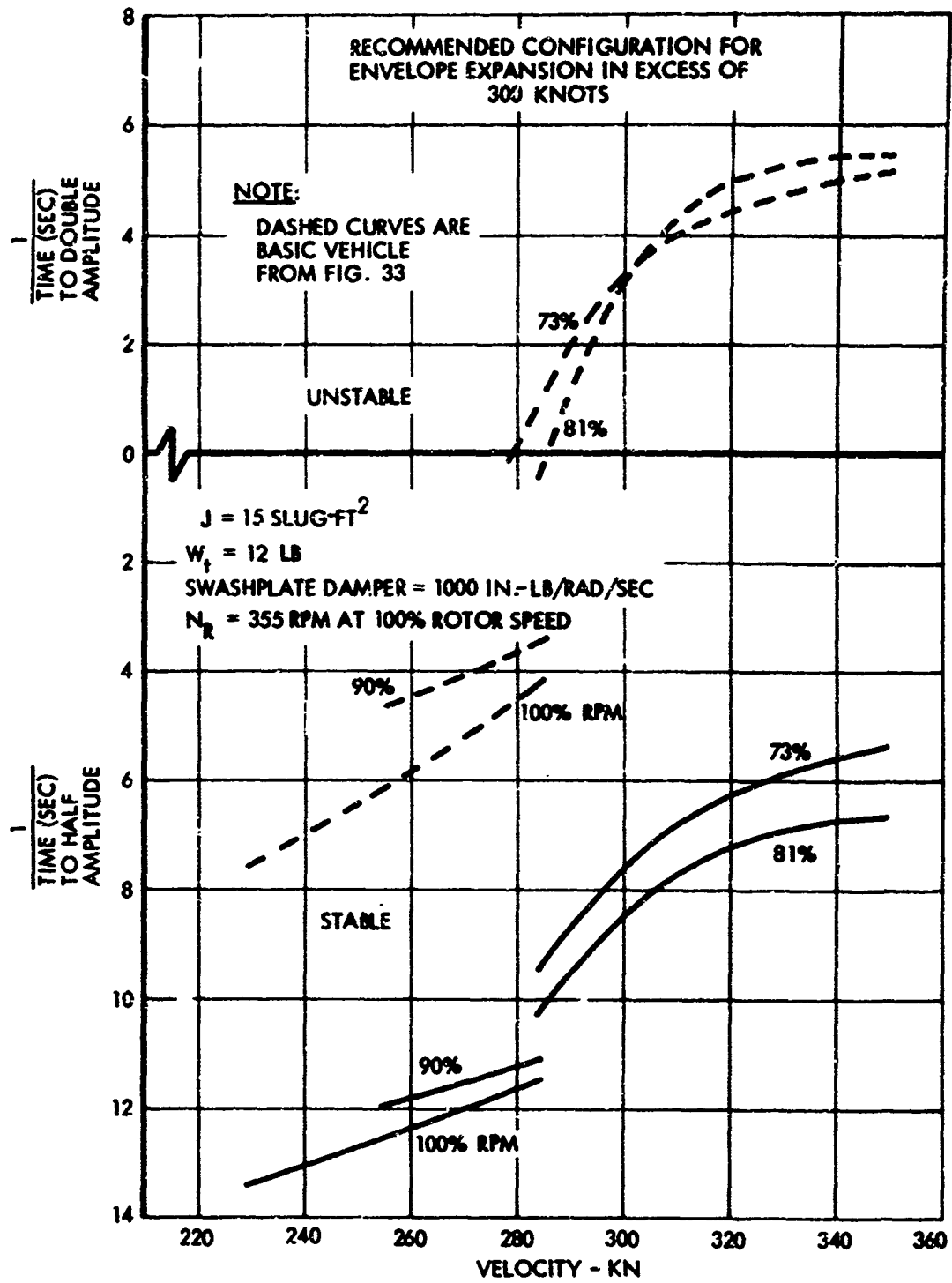


Figure 5. Stability of Rotor-Gyro Nutation Mode, Comparison of Basic and Recommended Configurations.

relatively large transient flapping responses. This effect is augmented by the more asymmetrical character of gust envelopment in the case of a slowly rotating rotor. At lowered rotor rotational speeds and high forward flight speeds, such transient flapping responses could manifest themselves in the form of high loads, possible blade divergence and/or vehicle instability.

In view of the aeroelastic constraints, there exists a limit to the reduction in rotor speed in combination with forward-flight speed which can be tolerated before significant structural and mechanical modifications become necessary. From the data developed, this limit appeared below 73% rpm at 300 knots. It will be shown that greater reductions in rotor rpm and higher forward flight speeds can be facilitated by the incorporation of a high-speed gyro and structural modifications.

Barring mechanical and structural alterations, the special aeroelastic phenomena associated with high-speed operation of the compound XH-51A rotor system at 50% of its original design speed can be attributed to three principal conditions: (1) excessive loss in flapping stiffness corresponding to the reduction in rotor speed, (2) diminution of gyro authority, and (3) inadequate frequency separation.

In addition to its influence on blade frequencies, substantial loss of flapping stiffness will result in flapping excursions. These become progressively larger as advance ratio is increased so that even though the intent is to maintain an unloaded rotor during flight at high advance ratios, the rotor will nevertheless become more sensitive to rotor incidence change, such as that occasioned by gust envelopment. Such flapping excursions would also have a significant effect on rotor torque and, hence, on rotor speed. Compensation for such cyclic disturbances is an innate characteristic of the gyro-controlled rigid-rotor system when the gyro possesses good gyroscopic characteristics. It should be mentioned that the centrifugal stiffness can be partially restored by adding tip weight to the rotor blades. The tip weight requirements and flapping motion dynamics are treated in the next section.

As the advance ratio approaches unity, a large area of the retreating side of the rotor is in reverse flow. Due to the large offset of the line of aerodynamic centers relative to the blade structural elastic axis, the blade in this reverse flow region will have an apparent "negative sweep" with respect to its feathering axis. This effect is destabilizing in that it generates the tendency to precess the control gyro so as to result in an increase in the rotor moment. This feedback loop results in the gyro-rotor system's tendency toward instability in a rotor cyclic divergence mode, due to its effect on rotor damping. These adverse characteristics will exist over a large area of the retreating side of the rotor for advance ratios near unity. Thus, the impedance of the gyro must be sufficiently large to forestall the effects of adverse feedback until the stabilizing conditions of the advancing side are reencountered.

With the rotor slowed to 50% rpm, it would not be feasible to furnish a control gyro of the conventional type since the size required would make the gyro unwieldy. The high-speed control gyro, which maintains its high rotational speed and, consequently, its ability to provide rotor control as the main rotor speed is reduced and restored, possesses important characteristics relative to the limitations referred to above.

Examination of control gyro size selection for pilot control and rotor response due to external disturbance indicates that the $J\Omega$ of the control gyro should be preserved when selecting a control gyro speed and polar inertia. This is equivalent to saying that the control gyro $J\Omega = J_H\Omega_H$, where the terms on the left pertain to the rotor speed gyro and the terms on the right pertain to the high-speed gyro system. This is seen most easily from the pilot side of the system; however, the rotor disturbance case can be simplified as follows.

Given an external moment acting to precess the main rotor, the blade sweep is then acting to precess the gyro. This feedback results in an automatic adjustment of cyclic pitch to alleviate the moment. The precession rate of the gyro is inversely proportional to its angular momentum. Therefore, the basic control input must be increased as $J\Omega$ is increased and the sweep angle (feedback) must also be increased to maintain a balance. The data presented in Appendix II show that the gyro stiffness (i.e., $J\Omega^2$) is most important for the high advance ratio case. Preservation of $J\Omega = J_H\Omega_H$ clearly benefits the stiffness when the gyro is operated at high speed, since the stiffness increases by the ratio Ω_H/Ω . Therefore, a favorable balance between pilot effort and blade sweep results while obtaining the benefits of the large stiffness of the high-speed gyro.

Maintenance of $J_H\Omega_H$ while varying the main rotor rpm affects the basic relationships described relative to gyro angular momentum, but to a second-order degree; i.e., 75% rotor speed would appear approximately as a 4/3 larger gyro angular momentum when viewed from the rotor. The rpm level below which a rotor speed gyro is no longer practical is between 50% and 75% normal rotor rpm.

The high-speed control gyro is also characterized by a very high nutation frequency. Thus, the swashplate damping required to stabilize the 2P nutation mode of the high-speed control gyro is reduced to a small fraction of that required for the rotor speed gyro.

Reference 5 reports on the background experience in slowed- and stopped-rotor technology which is used for the lower rpm range. A summary of previous model test experience in slowed-rotor and high-speed gyro technology is presented in Appendix II.

DYNAMICS OF FLAPPING MOTION

The flapping equation of motion (Reference 6) is expressed as follows:

$$\frac{2}{\gamma} \ddot{\beta} + \Omega \dot{\beta} c(\psi) + \Omega^2 \beta [K_0 + K(\psi)] = \Omega^2 \sum f(\psi)$$

where the terms have all been divided by $R^4 Ca\rho/2$.

This equation represents a forced single-degree-of-freedom system with periodically (but not harmonically) varying coefficients; i.e., it is a typical Hill-type equation. K_0 represents a combined structural and centrifugal stiffness, the latter being highly dependent on rotor inertia (e.g., tip weights).

Figure 6 shows the variation of aerodynamic stiffness around the azimuth as a function of advance ratio, μ . As can be noted in Figure 6, for $\mu > 0$ the aerodynamic stiffness assumes a negative value in the azimuth region $90 < \psi < 270$ degrees. Since K_0 is always positive, its value will determine whether a net negative stiffness is experienced by the system in some azimuth region.

A very conservative criterion is afforded by the requirement that $K_0 + K(\psi) > 0$ be established for stability. Figure 7 shows the variation of K_0 at various rpm for an unmodified XH-51A blade and the effect of tip weights on this rotor. The curves on this figure are obtained from the evaluation of the first flapwise mode of the blades. The variation of the ratio of the first flapping frequency to rotor rotational speed as a function of percent of rotor speed for three tip weights (0, 10, and 20 pounds) is shown in Figure 8. These data indicate that for operation of this rotor at 50% rpm with a 20-pound tip weight, a structural flapwise stiffness increase of 53% is required. This increase would be located principally in the hub and inboard end of the blade.

ROTOR NATURAL FREQUENCIES

Natural frequencies and mode shapes are computed for various rotor speeds from 50% to 100% normal rotor rpm using the mass and stiffness properties described in Figure 9. The variation of the natural frequencies with rotor rpm at two different collective settings of the main rotor blade is shown in Figure 10. Between 75% and 100% rotor rpm, the natural frequencies of the lower modes of vibration are well separated from the harmonics of rotor rpm (with the usual exception of the first normal bending mode, which approximates the frequency of the first harmonic; this mode is strongly damped).

Natural frequencies of the tail rotor are shown in Figure 11. The tail rotor is a teetering two-bladed system, which requires the investigation of both the collective and the cyclic modes. The collective modes (symmetric normal bending, antisymmetric in-plane bending) are excited at the

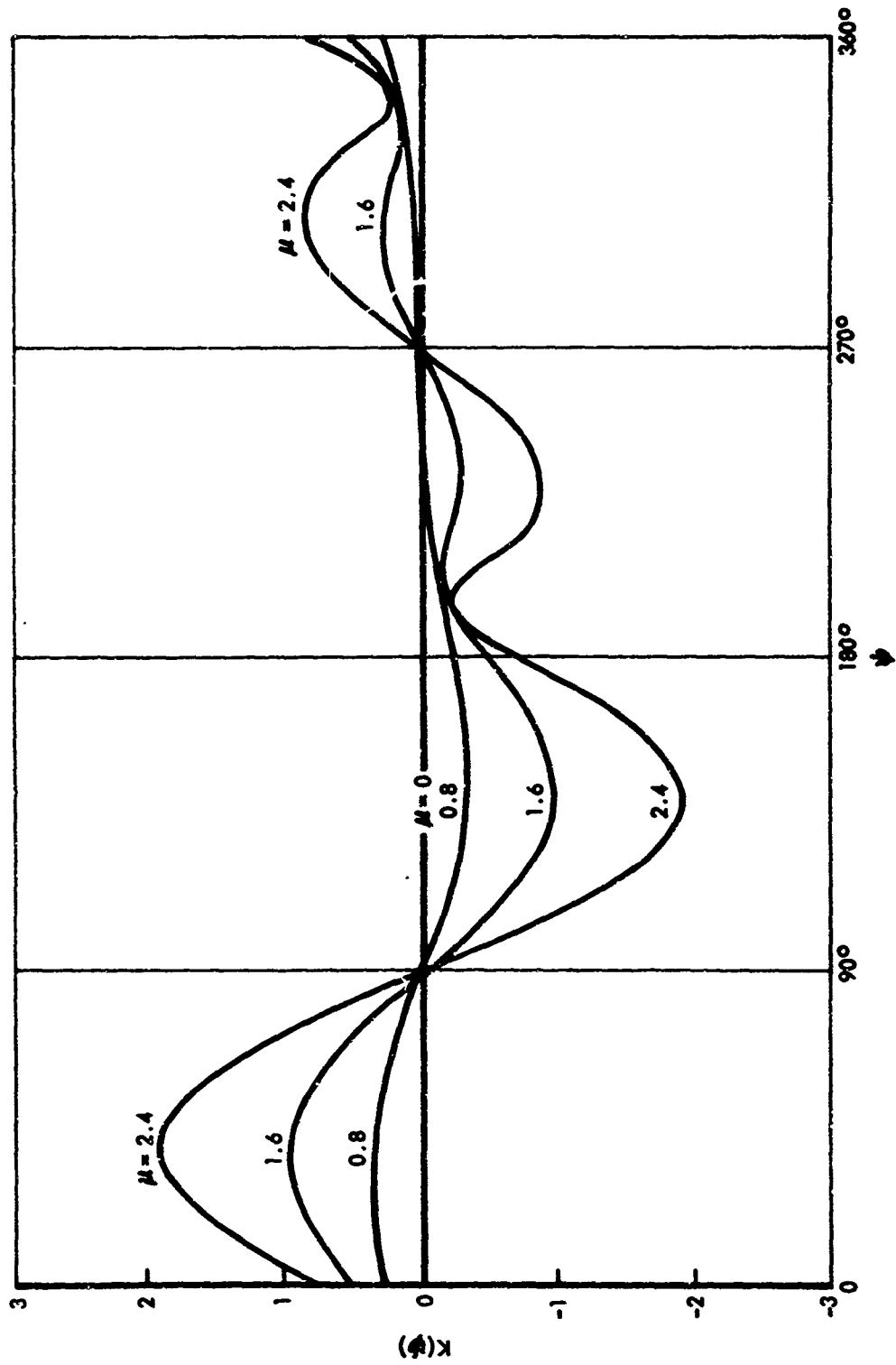


Figure 6. Effect of Advance Ratio on Aerodynamic Spring Rate.

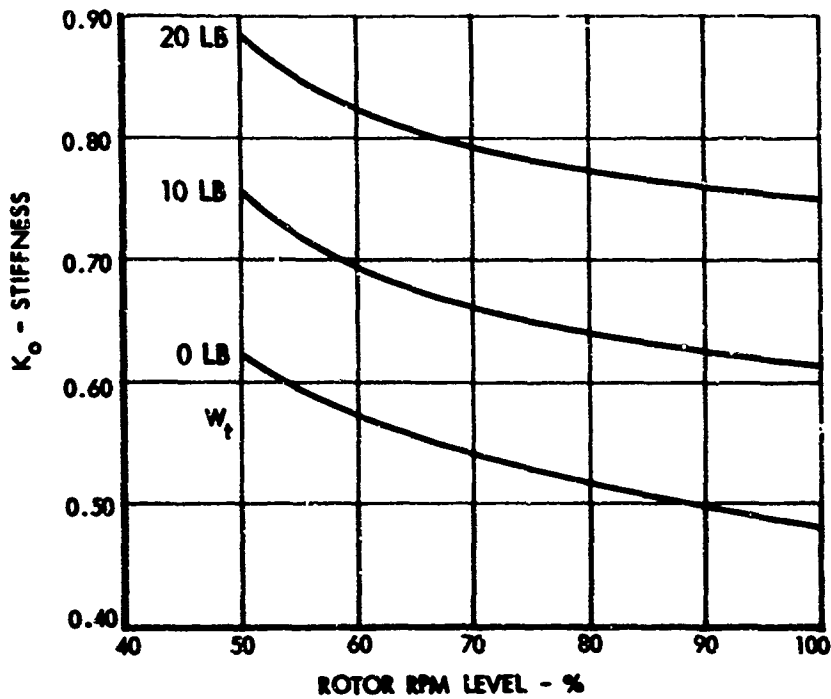


Figure 7. Variation of K_0 with Tip Weight, XH-51A Fotor.

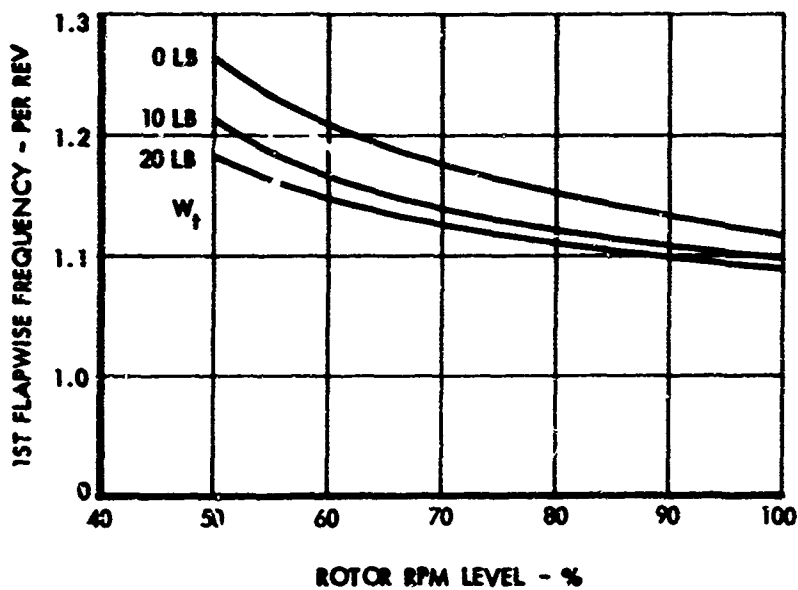


Figure 8. Variation of XH-51A Rotor First Flapwise Frequency with Tip Weight.

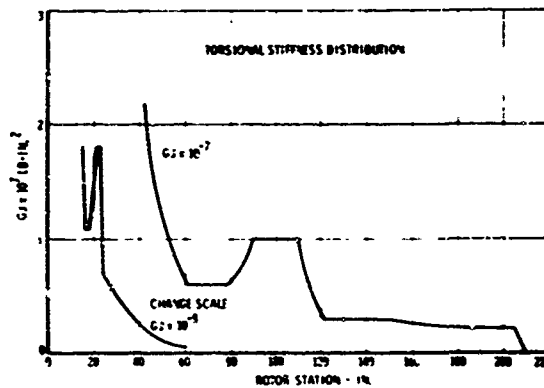
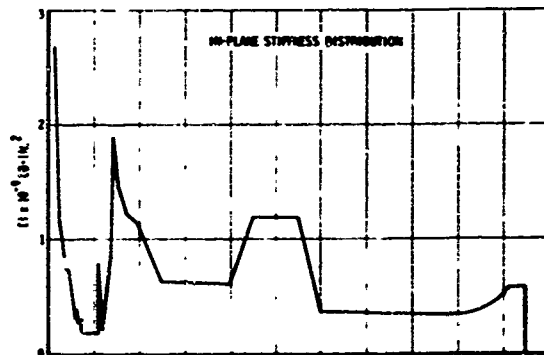
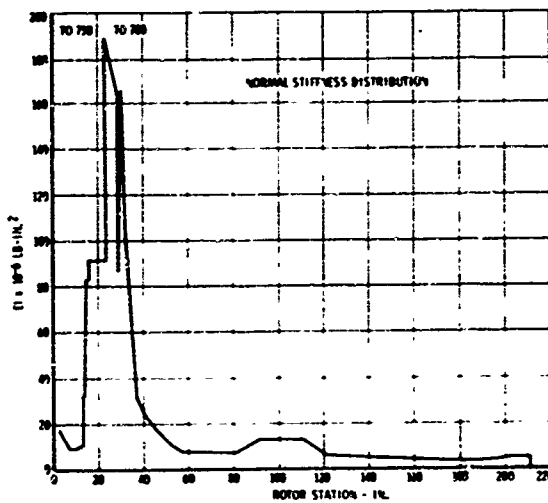
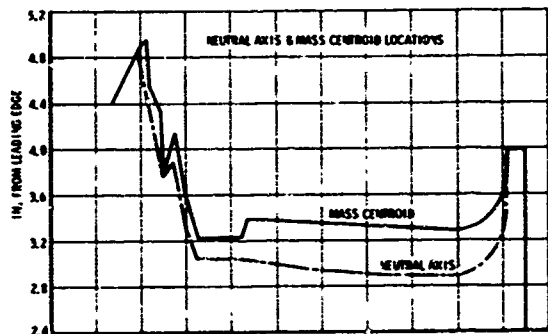
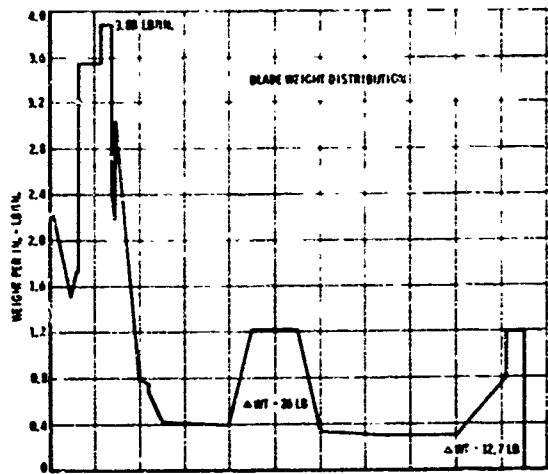


Figure 9. Main Rotor Mass and Stiffness Properties.

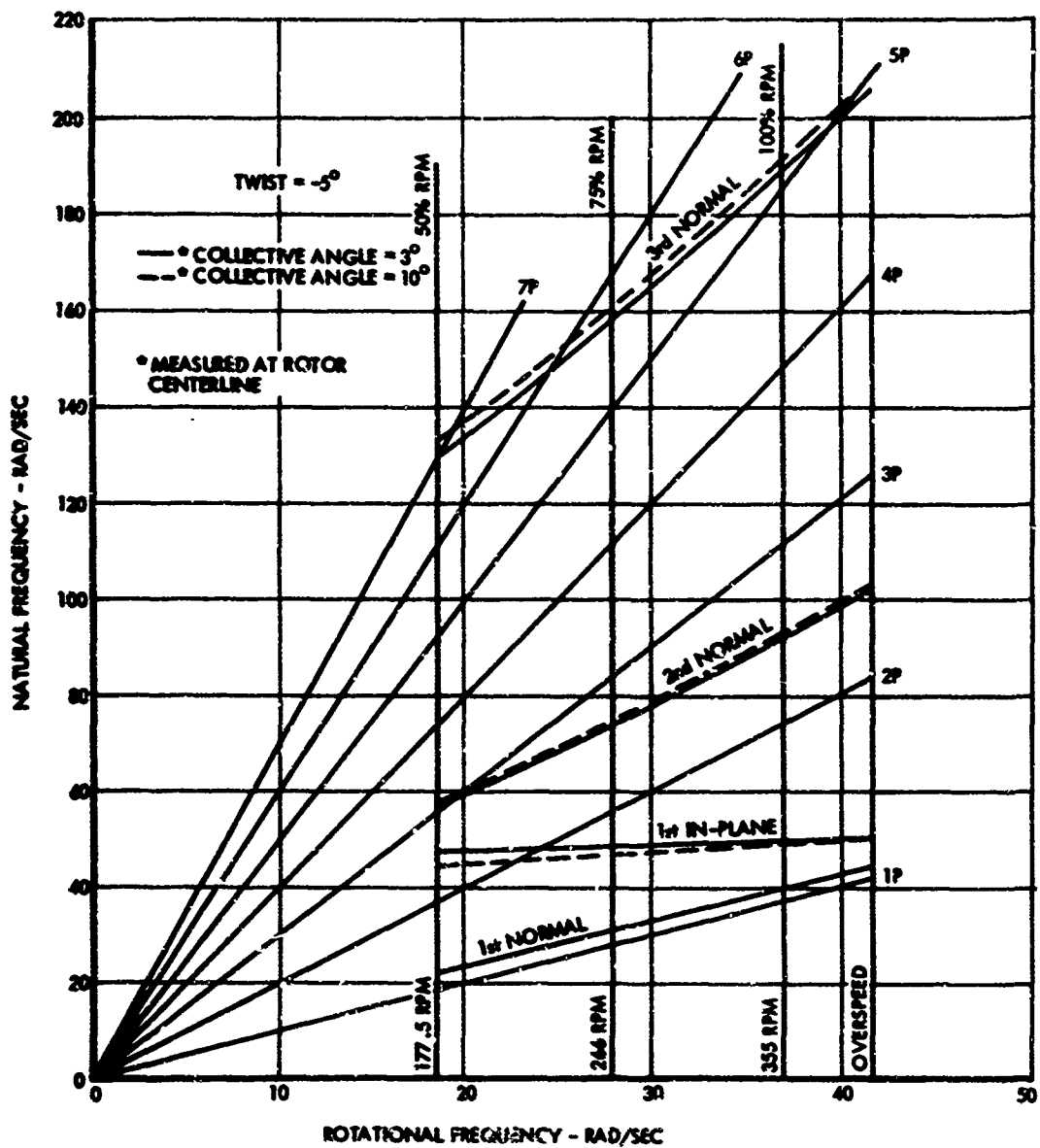


Figure 10. Main Rotor Natural Frequencies.

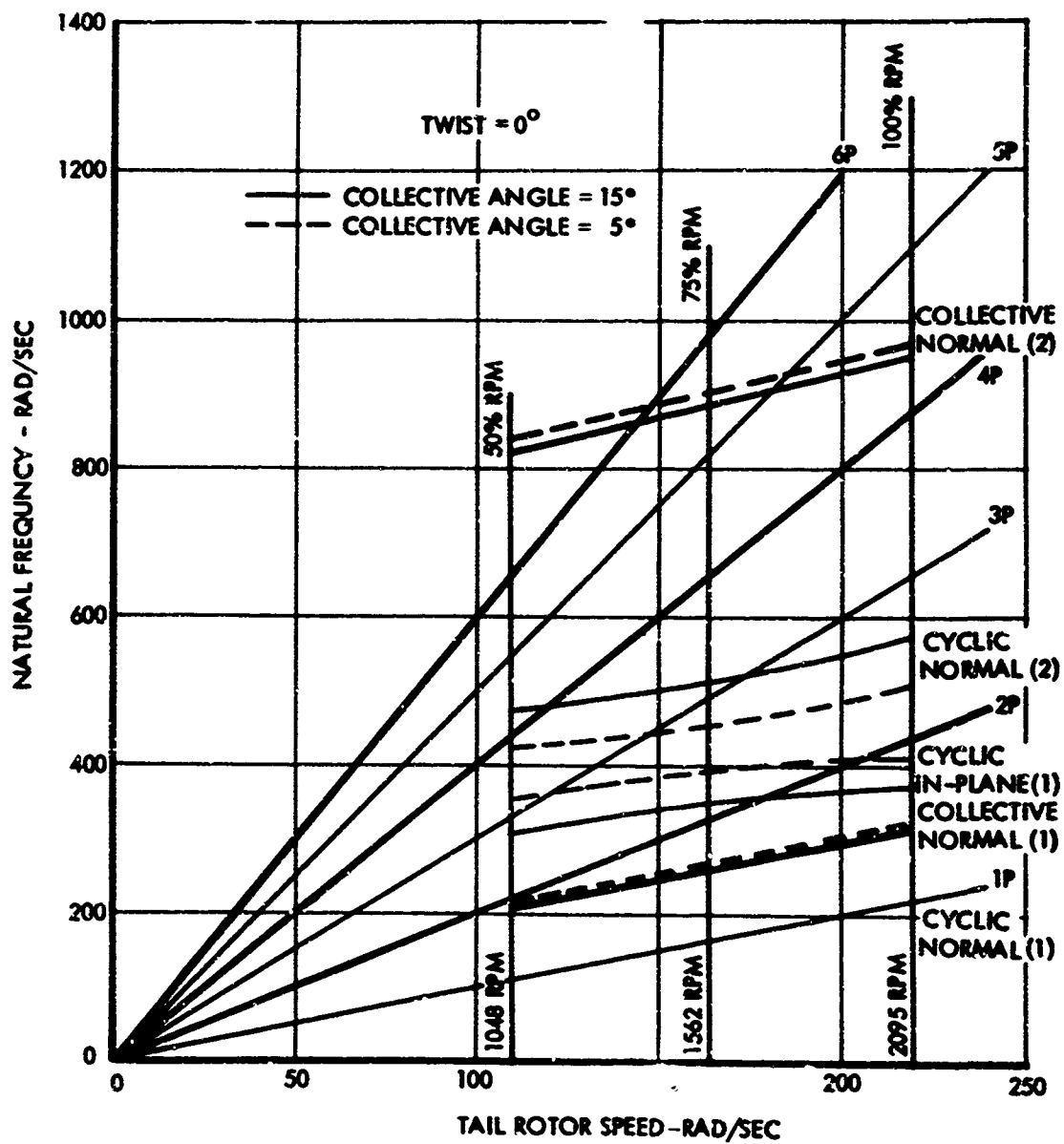


Figure 11. Tail Rotor Natural Frequencies.

even harmonic frequencies, shown by heavy lines. The cyclic modes (anti-symmetric normal bending, symmetric in-plane bending) are excited by the odd harmonic frequencies, shown by the thin lines in the figure. At normal rotor speed (2095 rpm), the natural frequencies of the rotor are well separated from the exciting harmonics at all collective angles. At 75% normal rotor speed, the tail rotor is operated at low collective angles; therefore, the second cyclic normal bending mode will not coincide with the third harmonic.

The operation of a 50% rpm rotor system necessitates further tailoring of main and tail rotor natural frequencies. Due to the extreme range of rpm variation in this case, it would be impossible to design a system completely devoid of resonance conditions over the entire range. Therefore, at some moderate flight speed, the range of rpm where resonances occur must be passed through rapidly in order to avoid high vibrations and loads.

1P-2P INSTABILITY

A phenomenon described as a 1P-2P instability has been experienced in gyro-controlled rigid-rotor operation. The phenomenon occurs at flight conditions where high hub moments requiring large blade flapping deflections must be generated. High blade flapping deflections cause a 2P in-plane excitation due to Coriolis forces. Flapping deflections feeding back as a moment on the control gyro through forward blade sweep tend to stabilize the hub moment. The 2P in-plane response of the rotor creates a moment opposing the stabilizing feedback. When this destabilizing moment becomes dominant, the rotor becomes unstable. The magnitude of hub moment at which the mode becomes unstable is dependent on rpm and is a minimum for the rpm at which the first in-plane natural frequency is 2P.

The response to this instability builds up slowly enough that the pilot has no problem controlling the rotor as long as he is given the cues to know that it is developing. Any increase of moment in flight results in motion of the vehicle for which the pilot can correct. In this respect, the phenomenon can be compared to an unstable phugoid or spiral mode which is not a problem to the pilot as long as he is provided with reasonable cues.

The possibility of exciting the unstable 1P-2P divergence exists in slowing the rotor from 75% to 50% rpm, if at the same time a large hub moment is required for trim. In addition to reducing rpm quickly to avoid operation at resonance of the first in-plane mode, it will be desirable to be operating at as low a hub moment as possible. In-plane natural frequencies for the 50% rpm rotor system will be tailored to avoid 1P-2P instability.

ROTOR CONTROL

In previous flight programs, the only control problem which has been encountered has been a right-hand stick displacement for trim. This displacement is required to balance a gyro moment caused by the feedback of a steady feathering moment due to the one-per-revolution high local drag acting on the underconed advancing blade at low lift. However, this stick displacement is small, and sufficient travel remained for adequate control margin.

The primary concerns with the control of a slowed-rotor compound are (1) the possible need for a phase shift of control with rpm reduction due to variation in cross coupling, and (2) the possible need for auxiliary fixed-wing-type control surfaces to supplement the available rotor hub moment at reduced rpm. The digital computer simulation described in Appendix I is used to evaluate main rotor control cross coupling and capability at low rpm. In this section the results of a study of slowed-rotor control cross coupling and control capability are presented.

CONTROL AT REDUCED RPM

In evaluating control cross coupling and capability, the parameters \bar{x} and \bar{y} , normalized stick displacements, are used in lieu of x_{cs} and y_{cs} , actual stick displacements, for two reasons: first, the functions p/y , q/x , etc., are dimensionless; second, these functions do not reflect a specific value for either K_{xcs} or $K_{y cs}$, dimensionless control moment spring constants. Eliminating the effect of these spring constants on the results allows the curves to be used as design tools in determining values for the control system spring constants.

The functions

$$\left(\frac{q}{\bar{x}}\right) \sqrt{\Omega}, \left(\frac{p}{\bar{y}}\right) \sqrt{\Omega}, \left(\frac{q}{\bar{y}}\right) \sqrt{\Omega}, \text{ and } \left(\frac{p}{\bar{x}}\right) \sqrt{\Omega}$$

are plotted in Figures 12 through 17. Dividing the basic functions $\frac{q}{\bar{x}}$... by the rotor speed ratio allows changing rotor speed to affect the amplitudes of the curves as well as the timing of them. Since the character of these responses is the same for various blade tip weights and rotor gyro inertias, all of the data presented in Figures 12 through 17 are for a tip weight of 15 pounds and a gyro inertia of 17.5 slug-ft². The response characteristics are not particularly sensitive to moderate variations about these values.

In general, the final amplitudes of the functions

$$\left(\frac{q}{\bar{x}}\right) \sqrt{\Omega} \text{ and } \left(\frac{p}{\bar{y}}\right) \sqrt{\Omega}$$

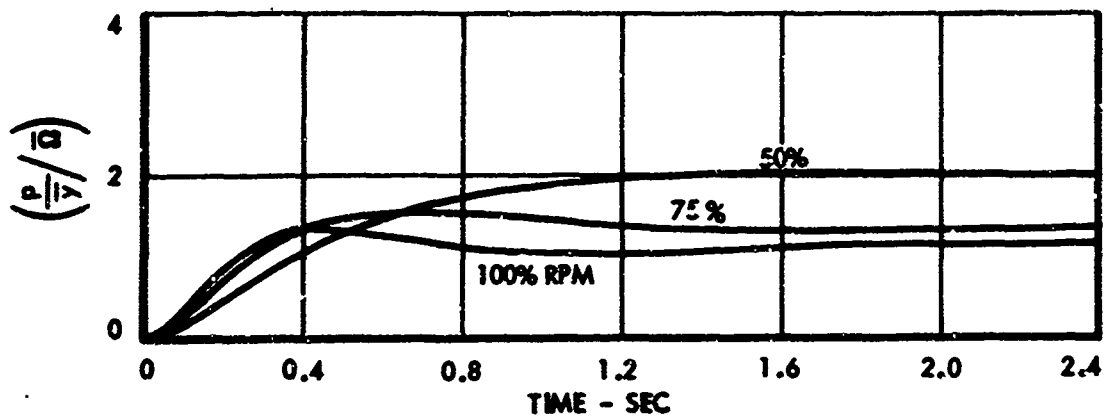
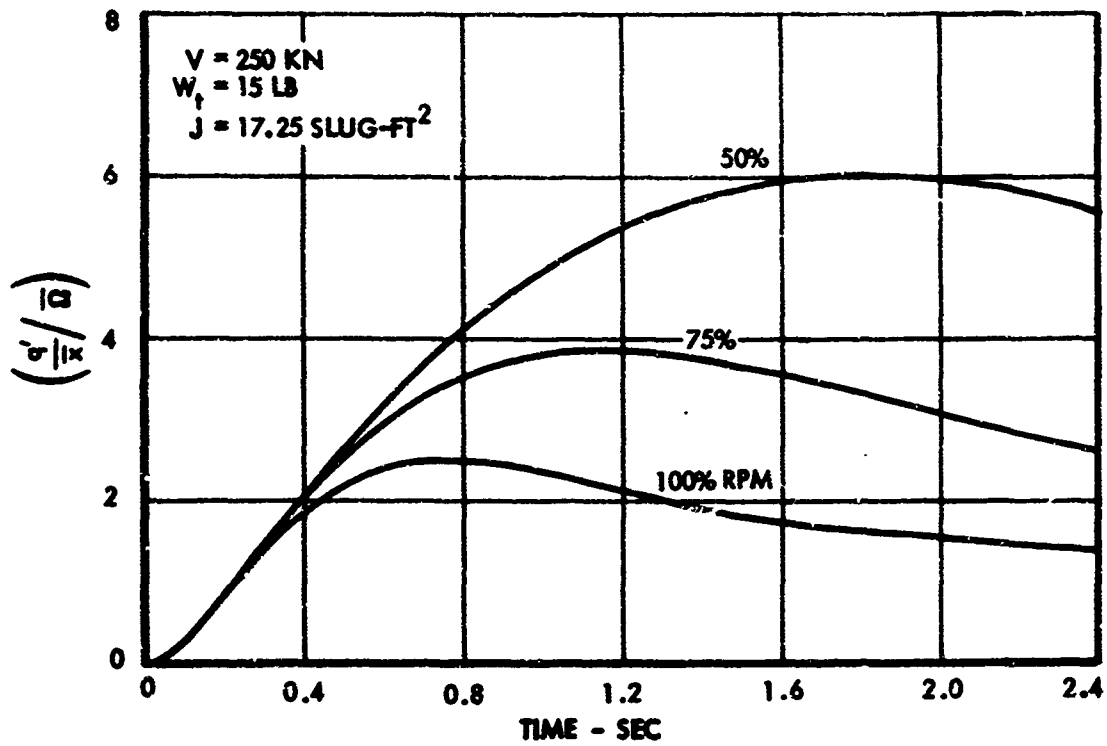


Figure 12. Pitch and Roll Control Sensitivity at 250 Knots.

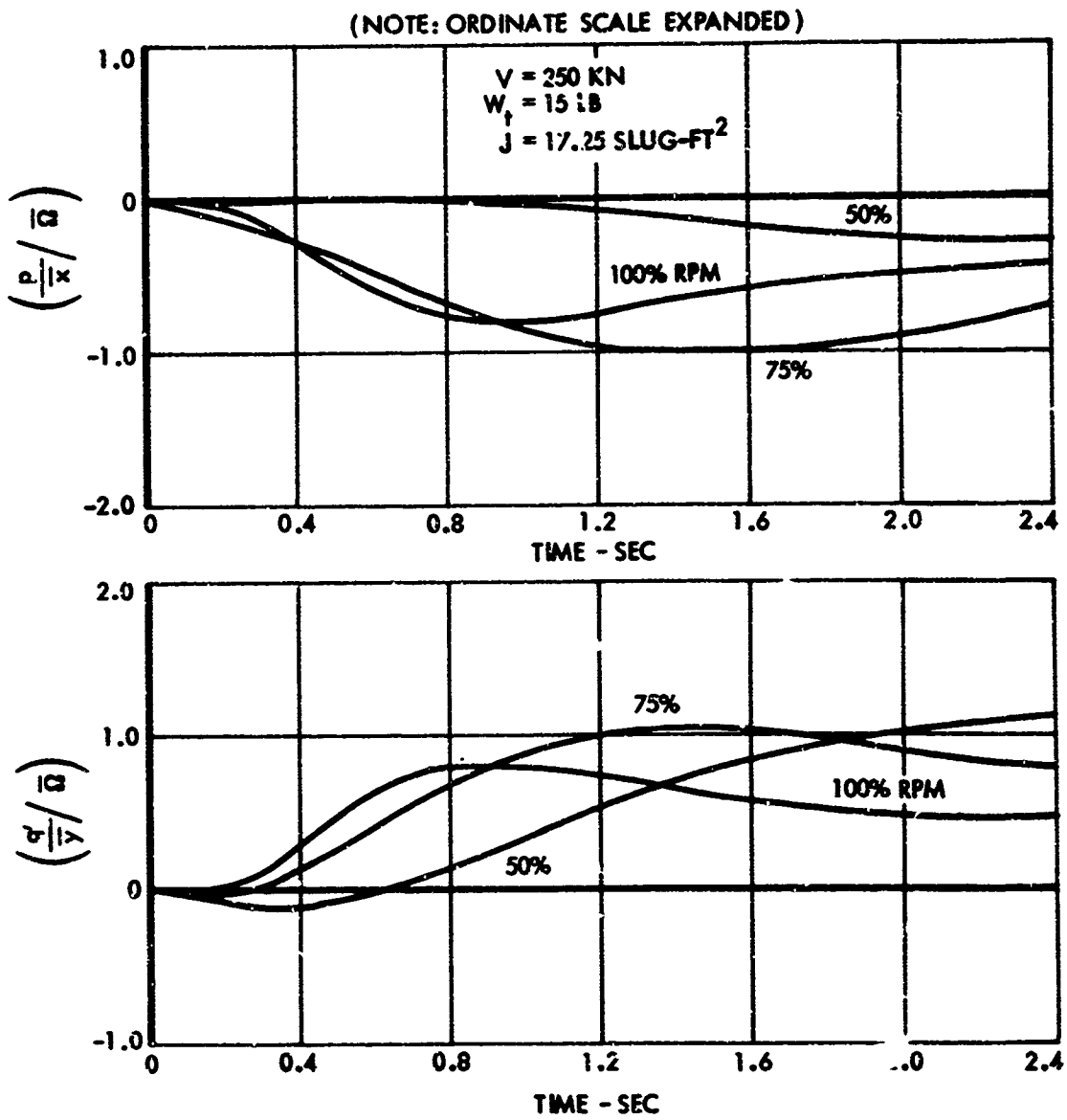


Figure 13. Cross Coupling at 250 Knots.

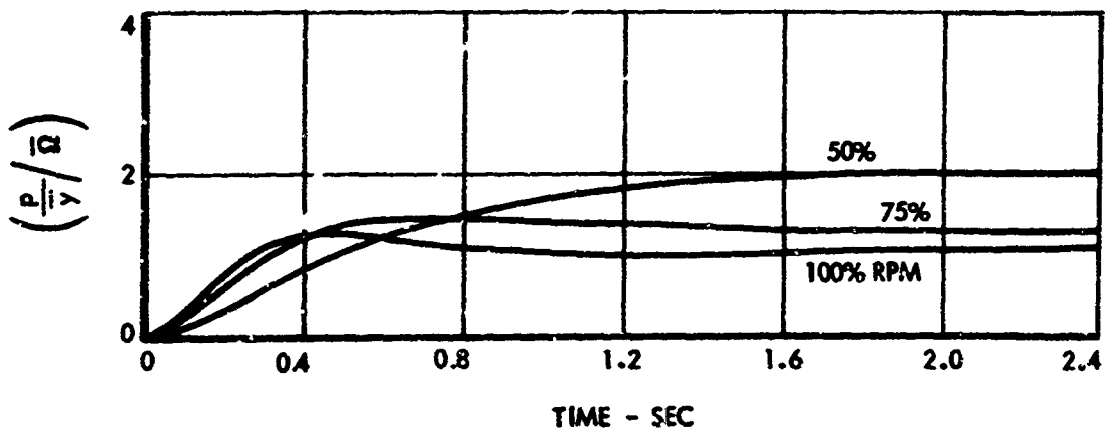
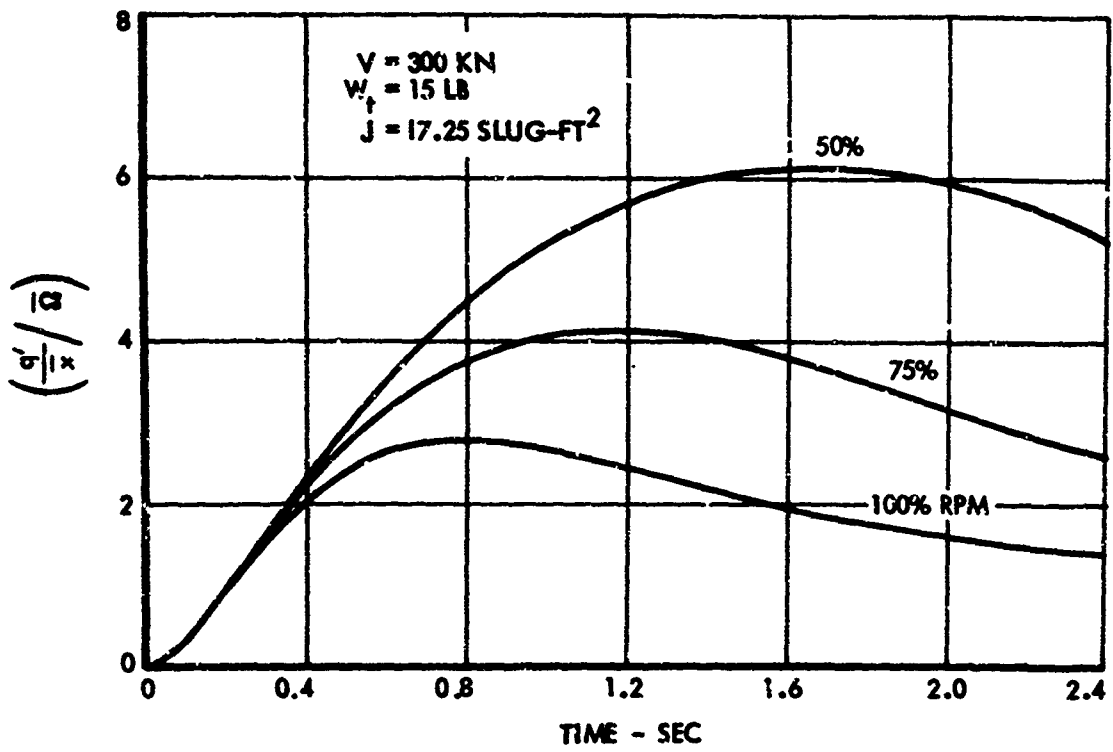


Figure 14. Pitch and Roll Control Sensitivity at 300 Knots.

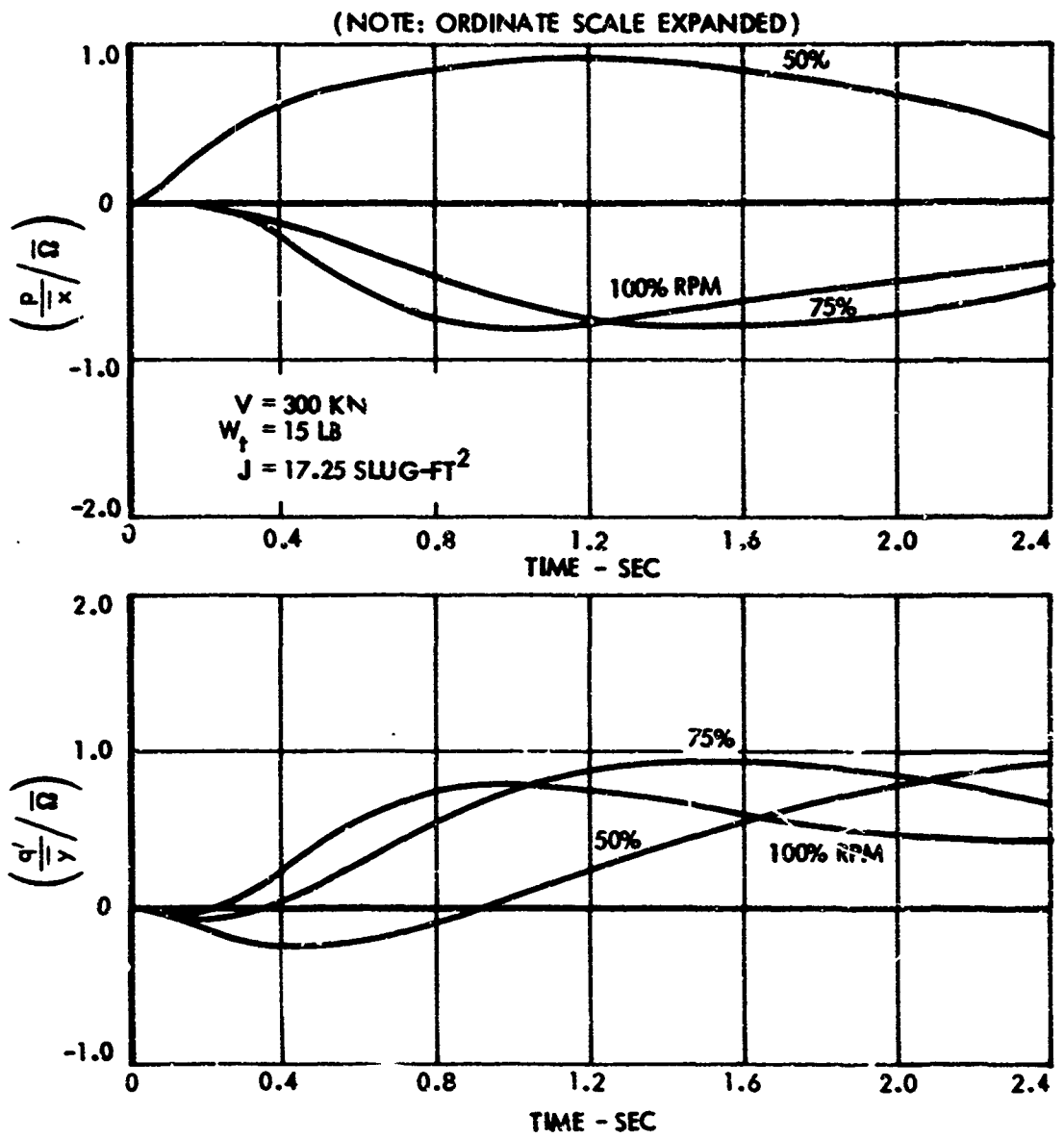


Figure 15. Cross Coupling at 300 Knots.

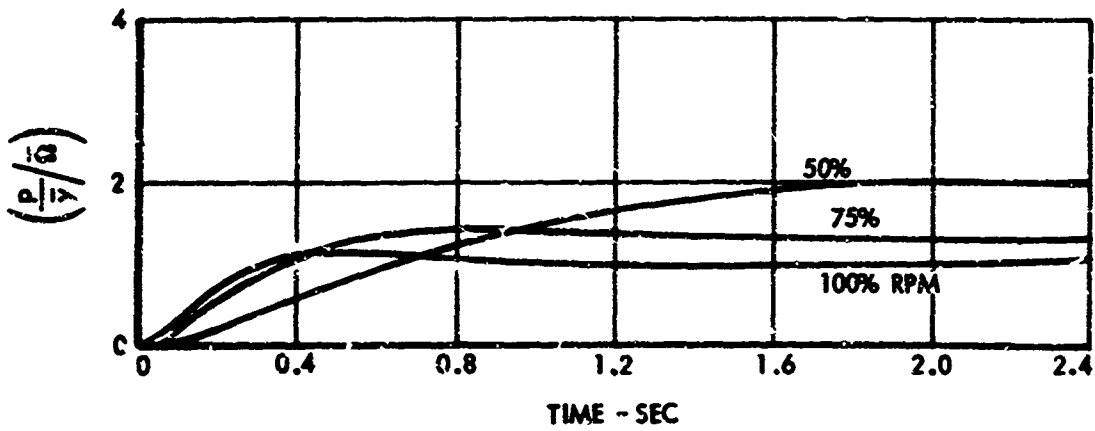
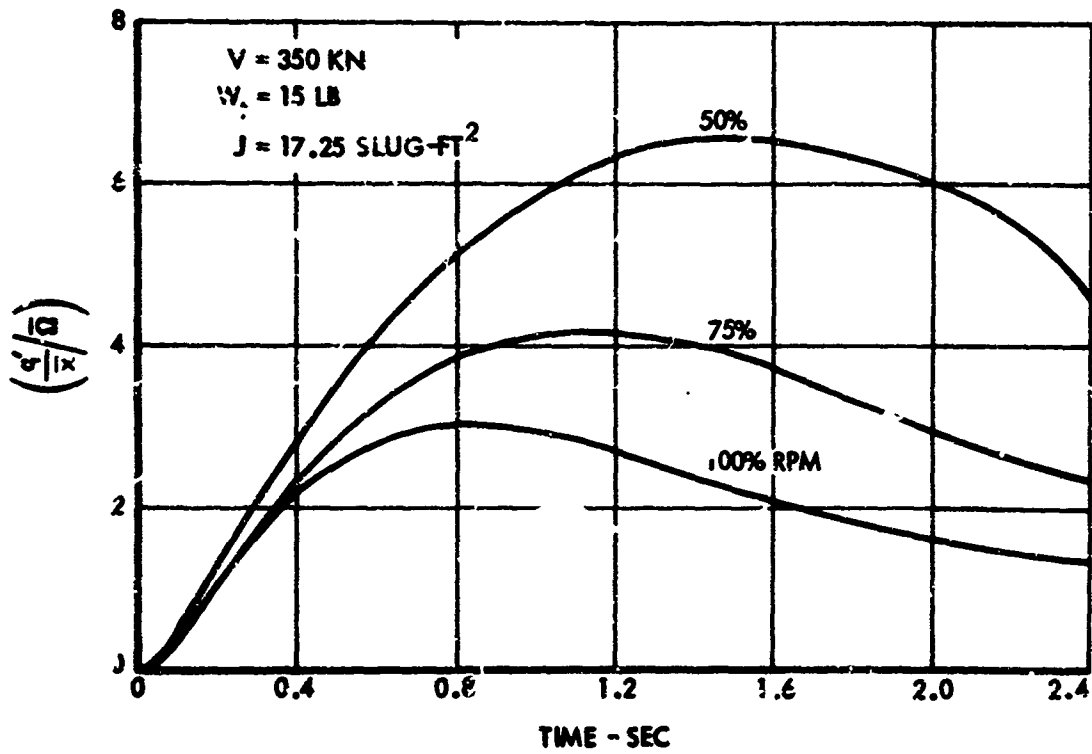


Figure 16. Pitch and Roll Control Sensitivity at 350 Knots.

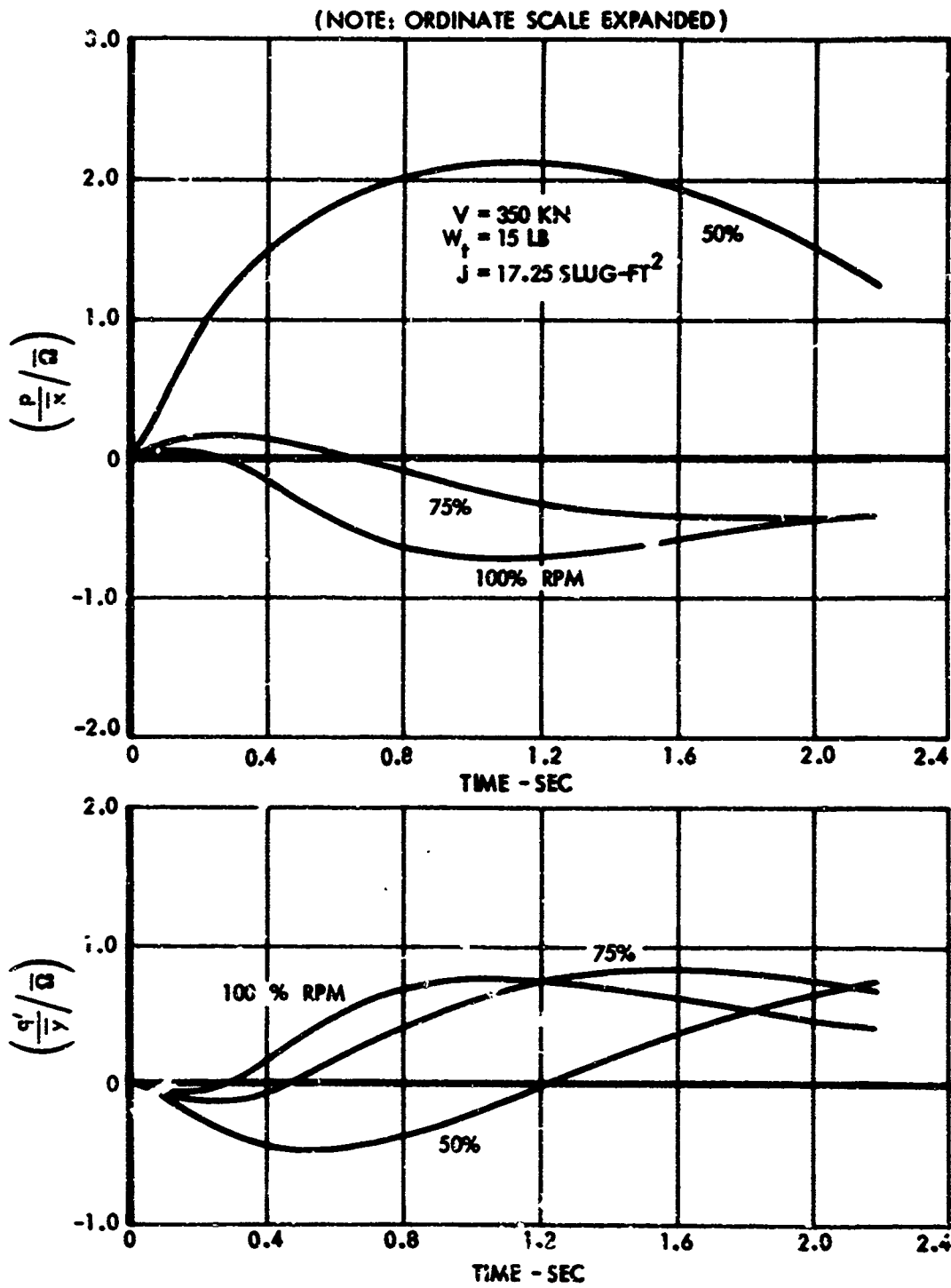


Figure 17. Cross Coupling at 350 Knots.

at a given flight speed vary as a function of the inverse of the rotor speed, Ω . For example, final amplitude of the 50% rpm curve of Figure 14 is nearly twice that of the 100% rpm curve. One may expect these amplitudes to ratio exactly with $1/\Omega$. However, since changing Ω slightly affects cross coupling (e.g., p/q' vs. time for an \bar{x} input), response is traded between pitch and roll in varying amounts as Ω changes. This effect accounts for any deviation of final amplitudes from exact proportions of $1/\Omega$.

The following conclusions on the sensitivity of handling qualities to rotor rpm and flight speed are based on the response functions shown in Figures 12 through 17 and on characteristics of existing helicopters.

1. The rigid-rotor system has intrinsic qualities of high-frequency, short-period, pitch and roll modes with high damping. The high-frequency (fast-response), highly damped characteristic can be closely matched, as in the XH-51A, to the pilot's response. Precision rate control may be achieved in response times (63% of time to maximum amplitude) of 0.5 second or less. Conventional helicopters display low damping, and angular rate results from a basic control input followed by a control adjustment to minimize overshoot. The response time to stabilize at a desired angular rate is from 2 to 5 seconds. Figure 18 illustrates how the two types of response match stick pulse inputs in hover. Simulation results show that the slowed-rotor vehicle can be adequately responsive at the rotor and flight speeds of interest. It is concluded that no additional control surfaces will be required to augment the rotor's cyclic control capabilities at rpm reductions down to 50%.
2. Cross coupling is not being altered enough by varying flight conditions to warrant compensation with special adaptive servo systems. This judgment is made after considering the cross-coupling levels encountered by pilots flying the XH-51A compound helicopter. The pilots are able to fly the aircraft safely with levels of coupling higher than those computed for the 50% rpm system. Flight test experience with the XH-51A in the high-speed regions (see Reference 3) indicates that the cross-coupling effects were dependent on, and inversely proportional to, the degree of control sensitivity. This is a controlled variable in the XH-51A control system and is adjusted by modifying hydraulic boost gain.
3. The vehicle becomes somewhat more amplitude-sensitive (considering ultimate response amplitude per unit of control input) with decreasing rotor speed. The sensitivity is not a strong function of airspeed. As discussed above, the amplitudes of Figures 12 through 17 do not reflect the control spring constants K_{xcs} and $K_{y cs}$. These spring coefficients directly affect the amplitude sensitivity of the vehicle, and their values can be determined in a final design process to provide a compromise between the sensitivities at minimum and maximum rotor speeds.

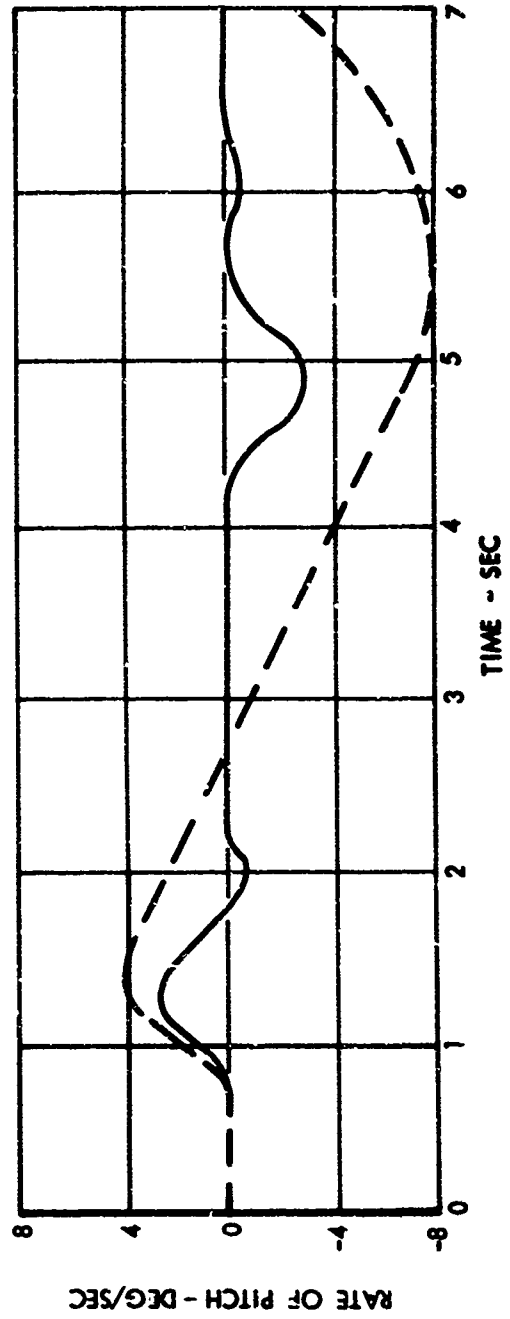
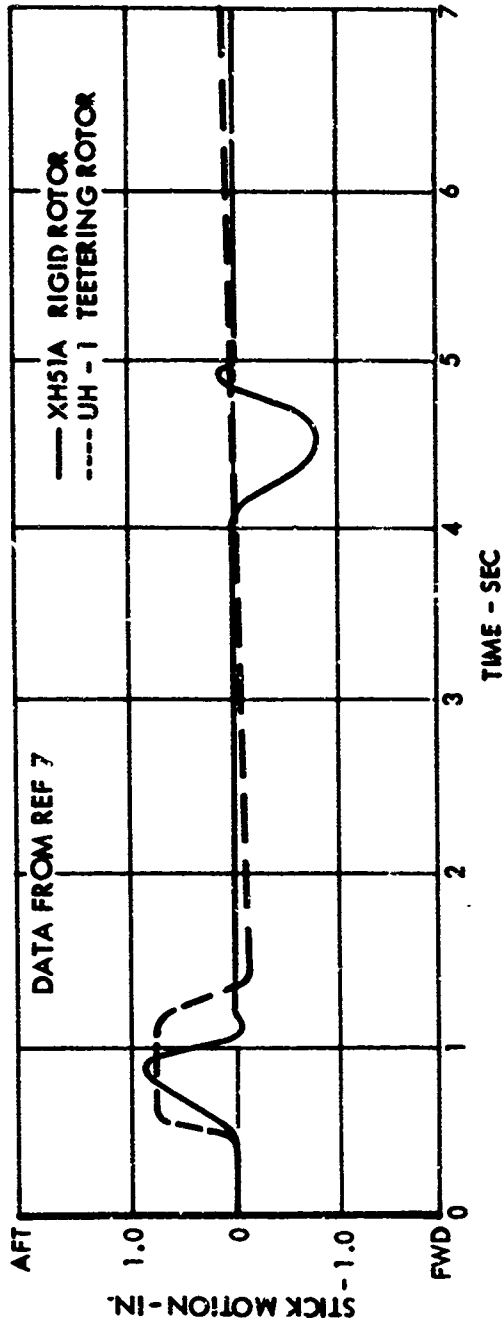


Figure 18. Response to Stick Motion in Hover.

ROTOR LOADS

The critical loading conditions for the rotor throughout the speed range are analyzed; the effect on loads of twist, coning angle and droop are assessed; and fatigue data are presented. The basic loads data are generated by the method indicated in Appendix I using the blade characteristics presented in Figure 9.

DESIGN LOADING CONDITIONS

Limit design loads on the main rotor are developed for 11 flight conditions following the rotor thrust capability diagram of Figure 19. Each of the circled numbers identifies a potential critical loading condition in the flight envelope which must be analyzed to determine the limit design loads. The high-speed loading conditions are evaluated at various reduced rotor speeds to provide a range of data to cover any selected rotor speed.

In addition to the limit design load conditions 1 through 11, other loading conditions for fatigue analysis are investigated. At the lower speeds, the collective control angle is used to obtain the rotor thrust specified. At the higher speeds (conditions 21 through 24 of Table II), the collective control angle is maintained at 3 degrees and the rotor angle of attack is determined by the assigned vehicle load factor.

A summary of the loading conditions is given in Table II.

Condition 1 is a symmetrical hovering pull-up with maximum rotor thrust. Analysis shows that the maximum rotor thrust is obtained with a collective control angle of 23.4 degrees. Since this is beyond the physical capability of the control system, the calculated loads are considered to be conservative. Furthermore, the torque required to maintain this condition is considerably larger than the torque which can be delivered by any turboshaft engines considered for the aircraft. Therefore, the computed in-plane bending moments are conservative. The values of bending and torsion moments vs. blade span are shown in Figure 20. (Since this is a symmetrical condition, the loads are constant around the azimuth.)

Condition 2 is a low-speed (60 knots) pitching pull-up with maximum rotor thrust. The maximum rotor thrust at this speed is obtained with a collective control angle of 17.3 degrees. Again the rotor torque required to maintain this condition is higher than the available torque, indicating that the loads are conservative.

At forward speeds above 64 knots, the limit structural design envelope loads are determined by retreating blade stall. In these conditions, the maximum rotor thrust on the retreating side of the rotor disc is limited to a low value due to blade stall and a relatively low value of dynamic pressure,

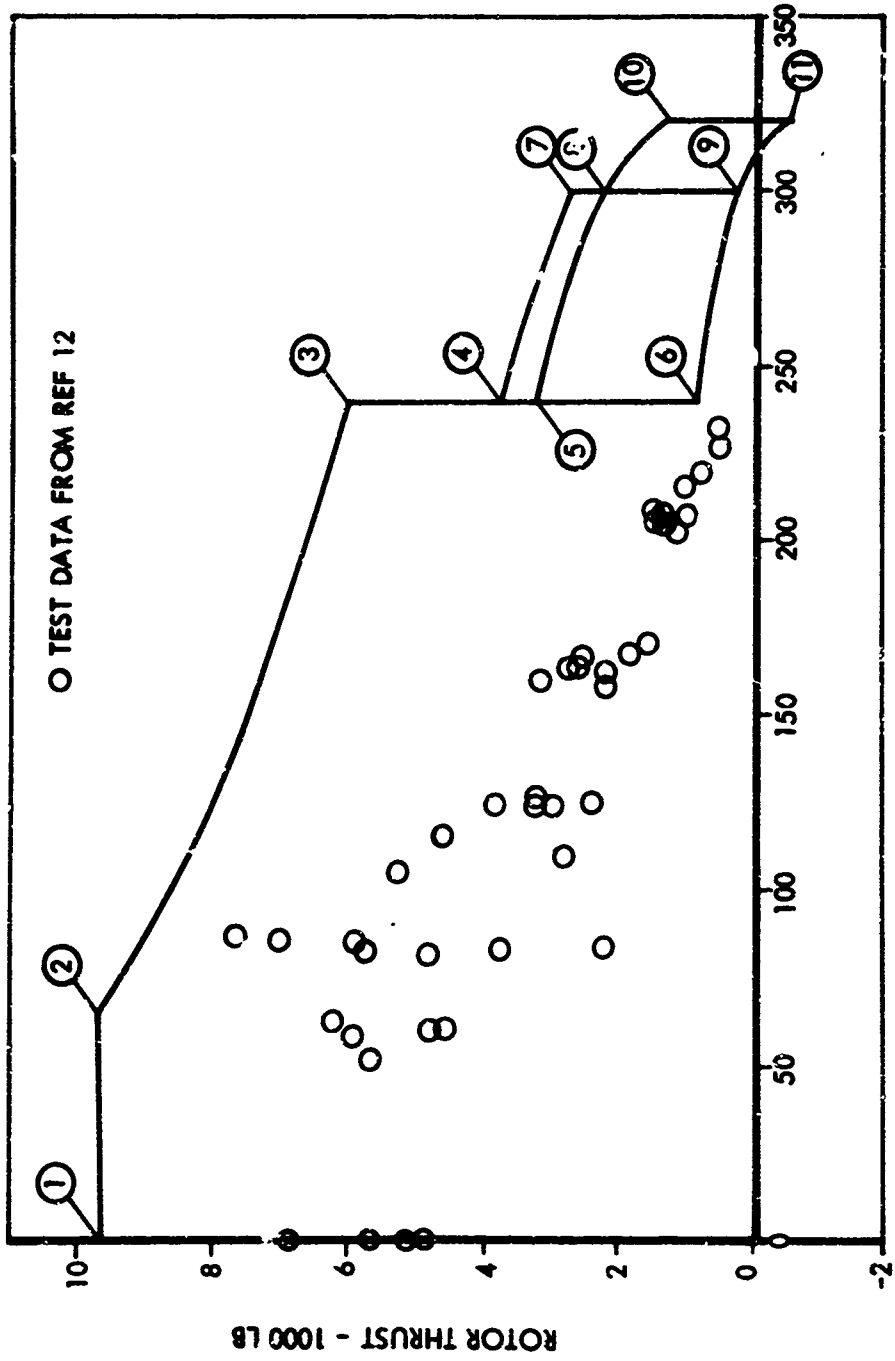


Figure 19. Rotor Thrust Capability Diagram.

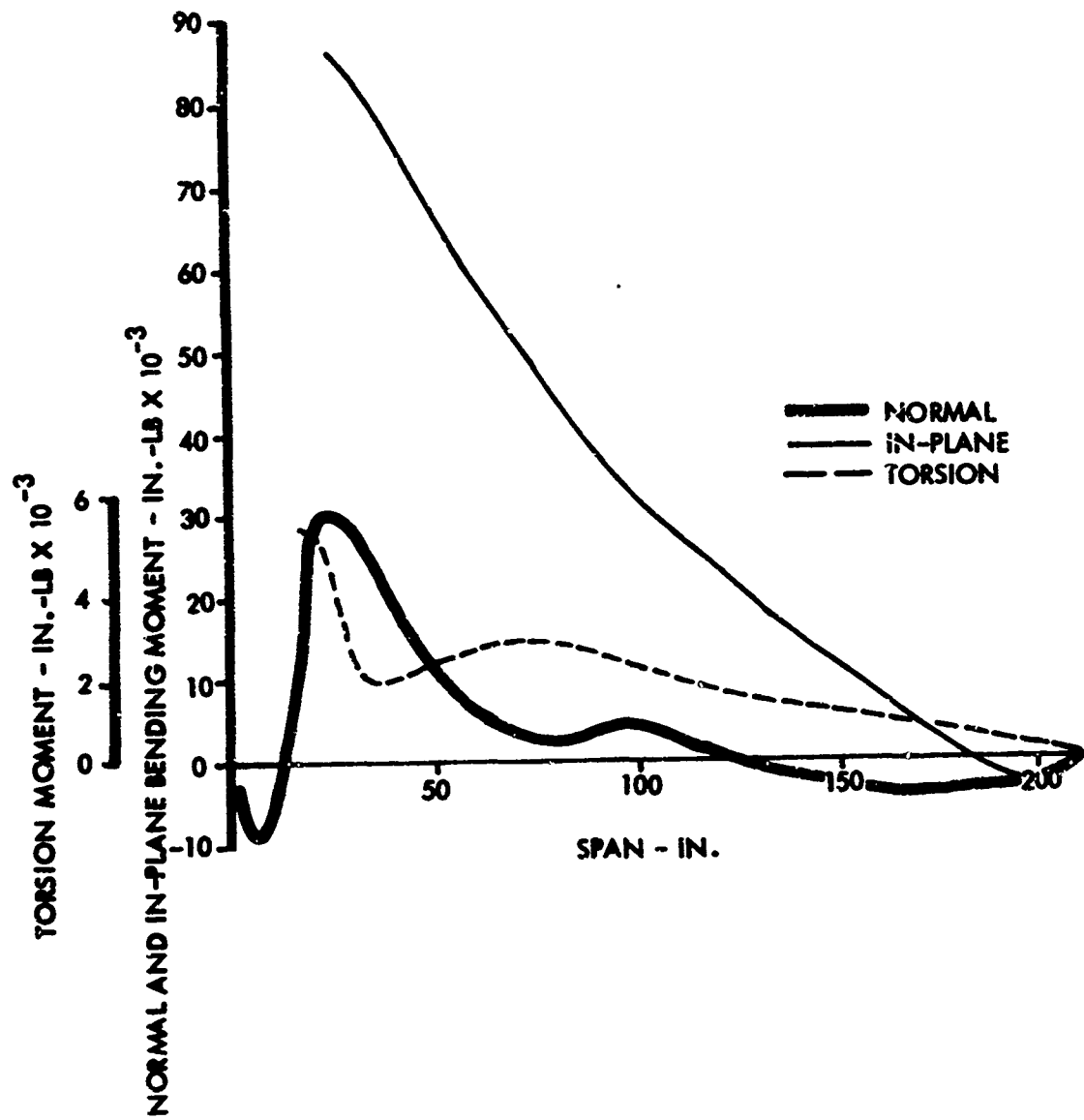


Figure 20. Spanwise Moment Envelope, Condition 1.

TABLE II. SUMMARY OF LOADING CONDITIONS

Cond. No.	Speed (kn)	RPM (%)	Vehicle Load Factor	Rotor Load (lb)	Vehicle Pitching Moment (in.-lb)	Pitch Rate (rad/sec)	Collective Angle (deg)	Cyclic Angle Cosine (deg)	Cyclic Angle Sine (deg)	Shaft Angle (deg)
1	0	100.0	1.75	10,500	0	0	23.4	0	0	0
2	66	100.0	1.82	11,040	0	0.24	17.3	1.45	-4.07	6.00
3	240	100.0	3.00	6,137	-75,000	0.16	10.15	2.32	-12.0	8.05
4	240	84.6	2.00	3,790	-50,000	0.08	11.71	2.22	-12.0	4.87
5	240	78.9	2.0	3,349	-50,000	0.08	11.30	2.37	-12.0	5.4
6	240	50.0	1.5	871	-37,500	0.04	10.29	3.21	-12.0	4.67
7	300	84.6	2.1	2,717	-52,500	0.07	11.74	2.43	-12.0	2.66
8	300	78.9	2.0	2,303	-50,000	0.06	11.85	2.51	-12.0	2.60
9	300	50.0	2.0	215	-50,000	0.06	10.40	3.49	-12.0	3.85
10	320	78.9	1.5	1,270	-37,500	0.03	12.83	2.62	-12.0	0.40
11	320	50.0	1.5	-592	-37,500	0.03	12.03	3.23	-12.0	1.47
12	0	100.0	1.0	6,000	-12,500	0	13.51	0.15	0	0
13	0	100.0	1.0	3,000	-6,250	0	9.56	0.07	0	0
14	64	100.0	1.0	6,000	-12,500	0	9.73	0.66	-2.72	1.0
15	64	100.0	1.5	0,000	-18,750	0.15	13.03	0.67	-3.72	6.0
16	120	100.0	1.0	4,200	-12,500	0	5.75	1.05	-2.61	6.0
17	120	100.0	1.5	7,171	-18,750	0.08	10.88	1.01	-7.0	6.0
18	180	100.0	1.0	3,000	-12,500	0	5.43	1.42	-2.72	3.0
19	180	100.0	1.8	6,000	-22,500	0.09	9.03	1.30	-7.44	6.0
20	240	100.0	1.0	2,400	-12,500	0	6.91	1.77	-4.38	1.0
21	260	84.6	1.0	2,400	-12,500	0	12.14	1.98	-10.36	0.5
22	260	84.6	1.0	1,400	-12,500	0	3.00	2.02	-1.01	3.0
23	260	84.6	2.0	1,686	-25,000	0.08	3.00	2.08	-0.23	2.0
24	320	78.9	1.0	871	-12,500	0	3.00	2.34	-1.8	1.0
25	320	78.9	1.0	281	-12,500	0	3.00	2.46	-0.41	0

while the thrust on the advancing side is determined by roll moment equilibrium.

The pitch rate q' which is developed in accelerated forward flight can be related to the vertical acceleration n_z :

$$q' = (n_z - 1) \frac{g}{V}$$

where g is the acceleration of gravity and V is the forward speed. Figure 21 shows a comparison of the theoretical pitch velocity and the measurements for the test conditions of Reference 8. The theoretical pitch rate computed from the vehicle load factor can be regarded as an upper limit.

A positive pitch rate (such as that in a pull-up) results in a gyroscopic moment on the rotor, which is relieved by aerodynamic forces. This requires additional rotor thrust on the advancing side of the rotor disc and increases the total rotor thrust. The maximum rotor thrust is developed in a condition which has the highest pitch velocity (i.e., the highest vehicle load factor) and the maximum cyclic control angle (12 degrees).

In Conditions 3 through 11, the rotor shaft angle of attack is determined by the vehicle load factor and the estimated rotor thrust. The sine component of the cyclic control angle is set at -12 degrees. The collective control angle and the cosine component of the cyclic control angle are determined from the shaft roll and pitch moment.

The most conservative phasing of the net shaft moment, in combination with the blade loads computed for zero shaft moment, is the phasing which follows from the aft c.g. position. The magnitude of these pitching moments is taken as 25,000 inch-pounds times the vehicle load factor. The maximum and minimum bending and torsion moments vs. blade span are shown in Figures 22 through 31.

A sample of the variation of bending moments over the azimuth is shown in Figure 32.

EFFECT OF TWIST, CONING ANGLE, AND DROOP

Figure 33 shows the effect of blade twist on cyclic normal bending moments at a given rotor thrust level. The data presented in this figure are based on linear theory. At the higher speeds and high rotor loads, the change in cyclic bending moment due to a change in built-in twist is of the order of 1% per degree.

A more complete analysis made for the design conditions 3, 7, and 10 by repeating the analysis for maximum rotor thrust without the built-in twist shows that a small increment of maximum rotor thrust is obtained by twisting the blades (Table III).

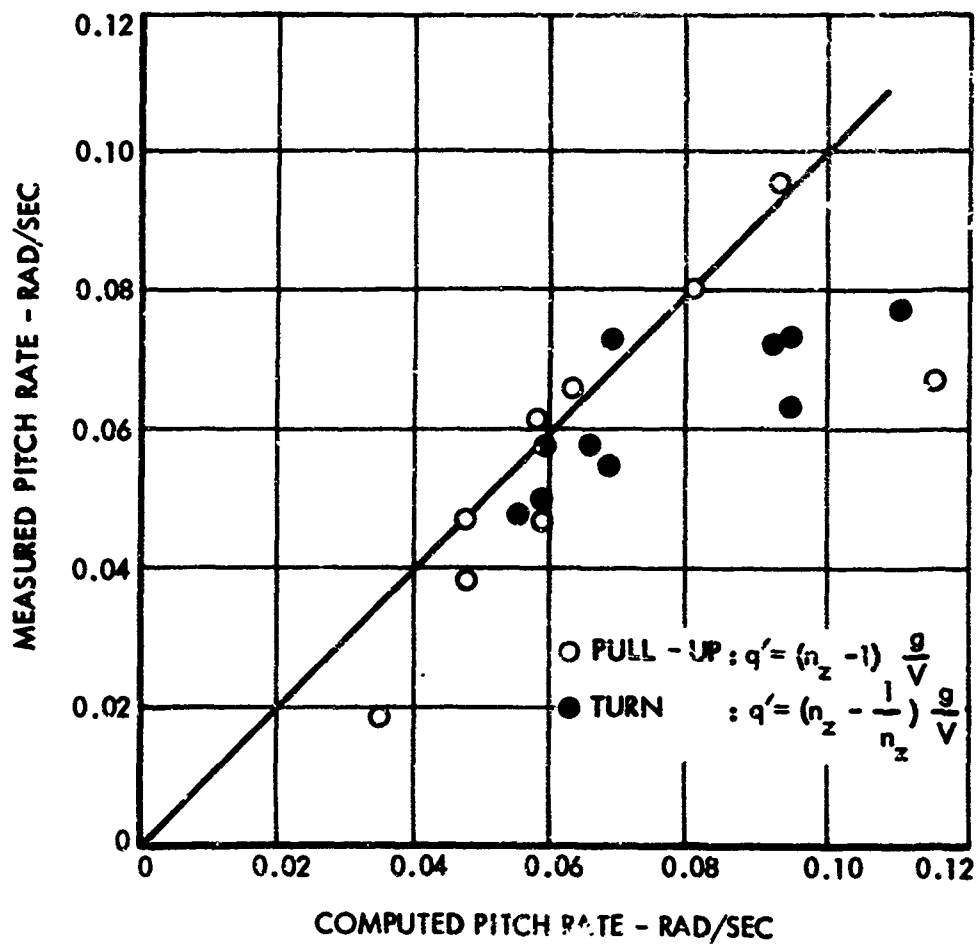


Figure 21. Measured Pitch Rate vs. Pitch Rate Computed from Load Factor and Speed.

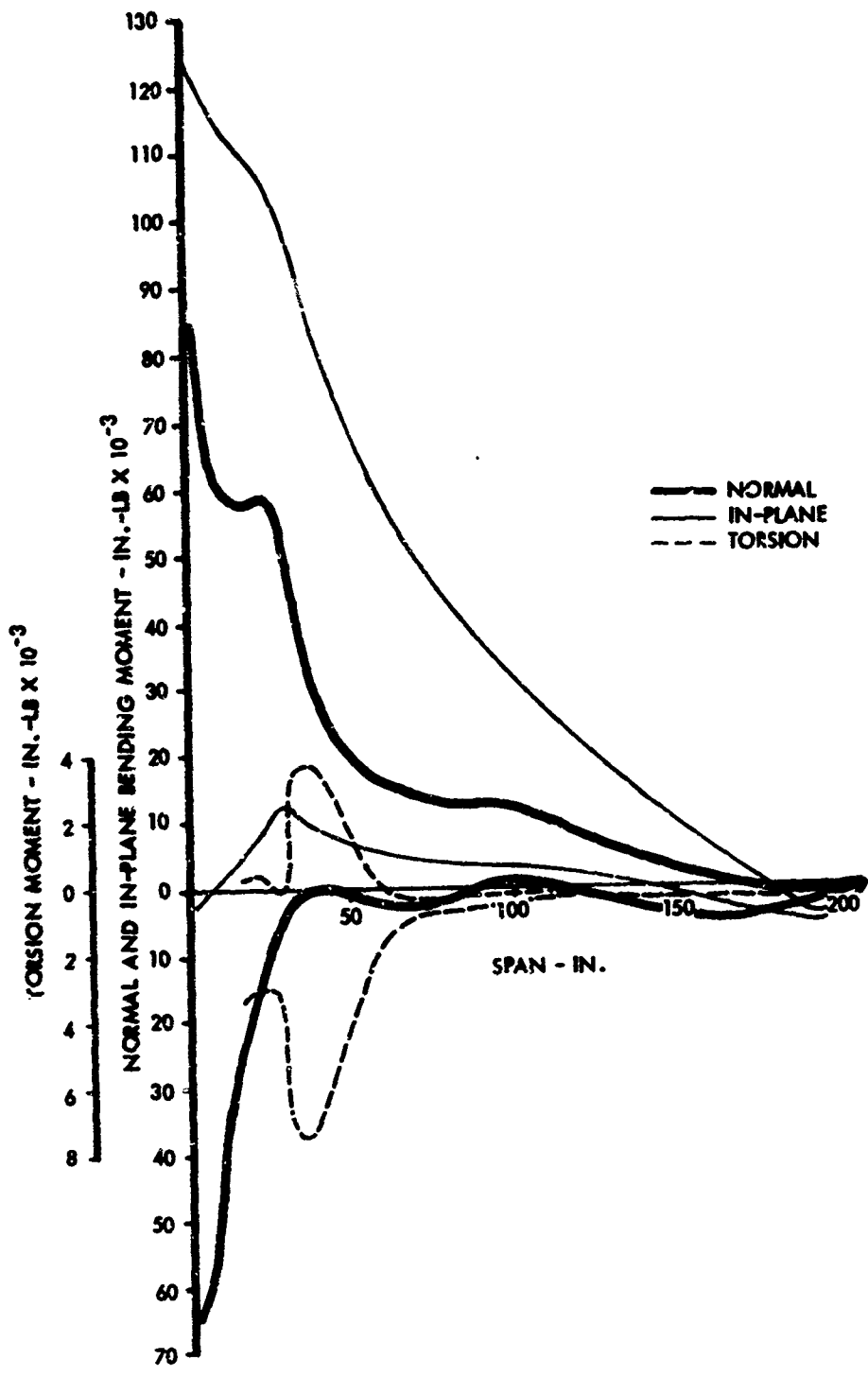


Figure 22. Spanwise Moment Envelope, Condition 2.

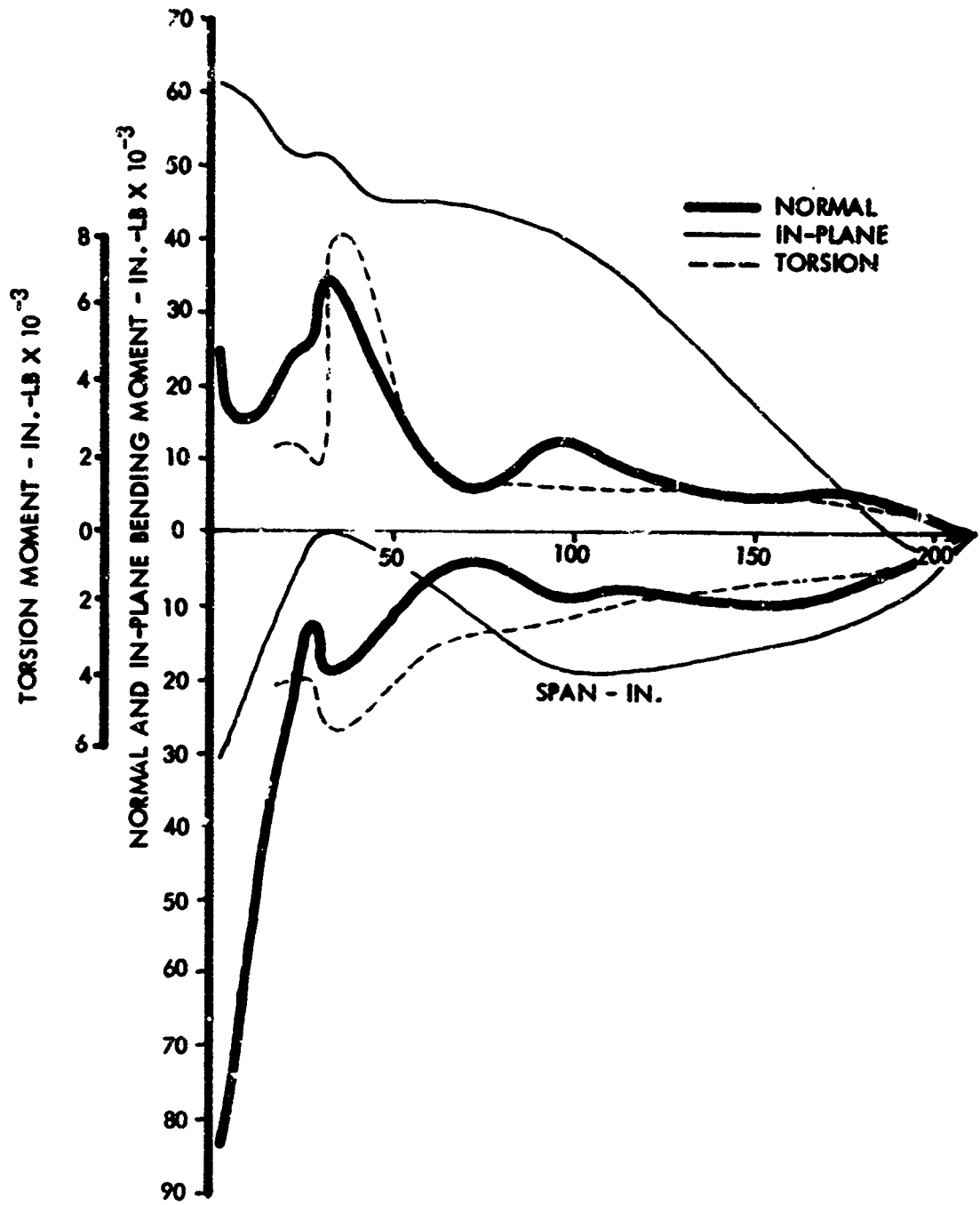


Figure 23. Spanwise Moment Envelope, Condition 3.

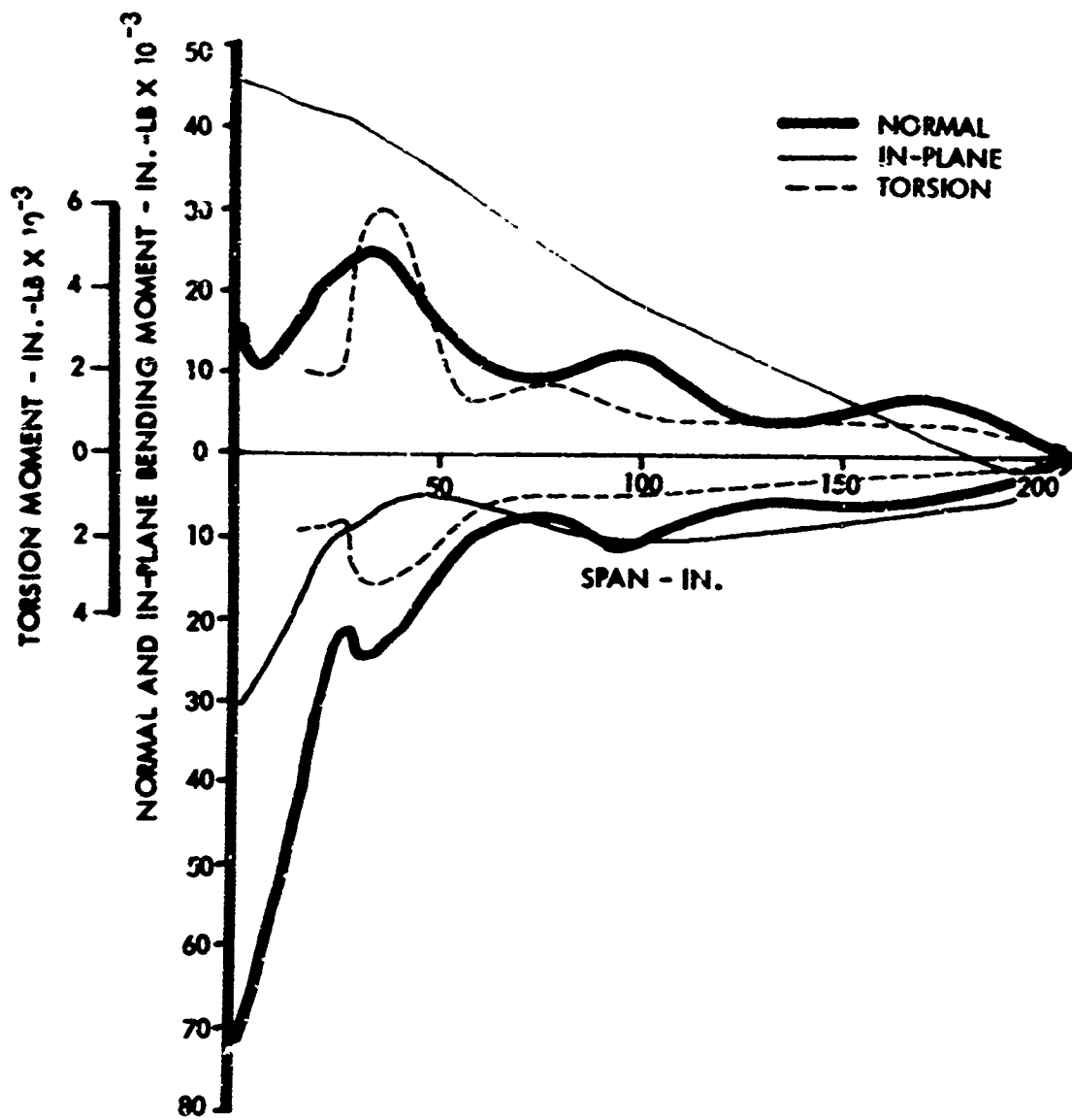


Figure 24. Spanwise Moment Envelope, Condition 4.

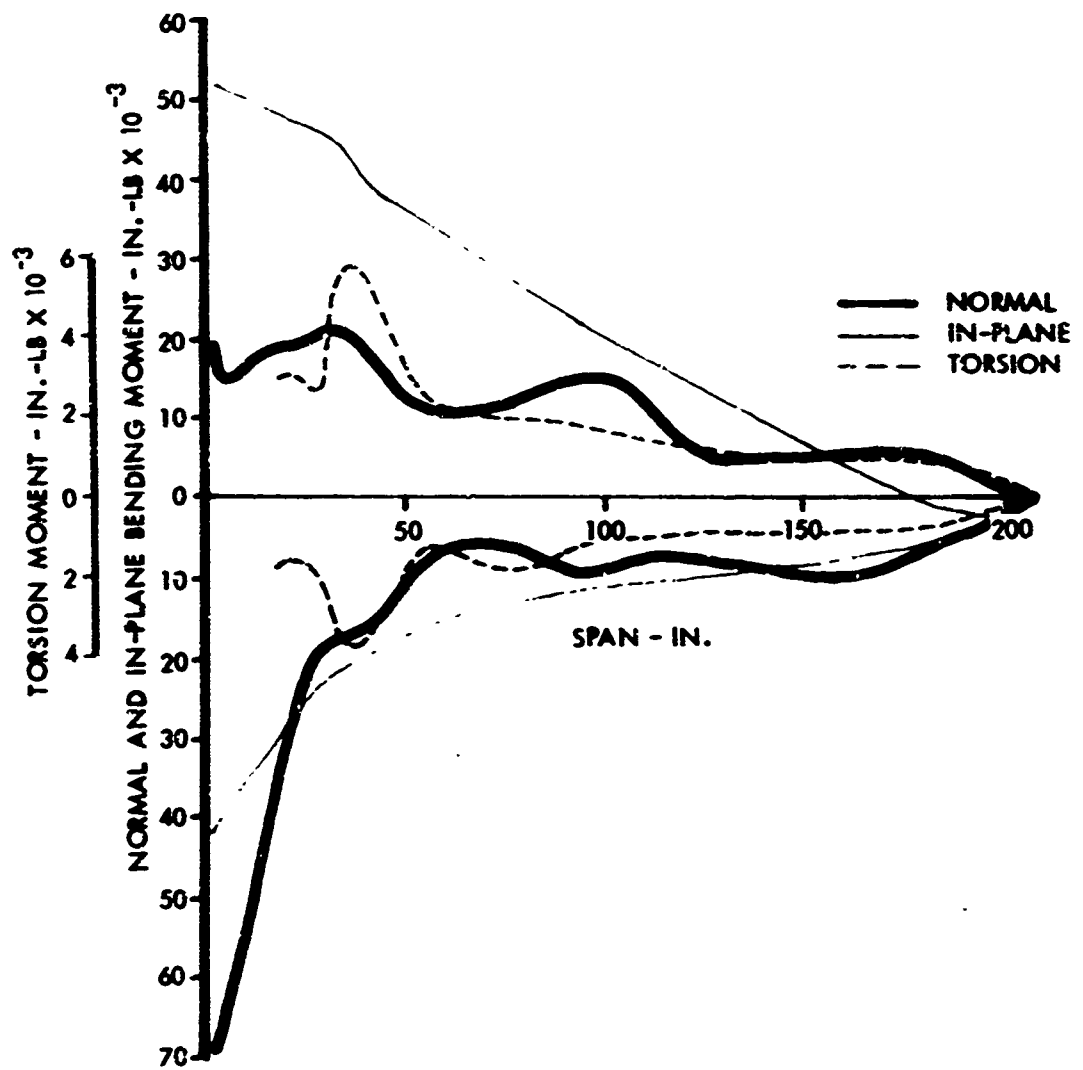


Figure 25. Spanwise Moment Envelope, Condition 5.

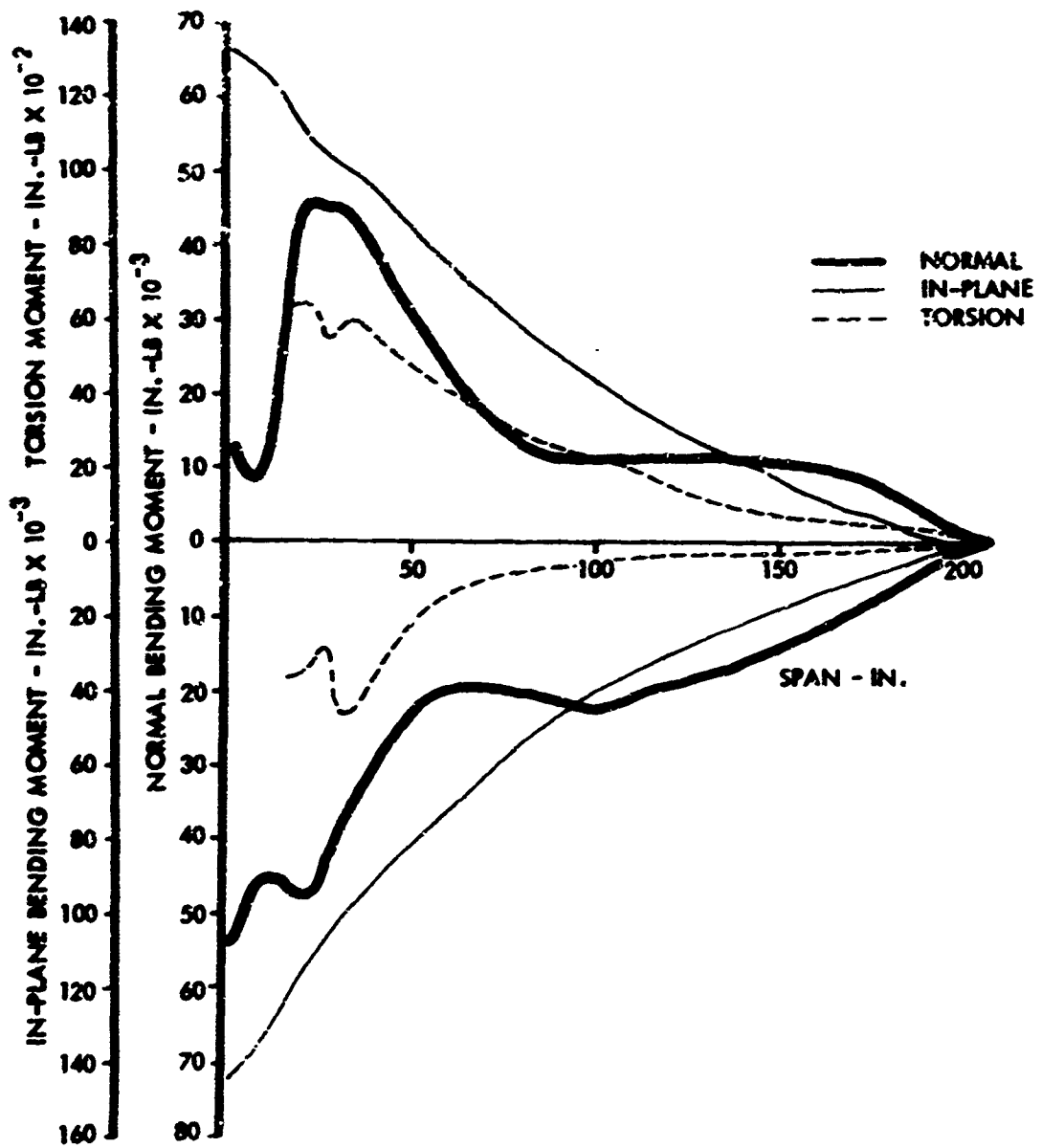


Figure 26. Spanwise Moment Envelope, Condition 6.

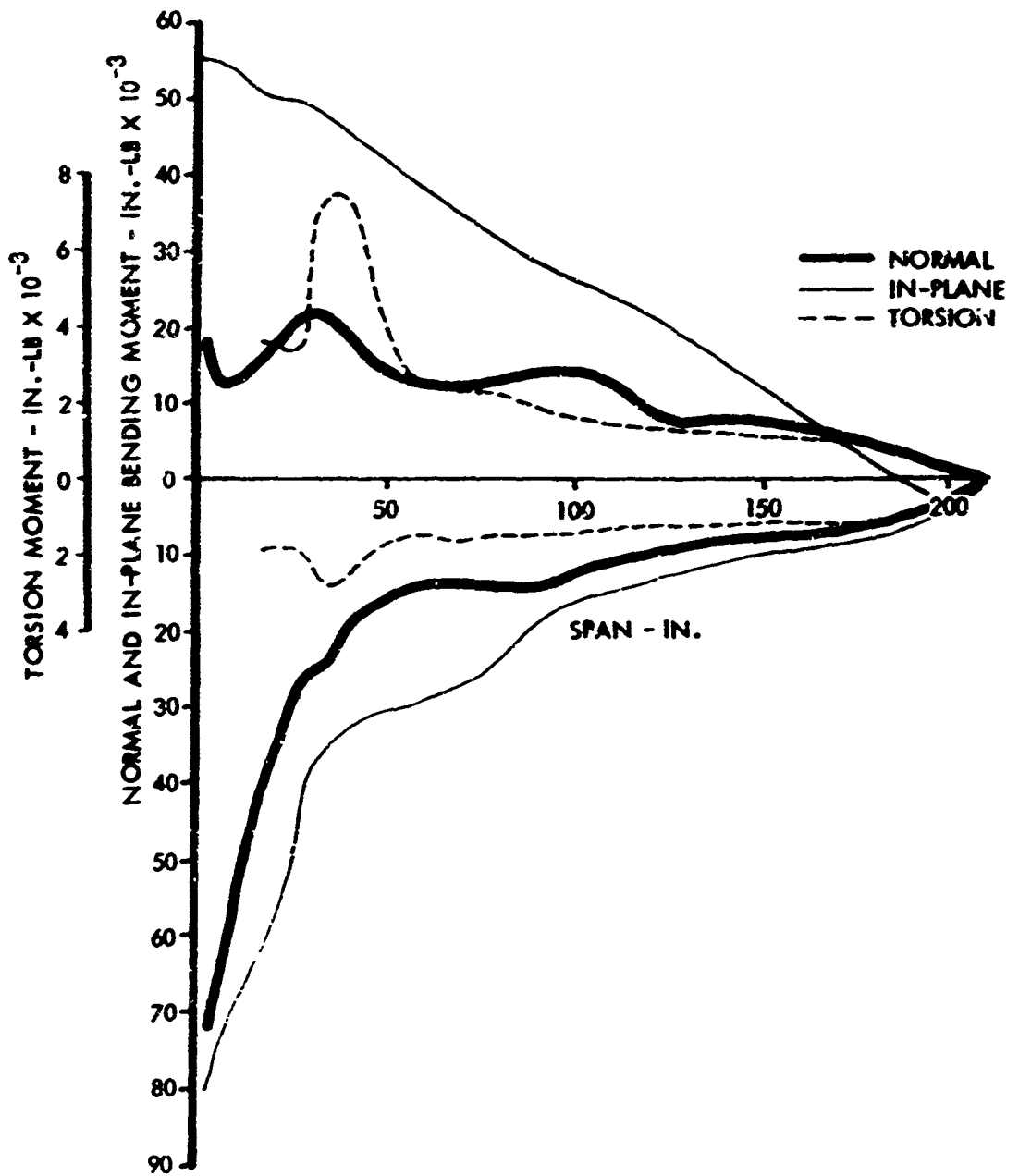


Figure 27. Spanwise Moment Envelope, Condition 7.

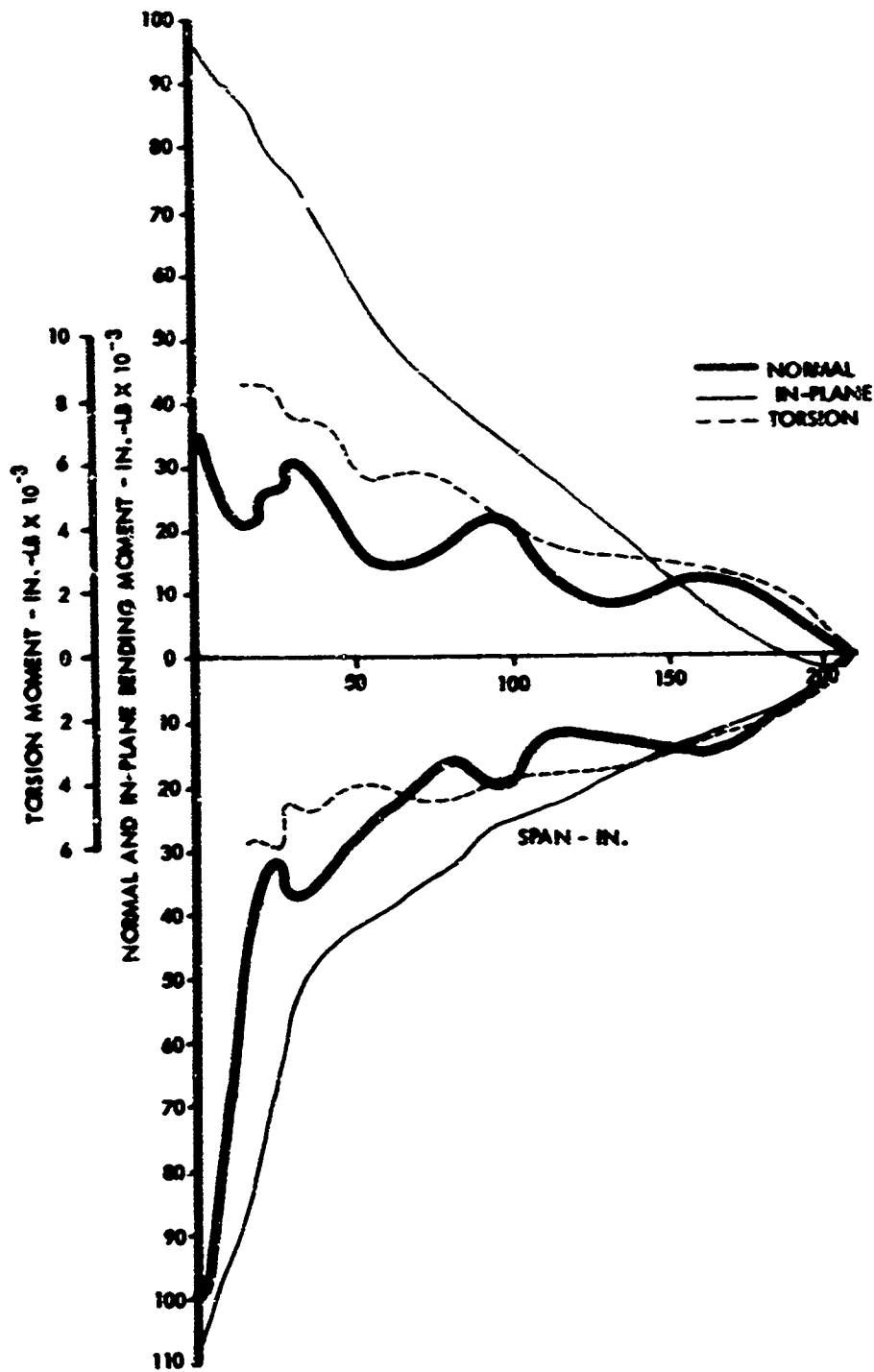


Figure 28. Spanwise Moment Envelope, Condition 8.

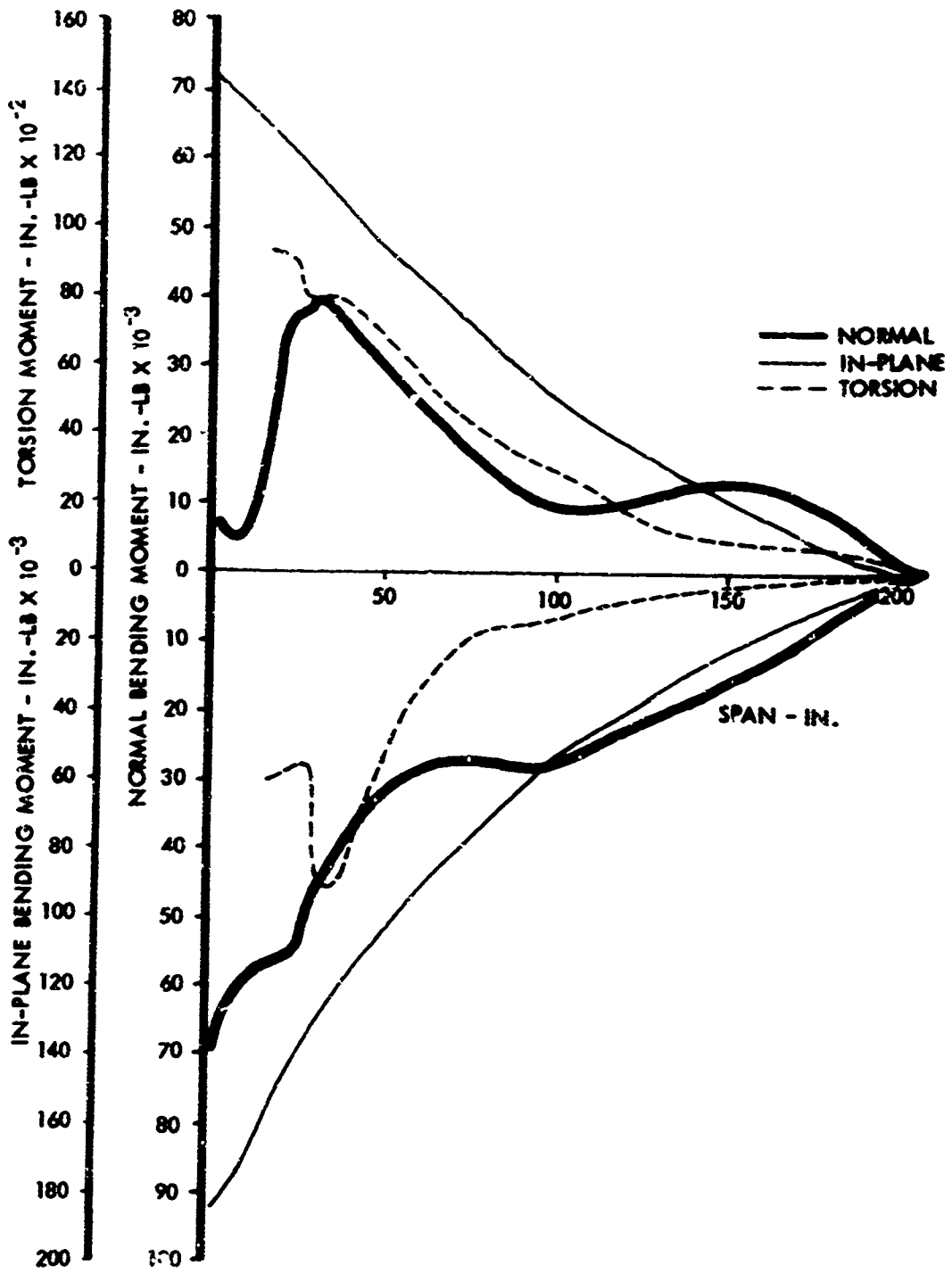


Figure 29. Spanwise Moment Envelope, Condition 2.

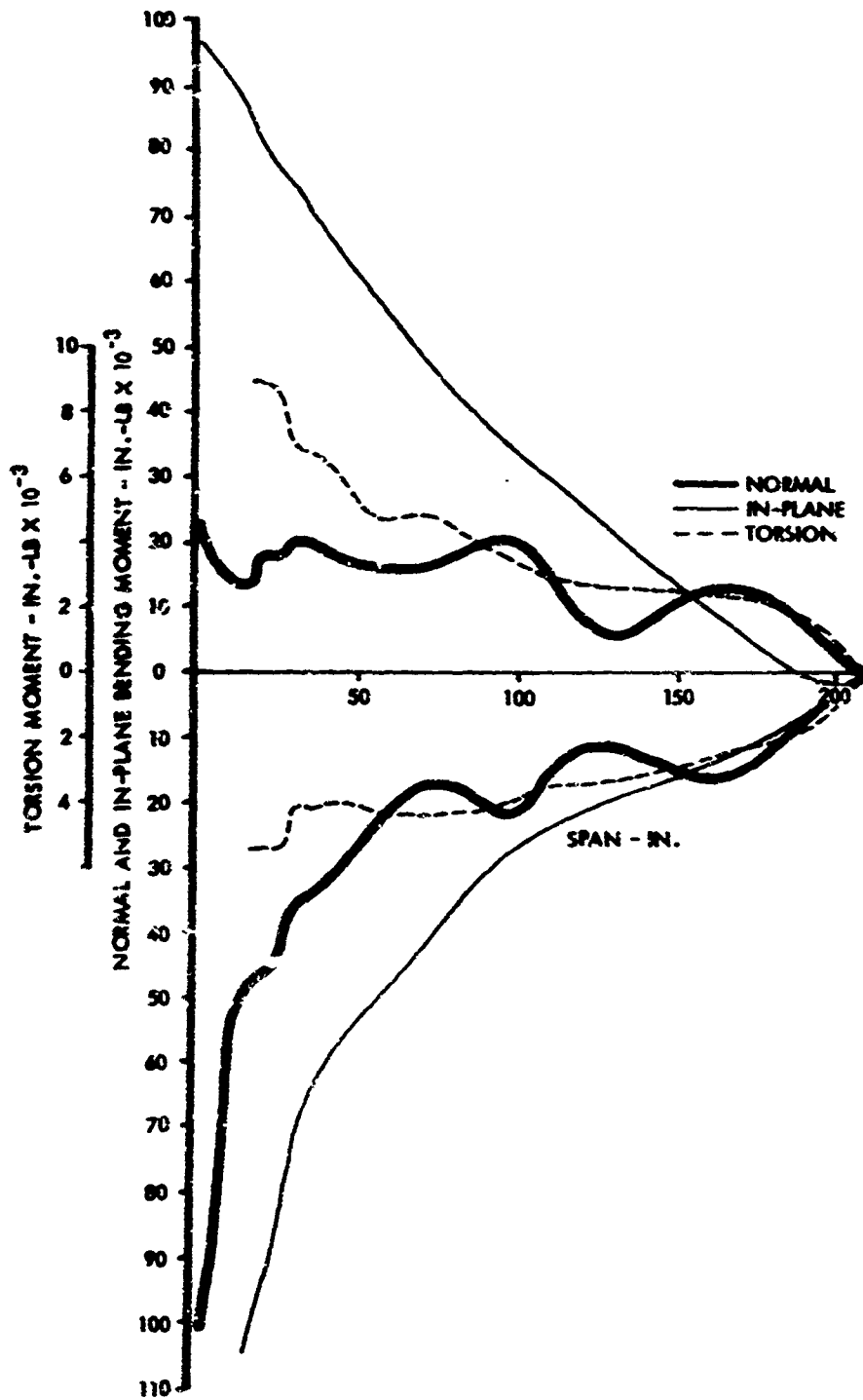


Figure 30. Spanwise Moment Envelope, Condition 10.

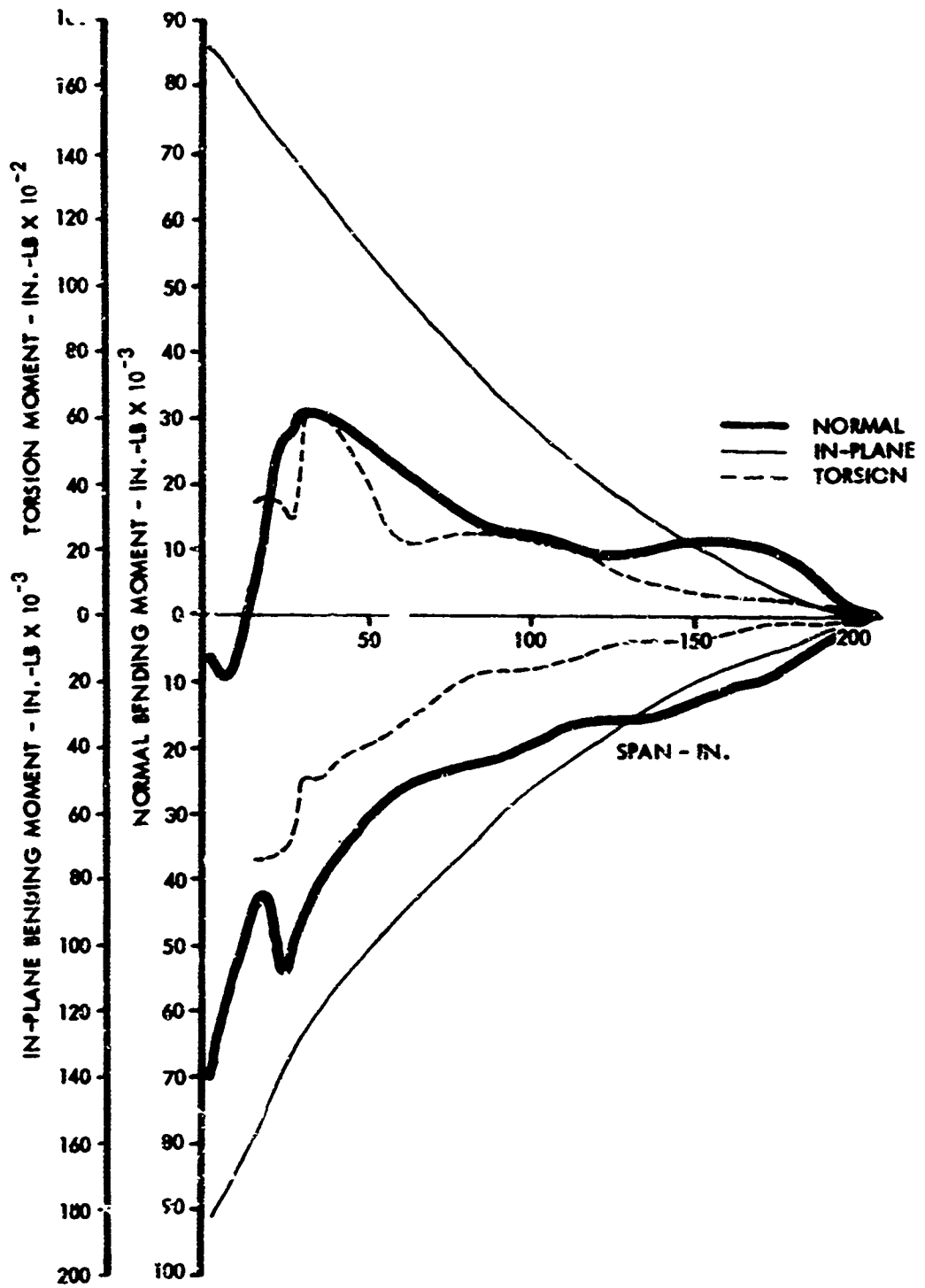


Figure 33. Spanwise Moment Envelope, Condition 11.

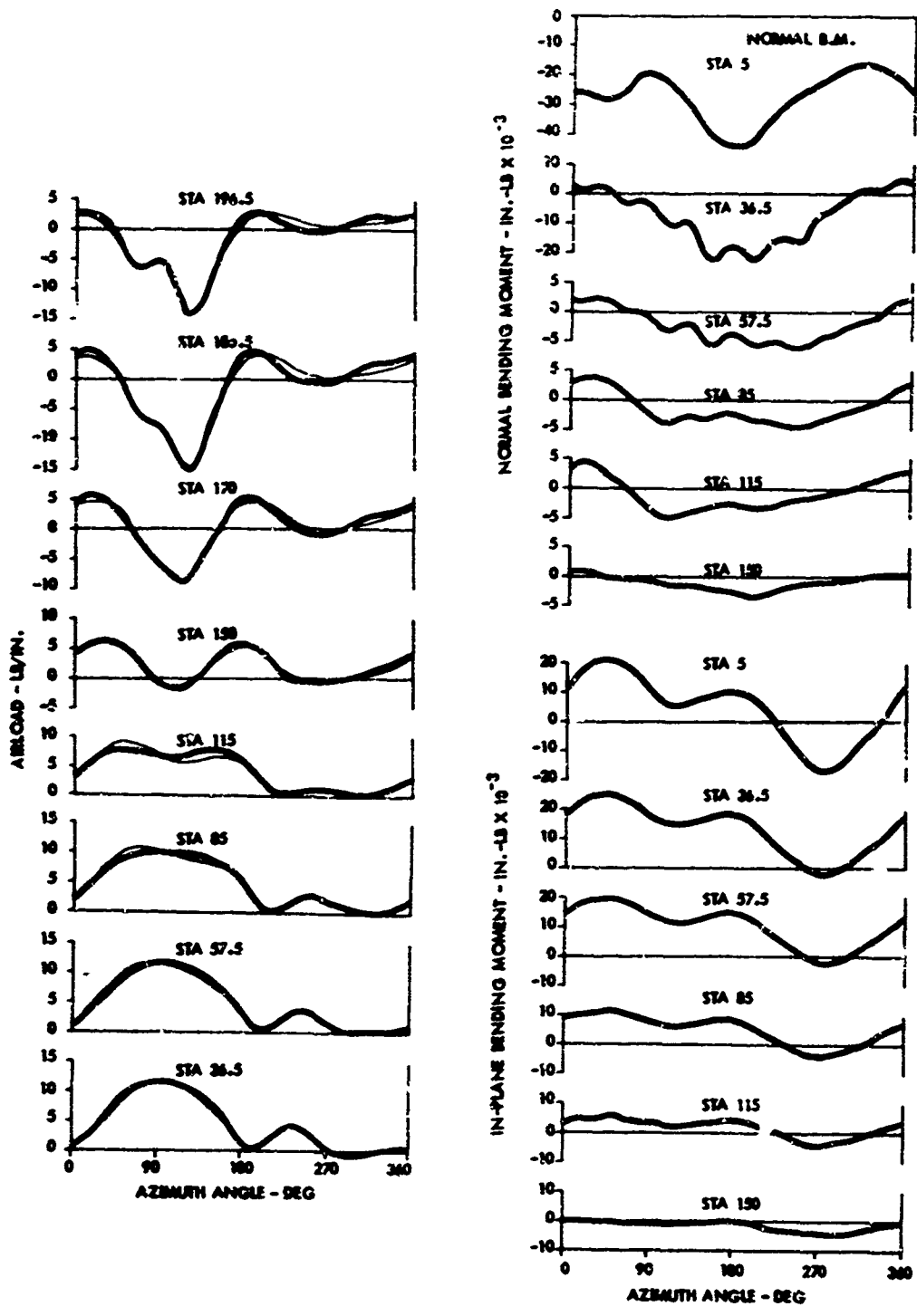


Figure 32. Main Rotor Blade Airloads and Response, Condition 22.

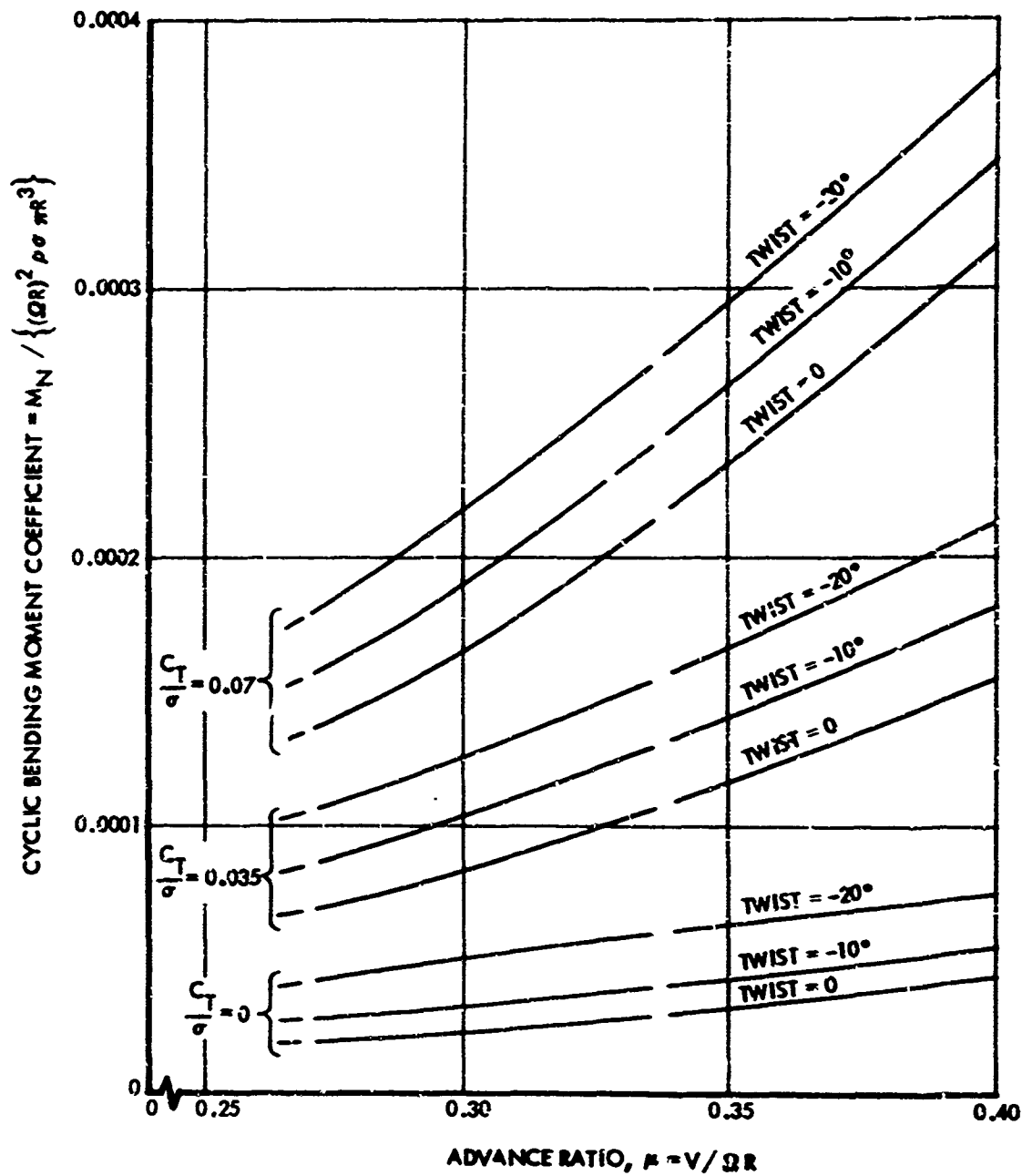


Figure 33. Effect of Twist on Cyclic Normal Bending Moments at Blade Root.

TABLE III. EFFECT OF TWIST ON LOADS		
Condition	Maximum Rotor Thrust (lb)	
	No Twist	-5 Deg Twist
3	5770	6137
7	2156	2719
10	749	1269

Normal and chordwise bending moments are compared in Figures 34 through 36. The effect of change in coning angle and droop angle is shown in Figure 37. At maximum rotor thrust essentially the same bending moments are obtained.

FATIGUE ANALYSIS

The spectrum of loading conditions used in determining the main rotor fatigue loading for analyses is shown in Table IV. The spectrum of stresses obtained from the fatigue loading spectrum is shown in Figure 38 for the hub of Rotor Station 5.0. Cumulative fatigue damage calculations for an XH-51A-type rotor hub subjected to this stress spectrum indicate negligible damage. To provide a base for further evaluating the cyclic stress environment, reference is made to the stress spectrum of the hub of the Lockheed Model 286 helicopter. This aircraft is a commercial version of the XH-51A helicopter. The stress spectrum to which the Model 286 hub was subjected in its certification fatigue test is compared with the XH-51A-type hub stress spectrum in Figure 38. This comparison shows that the cyclic stress environment for the Model 286 hub is much more severe than that anticipated for the hub in this design model.

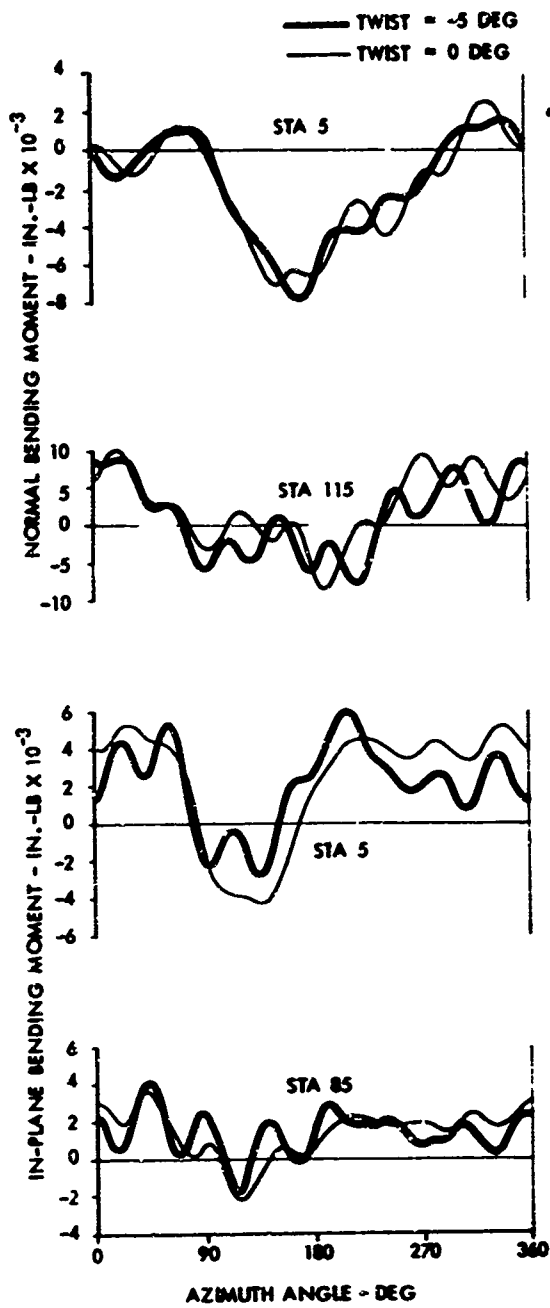


Figure 34. Effect of Blade Twist, Condition 3.

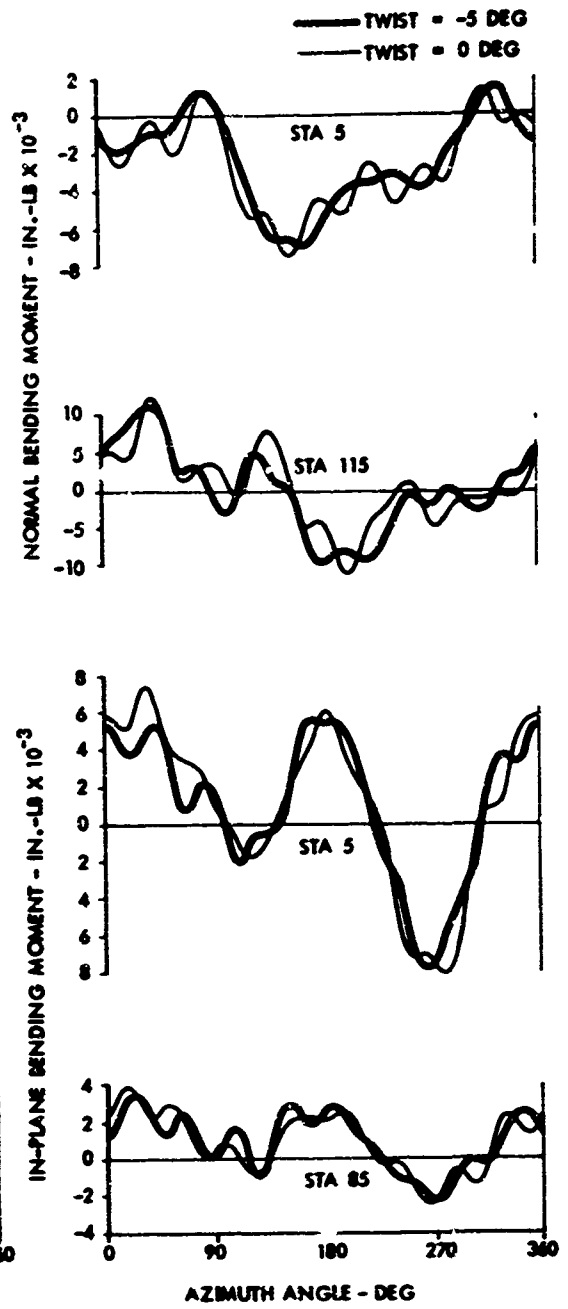


Figure 35. Effect of Blade Twist, Condition 7.

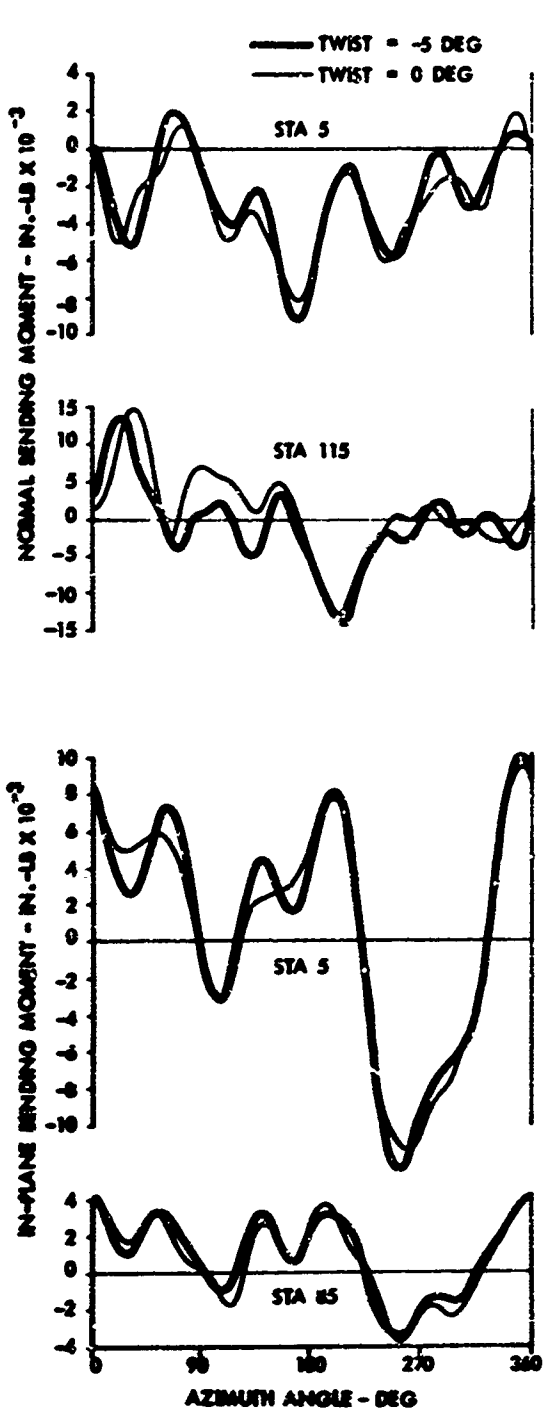


Figure 36. Effect of Blade Twist, Condition 10.

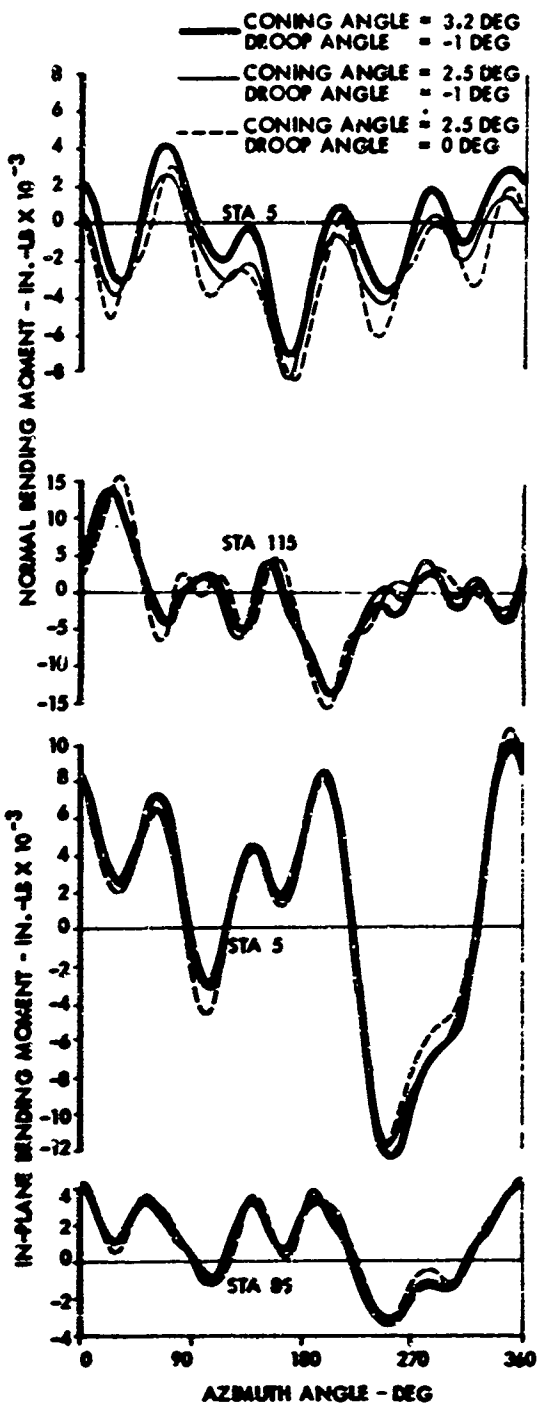


Figure 37. Effect of Blade Coning Angle and Droop, Condition 10.

TABLE IV. SPECTRUM OF FATIGUE LOADING CONDITIONS

Aircraft Operation	Number of Events	Time per Event (sec)	Total Time (min)	Condition (See Table II)
Ground Checkout				
On-Off	100	-	-	0-13-0
Steady Run	-	-	300	13
Tie-Down Testing				
On-Off	100	-	-	0-13-0
On-Off	50	-	-	0-12-0
Steady Run	-	-	1200	13
Steady Run	-	-	300	12
Cyclic Control Input	20	6	2	12
Flight Test				
On-Off Ground Runs	300	-	-	0-12-0
On-Off Ground Runs	300	-	-	0-13-0
Takeoff	300	3	15	12
Landing	300	3	15	12
Hover	600	15	150	12
Transition	300	15	75	14
Climb (Incl Maneuvers)	900	15	225	15
Steady Run, 64 Knots	-	-	618	14
Maneuvers, 64 Knots	400	6	40	15
Steady Run, 120 Knots	-	-	480	16
Maneuvers, 120 Knots	400	6	40	17
Steady Run, 180 Knots	-	-	360	18
Maneuvers, 180 Knots	400	6	40	19
Steady Run, 240 Knots	-	-	600	20
Maneuvers, 260 Knots	400	6	40	23
Maneuvers, 260 Knots	200	6	20	22
Steady Run, 300 Knots	-	-	120	24
Steady Run, 320 Knots	-	-	10	25

PERFORMANCE

A summary of performance data is presented and its impact on aircraft design requirements discussed. The impact of rotor tip speed, airfoil section thickness and camber distribution, and blade twist on rotor performance is evaluated. Data generated in performing a study to determine the effects of various design parameters on the hover and high-speed performance characteristics of the XH-51A compound helicopter are found in Appendix III.

DESIGN POINT PERFORMANCE AT HIGH SPEED

The XH-51A compound helicopter requires little power to overcome rotor drag and torque. Therefore, main rotor power requirements are not the limitation on vehicle performance at high speed. Rotor performance with appropriate blade geometry for each of two levels of rpm reduction (50% and 75% rpm) is presented in Table V. The required energy for overcoming blade drag and torque, at each rpm level, is resolved to an equivalent drag at the flight speed so that the total energy requirements may be compared on a common basis. At 300 knots, the difference in energy required for the rotors operating at these two levels of rpm is not sufficient to select one over the other without considering other aspects of the design requirements.

Since the power requirement for the rotor at low rpm and high speed is not the first limit on performance, the principal aspect of blade airfoil geometry selection now becomes that of alleviating compressible flow conditions which induce high oscillatory loads, a high vibration level and a feedback feathering moment to the gyro. However, this geometry selection must be optimized with the requirements for hover performance.

PERFORMANCE COMPARISONS

Data from the nondimensional hover characteristics of C_T/σ vs. C_P/σ of Figures 43 and 44 in Appendix III are extracted and tabulated in dimensional form in Table VI. These data provide a comparison to indicate trends and are simply made on the basis of an isolated rotor. This comparison, therefore, excludes the effects of engine and transmission losses, antitorque power, and aerodynamic download on the airframe. The basic blade geometry of the existing XH-51A compound is used for a reference base. This blade has a constant NACA 0012 airfoil section and includes a twist of -5 degrees. The comparison is made on the basis of 626 horsepower to the isolated rotor at standard sea level and at 5000 feet and 90°F. The blade geometric properties and corresponding hover lifts are noted in Table VI.

TABLE V. DESIGN POINT PERFORMANCE COMPARISON

Velocity: 300 Knots Altitude: Sea Level Temperature: Standard (50°F)		
% Normal Rotor RPM	50%	75%
Gyro-rotor speed ratio, N_C/N_R	40	1
J , slug-ft ²	0.9	17.25
Rotor blade geometry:		
θ_1 , deg	-5	-5
t/c	0.12	0.12
$c_{\theta 1}$	0	0
Drag of aircraft minus blades, lb	3051	3051
Rotor blade drag, lb	140	204
Aircraft drag, lb	3191	3255
Rotor shaft power, hp	31	130
Equivalent drag of shaft power, lb	34	141
Total equivalent blade drag, lb	174	345
Total equivalent drag, lb	3225	3396
(Blade drag/aircraft drag), %	4.39	6.97
(Total equivalent blade drag/ total equivalent drag), %	5.39	10.02

TABLE VI. COMPARISON OF ROTOR HOVER LIFT

Isolated Rotor, ONE								
Linear variation of t/c and c_{li} between noted radius stations. Actual blade begins at $x_c = .15$								
R = 17.5 ft			$M_{(1)} \leq .582$					
$\sigma = .0819$			$\Omega R = 650 \text{ fps}$					
Input Power, hp							626	
Alt, ft							S.L.	5000
Temp, °F							59	90
Twist, θ_1 , deg		Airfoil Distribution					Hover Lift, lb	
Effect of Twist		x	0	.7	.75	1.		
	0	t/c	.12			.12	6270	5870
		c_{li}	0			0		
	-5 (Ref Blade)	t/c	.12			.12	6450	6040
	c_{li}	0			0			
	-10	t/c	.12			.12	6590	6170
	c_{li}	0			0			
Effect of Airfoil Geometry	-5 (Ref Blade)	t/c	.12			.12	6450	6040
		c_{li}	0			0		
	-5	t/c	.12	.12		.06	6370	5820
		c_{li}	0			0		
	-5	t/c	.12	.12		.06	6420	5950
	c_{li}	0	0	.27	.09			
	-5	t/c	.12			.06	6330	5720
	c_{li}	0			0			
	-5	t/c	.12			.06	6420	5930
	c_{li}	.09			.09			

The first comparison shows the effect of twist at constant airfoil geometry. The reference blade with -5 degrees of twist shows a lift of 170 to 180 pounds more than that without twist and 130 to 140 pounds less than that for -10 degrees of twist when compared at the two altitude and temperature conditions. A study of loads over the required flight spectrum in the Rotor Loads section of this report shows an increase of only 10% in blade loads for -5 degrees twist when compared with the loads on a blade of no twist. As the amount of twist increases more than 5 degrees, blade loads increase too rapidly to warrant application of the additional twist. A comparison of Figures 63, 64, and 65 with Figures 47, 52, and 57 in Appendix III indicates that there is no discernible difference in performance at the high-speed forward-flight condition due to -5 degrees of twist. Therefore, the -5 degrees of twist which provides an increase in hover performance without a significant penalty at other conditions is recommended for use.

The second comparison is made to evaluate the decrease in lift due to the use of thinner blade tip sections in the case of the 75% rotor rpm reduction design. All of these blades, with -5 degrees of twist, are compared with the reference 12% constant section blade having no camber. The blades which have thin tip sections without the addition of camber show the greatest losses in hover lift, and the loss is more severe for the hot-day altitude condition. Of the two blades without camber, the one which is tapered in thickness along the entire radius shows the poorest hover performance. The use of camber in the sections which are reduced in thickness provides a reasonable recovery in performance for both types of tapered thickness blades. Camber is reduced toward the tip to obtain as much benefit as possible without precipitating adverse compressibility effects with high advancing tip Mach number.

The portion of the blade radius to which tapered thickness and compensating camber are used is, in part, dependent on the blade fabrication process. The linear variation from root to tip is more suited to quantity metal blade production techniques. The outboard use of tapered thickness and compensating camber may be suited to the modification of an existing constant section design. Both can be tailored to work nearly as well for the same high-speed and hover design requirements.

Although it is not required for the 300-knot speed objective, a thin tip section may be used to alleviate compressibility effects with increased margins in the case of the 75% rpm design; in that event, compensating camber is recommended for recovering hover performance. For the 50% rpm design, a constant 12% symmetrical airfoil as used on the current XH-51A rotor blades could be used on the basis of aerodynamic considerations. However, dynamic considerations covered in the section on Rotor Dynamics and Aeroelastic Stability show that increased structural flapwise and torsional stiffness is required for operation at this reduced rpm level. For flight speeds which exceed 300 knots, i.e., 325 to 350 knots, the increase in advancing tip Mach number again introduces the consideration

of tapered thickness blades with thin tip sections for the 50% rpm system. Compensating camber diminishing toward the tip is again recommended for blades with this type of thickness distribution.

CONCLUSIONS AND RECOMMENDATIONS

CONCLUSIONS

Proper selection of rotor design parameters for slowed-rotor operation will remove flight limits previously encountered with the XH-51A compound helicopter. Analysis, simulation, and conservative extrapolation of previous test results show that an XH-51A-type rigid-rotor compound helicopter can be flown at speeds up to 300 knots. The primary goal in slowing the rotor is to eliminate vibration due to compressibility effects on the advancing blade at high speed, although a decrease in cruise power required at moderate speeds is also realized.

The results of the study show that:

1. Slowing the rotor to 75% rpm will provide a speed capability of 300 knots without encountering undesirable compressibility effects.
 - The onset of compressibility effects occurs at an advancing tip Mach number of 0.91. Operation at 300 knots at 75% rpm corresponds to an advancing tip Mach number of 0.891.
 - The 75% rpm rotor system includes increases in swashplate damping, gyro inertia, and blade tip weight to maintain rotor stability at reduced rpm with a 1:1 gyro-rotor rpm ratio.
 - Rotor frequencies are placed to avoid proximity to integer values in the design rpm range. Operation at almost any rpm within the design range consistent with an acceptable advancing tip Mach number is feasible.
2. Slowing the rotor to 50% rpm provides larger operating margins before the onset of compressibility effects at 300 knots and a potential for speed increase to between 325 and 350 knots.
 - The 50% rpm rotor system makes frequency placement more difficult due to the large magnitude of operational rpm change. It requires that the rotor rpm pass rapidly through a resonant frequency range at a low or moderate flight speed.
 - The 50% rpm rotor system includes increased blade structural flapwise and torsional stiffness and a high-speed gyro to provide rotor blade stability at 50% rpm and compatible gyro-rotor precession rates with a reasonable gyro size.

3. For both systems:

- A stiff-mounted transmission is required.
- Increased operating margins before the onset of compressibility can be obtained by reducing section thickness near the blade tip. However, when blade thickness taper is used, camber must be added to the blade section to minimize losses in hover performance resulting from the use of thin blade sections.

RECOMMENDATIONS

A research flight test program should be conducted to confirm and supplement the analytical predictions with experimental data.

REFERENCES CITED

1. Foulke, William K., EXPLORATION OF HIGH-SPEED FLIGHT WITH THE XH-51A RIGID ROTOR HELICOPTER, Lockheed-California Company; USAAML Technical Report 65-25, U.S. Army Aviation Materiel Laboratories, Fort Eustis, Virginia, June 1965, AD 617966.
2. Wyrick, Donald R., EXTENSION OF THE HIGH-SPEED FLIGHT ENVELOPE OF THE XH-51A COMPOUND HELICOPTER, Lockheed-California Company; USAAVLABS Technical Report 65-71, U.S. Army Aviation Materiel Laboratories, Fort Eustis, Virginia, November 1965, AD 627372.
3. Lentine, F.P., Groth, W.P., and Oglesby, T.H., RESEARCH IN MANEUVERABILITY OF THE XH-51A COMPOUND HELICOPTER, Lockheed-California Company; USAAVLABS Technical Report 68-23, U.S. Army Aviation Materiel Laboratories, Fort Eustis, Virginia, June 1968.
4. Gockel, M.A., AN EXPERIMENTAL AND ANALYTICAL INVESTIGATION OF THE EFFECTS OF TIME VARYING CERTAIN CHORD MODE FREQUENCY RATIOS, Lockheed-California Company, LR 22365, 1 April 1969.
5. Composite Aircraft Program, EXPLORATORY DEFINITION AND PROPOSAL FOR FULL-SCALE FOLLOW-ON PROGRAM, Draft Final Lockheed-California Company Report to U.S. Army Aviation Materiel Laboratories under Contract DAAJ02-67-C-0045, 31 July 1967, Burbank, California.
6. Sissingh, Dr. G.J., DYNAMICS OF ROTORS OPERATING AT HIGH ADVANCE RATIOS, Lockheed-California Company Paper Presented at Specialists' Meeting of the Fluid Dynamics Panel of AGARD, Gottingen, Germany, September 1967.
7. Prouty, R.W., CONTROL SYSTEMS FOR UNARTICULATED ROTORS, Lockheed-California Company Paper Presented at the Society of Automotive Engineers A-18 Committee Meeting, Denver, Colorado, August 1966.
8. Sweers, J.E., IN-FLIGHT MEASUREMENT AND CORRELATION WITH THEORY OF BLADE AIRLOADS AND RESPONSES ON THE LOCKHEED XH-51A COMPOUND RIGID ROTOR HELICOPTER, VOLUME III, THEORETICAL PREDUCTION OF AIRLOADS AND STRUCTURAL LOADS AND CORRELATION WITH FLIGHT TEST MEASUREMENTS, Lockheed-California Company; USAAVLABS Technical Report 68-22C, U.S. Army Aviation Materiel Laboratories, Fort Eustis, Virginia, May 1968, AD 674195.
9. Carpenter, Paul J., LIFT AND PROFILE DRAG CHARACTERISTICS OF AN NACA 0012 AIRFOIL SECTION AS DERIVED FROM MEASURED HELICOPTER ROTOR HOVERING PERFORMANCE; NACA Technical Note 4357, National Advisory Committee for Aeronautics, September 1958.

REFERENCES CITED (Continued)

10. Sipe, O.E., Jr., and Gorenberg, N.B., EFFECT OF MACH NUMBER, REYNOLDS NUMBER, AND THICKNESS RATIO ON THE AERODYNAMIC CHARACTERISTICS OF NACA 63A - SERIES AIRFOIL SECTIONS, Lockheed-California Company; USAAML Technical Report 65-28, U.S. Army Aviation Materiel Laboratories, Fort Eustis, Virginia, June 1965, AD 619153.
11. Gessow, Alfred, and Crim. Almer D., A METHOD FOR STUDYING TRANSIENT BLADE-FLAPPING BEHAVIOR FOR LIFTING ROTORS AT EXTREME OPERATING CONDITIONS; NACA Technical Note 3366, National Advisory Committee for Aeronautics, January 1955.
12. Gessow, Alfred, EQUATIONS AND PROCEDURES FOR NUMERICALLY CALCULATING THE AERODYNAMIC CHARACTERISTICS OF LIFTING ROTORS; NACA Technical Note 3747, National Advisory Committee for Aeronautics, October 1956.

APPENDIX I

METHODS OF ANALYSIS

Test-based analytical methods are used to identify parameters critical to 300-knot flight speeds and to indicate values of those parameters which must be applied in achieving these speeds. The analyses selected for evaluation of the various aspects of this high-speed regime have been developed and correlated with prior high-speed flight experience and test results. This section contains a brief description of these methods as they relate to this study.

ROTOR PERFORMANCE

Both the hover performance and the forward-flight performance analyses employed in producing the rotor performance charts in Appendix III are of the numerical iterative type. They utilize two-dimensional data for airfoils with NACA four-digit basic thickness form. The mean lines of these airfoils are of the far-forward camber-type, five-digit series with maximum camber at the 15% chord station. The thinner sections of this family, when combined with a mean line which would produce a concave lower surface, are modified in the nose region to eliminate any concavity. Nose thickness is appropriately increased above and below the mean line to avoid an adverse pressure gradient at negative angles of attack.

The aerodynamic data representing these airfoil sections in both the hover and the forward-flight analyses are used in a tabular look-up format of c_L and c_D on the basis of blade element thickness ratio, camber design lift coefficient, angle of attack and Mach number. These data have been synthesized in the manner of the rotor blade section data of Reference 9. Variations for thickness ratios and camber have been generated using transonic similarity rules as indicated in Reference 10 and have been cross checked with numerous data sources found in the bibliography of Reference 10. These have been further verified through high-speed wind-tunnel tests.

The hover analysis employs a blade element momentum balance at each of a series of discrete blade radius stations and accounts for finite blade number on the basis of thrust produced. Integrated results of this analysis have shown good correlation with results of whirl tower tests. The forward-flight performance analysis consists of a modified and an expanded version of that reported in References 11 and 12. The method includes an iteration cycle on blade motion and tip path plane trim to the shaft normal plane. Accordingly, the data provided in Figures 44 through 65 of Appendix III represent trimmed flight rotor conditions in which the hub moments have been trimmed to zero by the application of appropriate cyclic pitch control. For these conditions, the tip path plane is parallel to the shaft normal plane.

Vehicle performance can be evaluated by the method indicated in the sample calculation in Appendix III.

AIRCRAFT CONTROL REQUIREMENTS

To evaluate control cross coupling and control at high speed, a digital computer simulation is used.

Nine degrees of freedom are incorporated in the digital simulation, as follows:

Rotor: 1 flapping degree of freedom x 4 blades -
4 degrees of freedom

Gyro: 2 degrees of freedom

Nonrotating airframe: 3 rigid-body degrees of freedom: pitch,
roll, and plunge (vertical velocity in
body coordinates)

The simulation is performed in two parts. First an isolated rotor solution is obtained using the 4-degree-of-freedom main rotor portion of the program. Forces and moments applied to the vehicle by the rotor are calculated as functions of shaft rolling, pitching, and plunging, and as functions of the cyclic pitch inputs. These responses are reduced to their "quasi-static"* components, thereby producing a set of rotor stability derivatives. These stability derivatives provide equations of the form

$$M_H = \frac{\partial M_H}{\partial A_{1s}} A_{1s} + \frac{\partial M_H}{\partial B_{1s}} B_{1s} + \dots$$

The second part of the simulation substitutes the rotor-stability derivatives

$$\frac{\partial M_H}{\partial A_{1s}}, \frac{\partial M_H}{\partial B_{1s}} \dots$$

*Quasi-static means that the transfer functions of the rotor (e.g., pitch hub moment/pitching rate) were reduced to constants. This is regarded as a good assumption, since the dynamic response of a rotor is quite fast compared with overall vehicle time constants and frequencies.

along with the appropriate nonrotating airframe derivatives, into a set of linear, constant coefficient differential equations. The gyro nutation mode is assumed to be adequately damped (this is equivalent to assuming that the gyro functions as a pure integrator with gain $J\Omega$), which reduces the number of vehicle dynamic equations to three.

These three differential equations are solved digitally, producing time-history vehicle responses to steps of lateral and longitudinal stick displacements.

ROTOR DYNAMIC STABILITY

The dynamic behavior of the XH-51A rigid-rotor system can be described as that of a gyroscope which is flexibly connected to the transmission and fuselage and which is slaved to a control gyroscope. The control gyro receives feedback information from the rotor and fuselage as well as command inputs from the pilot.

While the rotor is simply characterized above as a gyroscope, this analytical model of the compound rigid-rotor system has been described in a fully coupled collective-cyclic aerodynamic-mechanical formulation. This model includes the effects of Mach number and reverse flow in the flapping, the in-plane and the feathering relationships. The analytical model is described in terms of the basic degrees of freedom utilized in both the closed form and transient solutions obtained.

Table VII summarizes the specific degrees of freedom incorporated in the analytical model.

The space configuration of the elastic rotor system is approximated by the superposition of a finite number of fundamental mode shapes. Thus, the generalized coordinates numbered 3 through 8 represent multipliers that determine the amount that the normalized mode shapes contribute to any general deformation of the rotor.

The mechanical description of the rotor, the gyro, and the fuselage (anisotropic, describing the pitch, roll, and plunge of the fuselage as a rigid body) is formulated in the stationary coordinate system.

The rotor aerodynamic analysis is performed with a separate, rather elaborate program. Briefly, each blade is subdivided into 20 elements. The cyclic pitch necessary to trim the rotor system is calculated by an iteration procedure. The program yields virtually all rotor system characteristics, including resolved thrust, drag and pitching loads, on each blade element at each of 24 equal azimuth intervals. A harmonic analysis is performed on this loading, and the steady as well as the first six harmonics of blade loading are obtained. However, only the first two harmonics of the airload are introduced into the dynamic analysis discussed here; that is, the solution which is sought is concerned only with the dynamic aeroelastic stability of the system as it is represented by the

model discussed above. Mach number, stall, and reverse flow effects are taken into account by the use of two-dimensional airfoil data for the full spectrum of angles of attack encountered by the rotor blade elements.

TABLE VII. DESCRIPTION OF DEGREES OF FREEDOM

Degree of Freedom	Symbolic Designation	Description
1	V_x	Longitudinal velocity of rotor hub
2	V_y	Lateral velocity of rotor hub
3	$\bar{\beta}$	Collective component of rotor flapwise deflection
4	θ_R }	Cyclic components of rotor flapwise deflection
5	ϕ_R }	
6	$\bar{\epsilon}$	Collective component of rotor in-plane deflection
7	ϵ_x }	Cyclic components of rotor in-plane deflection
8	ϵ_y }	
9	\bar{z}_t	Vertical deflection of transmission
10	θ_t	Pitch angle of transmission
11	ϕ_t	Roll angle of transmission
12	θ_f	Pitch angle of fuselage
13	ϕ_f	Roll angle of fuselage
14	θ_G }	Cyclic components of gyro displacement
15	ϕ_G }	
16	V_{z_c}	Vertical velocity of aircraft center of gravity

The behavior of the system is defined by a set of 16 simultaneous total differential equations in the independent variable time. Two basic techniques have been applied to the solution of these equations. The first involves computation of the complex eigenvalues, which determine the characteristic frequencies and damping factors and which provide the necessary information to plot critical stability-rotor speed diagrams for specified flight speeds. The second technique employs a time-history solution to determine the dynamic response of the rotor-fuselage system to a time-dependent control input. The solution is initiated by imposing the swash-plate attitude that would be required for trim of the rotor system if it were perfectly rigid. Thereafter, the control gyro is allowed full cyclic authority. Time histories of all 16 degrees of freedom, as well as collective input and load factor, are obtained directly from a tape plotting system. These plots present the dynamic response with respect to the stationary coordinate system.

ROTOR LOADS AND NATURAL FREQUENCIES

A digital computer program which consists of a combination of airloads and response analysis is used for evaluating blade bending and torsion moments as well as natural frequencies of rotors with rigidly mounted blades. The airloads are computed in the same manner as in the performance analysis, employing the two-dimensional airfoil section data to compute total rotor thrust, pitch and roll moments, and rotor torque. The control angles required for a given trimmed condition are computed. The response analysis is used to compute blade deflections and inertia forces on the blade elements. Bending moments about two axes and torsion are found from the deflected blade geometry and the combination of airloads and inertia forces. The basic program has been extended to include the computation of blade stresses at selected points of various cross sections at each selected azimuth position. Blade natural frequencies are computed by setting airloads to zero and computing blade response characteristics.

APPENDIX II

SLOWED-ROTOR TEST EXPERIENCE

Various aeroelastic wind tunnel tests, both full scale and model scale, have been conducted in connection with fully stopped and stowed rotor programs. These tests also provide useful knowledge regarding the aeroelastic phenomena associated with slowed-rotor concepts, especially in regard to flight at high advance ratios. A full-scale stopped-rotor system, designated the CL-870, was sized for eventual flight test on a modified compound XH-51A. This relatively stiff, three-bladed rigid rotor incorporated an independently hydraulically driven high-speed gyro which maintained its rotational speed, and consequently its ability to provide control, as the main rotor speed diminished. Figure 39 shows the high-speed gyro installation on the model that was tested in the NASA-Ames 40- x 80-foot tunnel.

The rotor was both stable and easily controllable down to 15% rotor rpm at 140 knots and to lower percentages of rotor speed at lower forward speeds. In addition, substantial data relative to the structural loads and aeroelastic characteristics manifested by the CL-870 under a variety of conversion configurations, at various angles of attack and tunnel speeds up to 140 knots, were also obtained. The results of these tests are presented in Figure 40.

Prior to tests of the full-scale system, tests to study rotor in-flight stopping and starting were conducted on a dynamically scaled 7.42-foot-diameter rotor mounted over a representation of a wing/body as shown in Figure 41. This test was performed in an 8- x 12-foot low-speed wind tunnel. In lieu of a mechanical high-speed gyro, the rotor system was controlled by an electronic simulation of the high-speed gyro. The gyro rpm was eleven times the normal rotor rpm. For the gyro and rotor combination tested, the constant-speed gyro was in command of the rotor at rotor speeds down to less than 10% of the normal rotor rpm. The high-speed gyro functioned, in the manner that had been analytically predicted, as an effective control gyro. Figure 42 presents the stability boundary experimentally obtained in these tests.

These two wind tunnel test programs conducted during 1967 demonstrated that a constant high-speed gyro will satisfactorily control the rotor during a slowed-rotor operation. It was experimentally shown that the principal attributes of the high-speed gyro are that (1) it maintains a feathering frequency near 1P during very large excursions in rotor speed, (2) it provides a very high cyclic stiffness which accommodates operation at very low rotor speeds and high advance ratios, and (3) it results in a very high nutation frequency which is easily damped.



Figure 39. CI-870 Model, Modified to Incorporate a High-Speed Gyro, Installed in NASA-Ames 40- x 80-Foot Wind Tunnel.

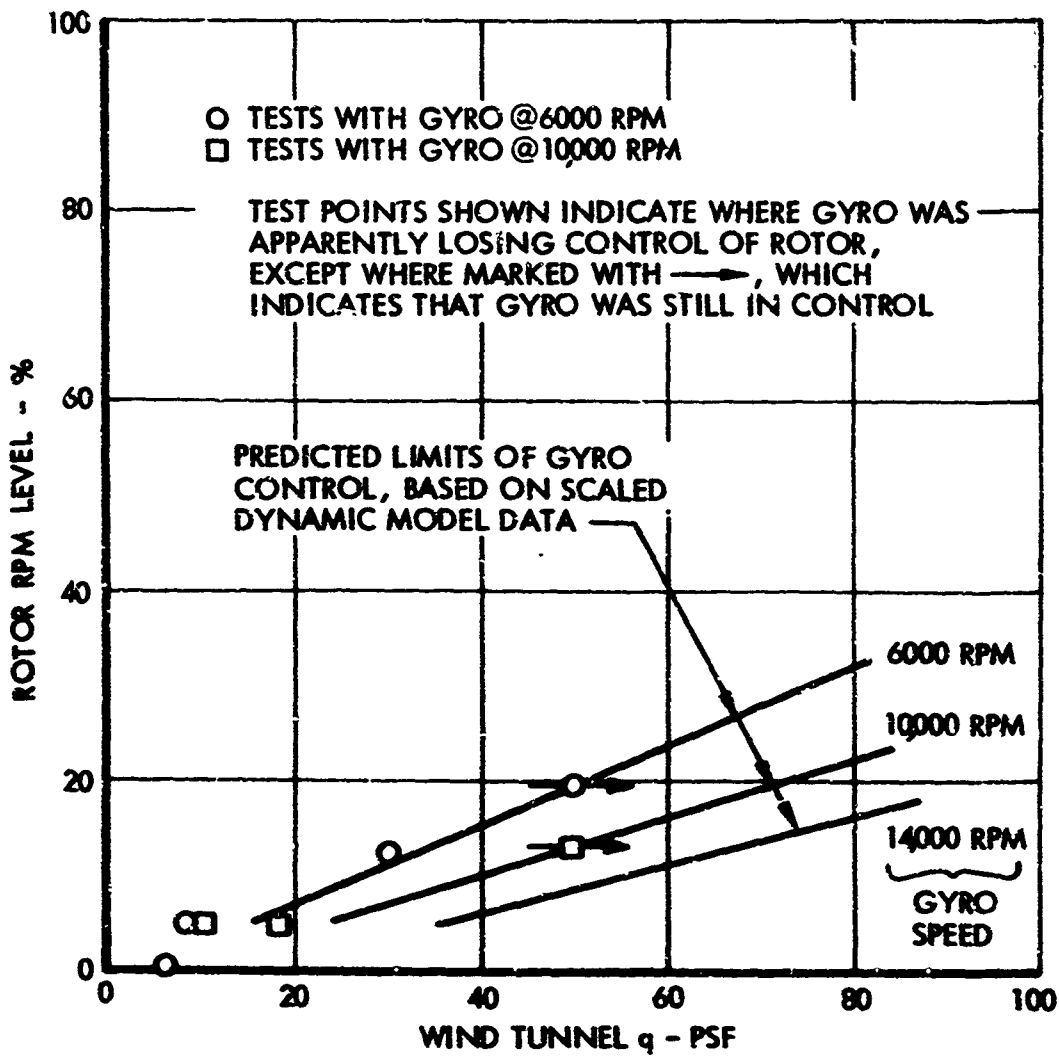


Figure 40. Results of Full-Scale Model Tests.



Figure 41. Dynamic Model in 8- x 12-Foot Low-Speed Wind Tunnel.

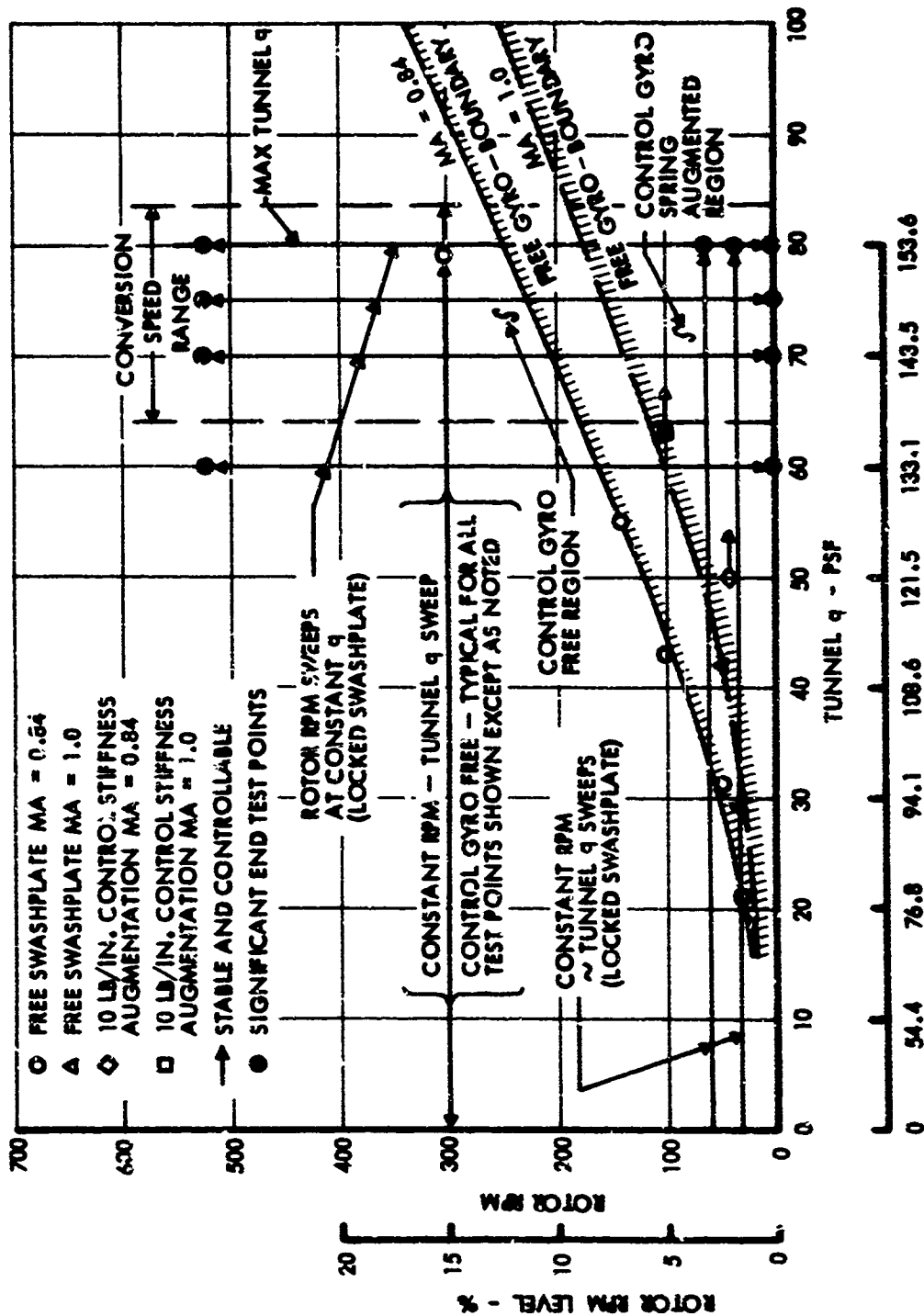


Figure 42. Summary of Dynamic Model Test Results, TUNNEL V - KN

APPENDIX III

ROTOR PERFORMANCE CHARTS AND SAMPLE CALCULATION

ROTOR PERFORMANCE CHARTS

Rotor performance data for high-speed flight at reduced rpm are identified in Table VIII for a range of airfoil distributions and include selected combinations of airfoil geometry and blade twist. These data are in general supplemented by corresponding information at the hovering condition (Figures 43 and 44). The blade airfoil thickness ratio and camber (design lift coefficient) distributions vary linearly between the points of the rotor radius stations at which each of these geometric properties is defined in all tables and figures. A rotorcraft flight condition spectrum is shown in Figure 45 for ease in identifying the operating realm of each of the high-speed flight design charts, Figures 46 through 65. The methods by which the rotor performance chart data were calculated are briefly described in Appendix I, Methods of Analysis.

The rotor flight path force components of lift and drag are nondimensionalized by the product of blade area and flight path dynamic pressure to give $C_{LR} = L_R/qS_b$ and $C_{DR} = D_R/qS_b$. The shaft power is modified to an equivalent drag along the flight path and is nondimensionalized in the same manner to give $C_{DQR} = 550 \text{ HP}_R/qS_b V$. Therefore, rotor total equivalent drag coefficient may be defined as $C_{DER} = C_{DR} + C_{DQR}$. These forms of nondimensional parameters are more suitable for comparing data at different rpm at the same flight path speed. The performance data charts also include the longitudinal cyclic pitch settings, B_1 , required for the noted flight conditions.

For the high-speed flight conditions, these performance charts may be used for other rotor solidities with little error in angle of attack or drag. These changes are only a function of the net induced effects, and at these high speeds the combination of low lift loading and high dynamic pressure with the relatively large span (the diameter) makes the induced effects negligible. Also, shaft power is essentially independent of these effects.

The high-speed performance data charts are developed to provide adequate information consistent with the unloaded rotor mode of operation applied in high-speed flight. The basic data regime in each case is that for a zero three-quarter-radius collective pitch setting at an angle of attack range between zero rotor lift and zero rotor shaft horsepower (autorotation). As the advancing tip Mach number increases at the same flight speed (Figures 47, 48 and 49 in reverse order), there is a tendency for the shaft power curve not to pass through the autorotation point, $C_{DQR} = 0$, even at a low collective pitch setting, precluding autorotation. This trend becomes more severe at higher collective pitch settings.

TABLE VII. ROTOR PERFORMANCE DATA FOR HIGH-SPEED FLIGHT

Rotor	R (ft.)	σ	Blade Geometry					Flight Condition						Case	Fig No.	
			x	0	Airfoil Distribution			V (km)	q (psf)	ΩR (rpm)	μ	M _(1,50)				
					t/c	.12	.75						1.0			θ ₁ (deg)
Main	17.5	.0819	t/c	.12				250	212	550	84.6	.768	.870	1	46	
			cf1	0			0	300	305	550 488	84.6 75.	.921 1.890	.946 .890	2	47	
								325	358	488	75.	1.559	.745	3	48	
								325	358	488	75.	1.126	.928	.928	4	49
								300	305	550 488	84.6 75.	1.689	.782	.946	5	50
								300	305	550	84.6	.921	.946	.946	6	51
								325	358	488	75.	1.039	.890	.890	7	52
								325	358	488	75.	.998	.983	.983	8	53
								325	358	488	75.	1.126	.928	.928	9	54
								325	358	488	75.	1.126	.928	.928	10	55
Tail	3.25	.1273	t/c	.12				250	212	550	84.6	.768	.870	11	56	
			cf1	0			.06	300	305	550 488	84.6 75.	.921 1.039	.946 .890	12	57	
								325	358	488	75.	1.039	.890	.890	13	58
								300	305	488	75.	1.039	.890	.890	14	59
								300	305	488	75.	1.039	.890	.890	15	60
								300	305	488	75.	1.039	.890	.890	16	61
								300	305	488	75.	1.039	.890	.890	17	62
								300	305	488	75.	1.039	.890	.890	18	63
								300	305	488	75.	1.039	.890	.890	19	64
								300	305	488	75.	1.039	.890	.890	20	65
Tail	3.25	.1273	t/c	.07				300	305	601	84.6	.843	.991	21	66	
			cf1	0			0	300	305	533	75.0	.952	.930			
								300	305	355	50.0	1.427	.786			

*Abbreviated data range

BLADE SECTION CHARACTERISTICS

x	t/c	c _l
0	0.12	0
1.0	0.12	0

θ_1	DEG
---	0
---	-5
---	-10

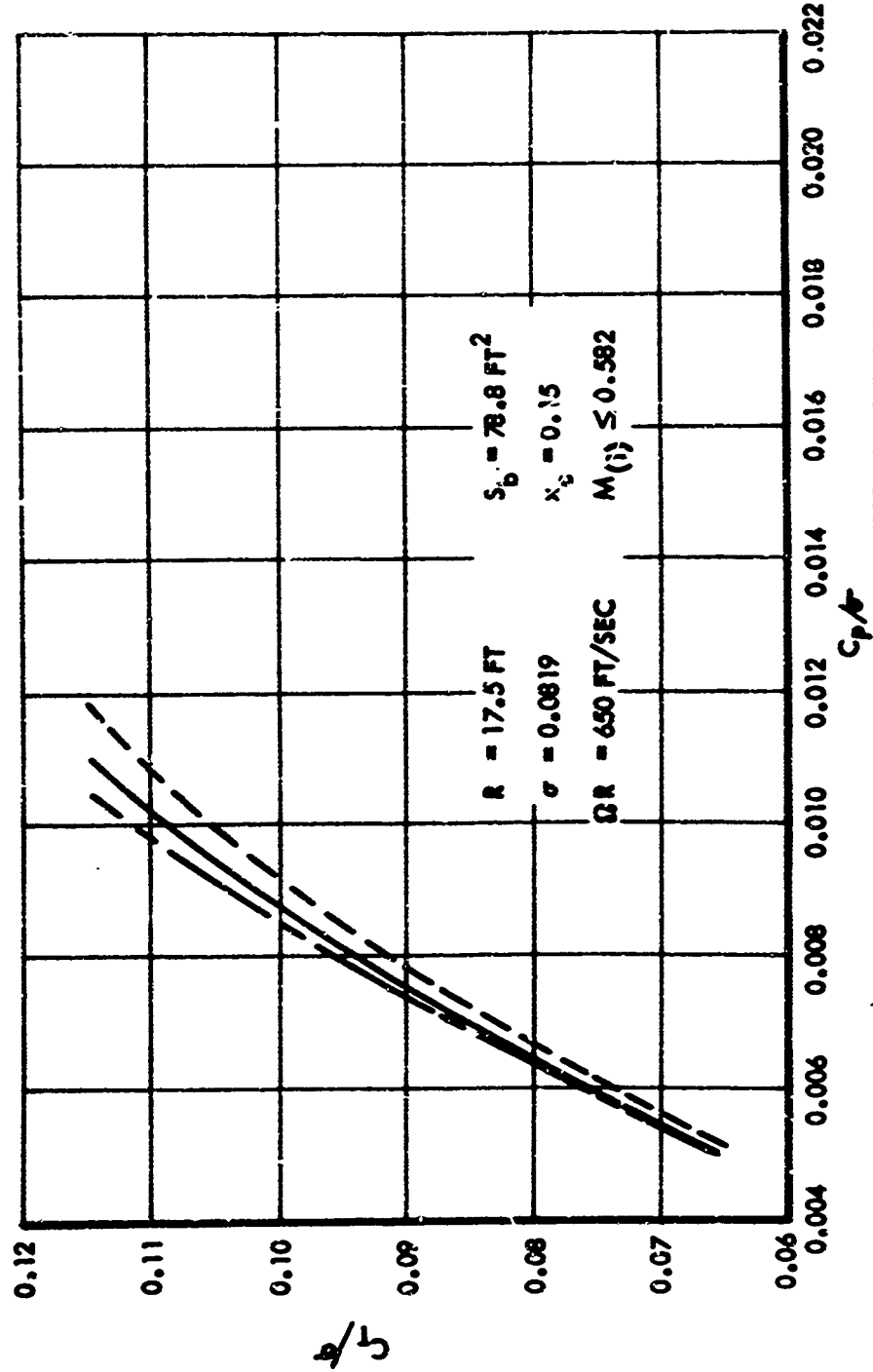


Figure 43. Rotor Hovering Performance, Effect of Twist.

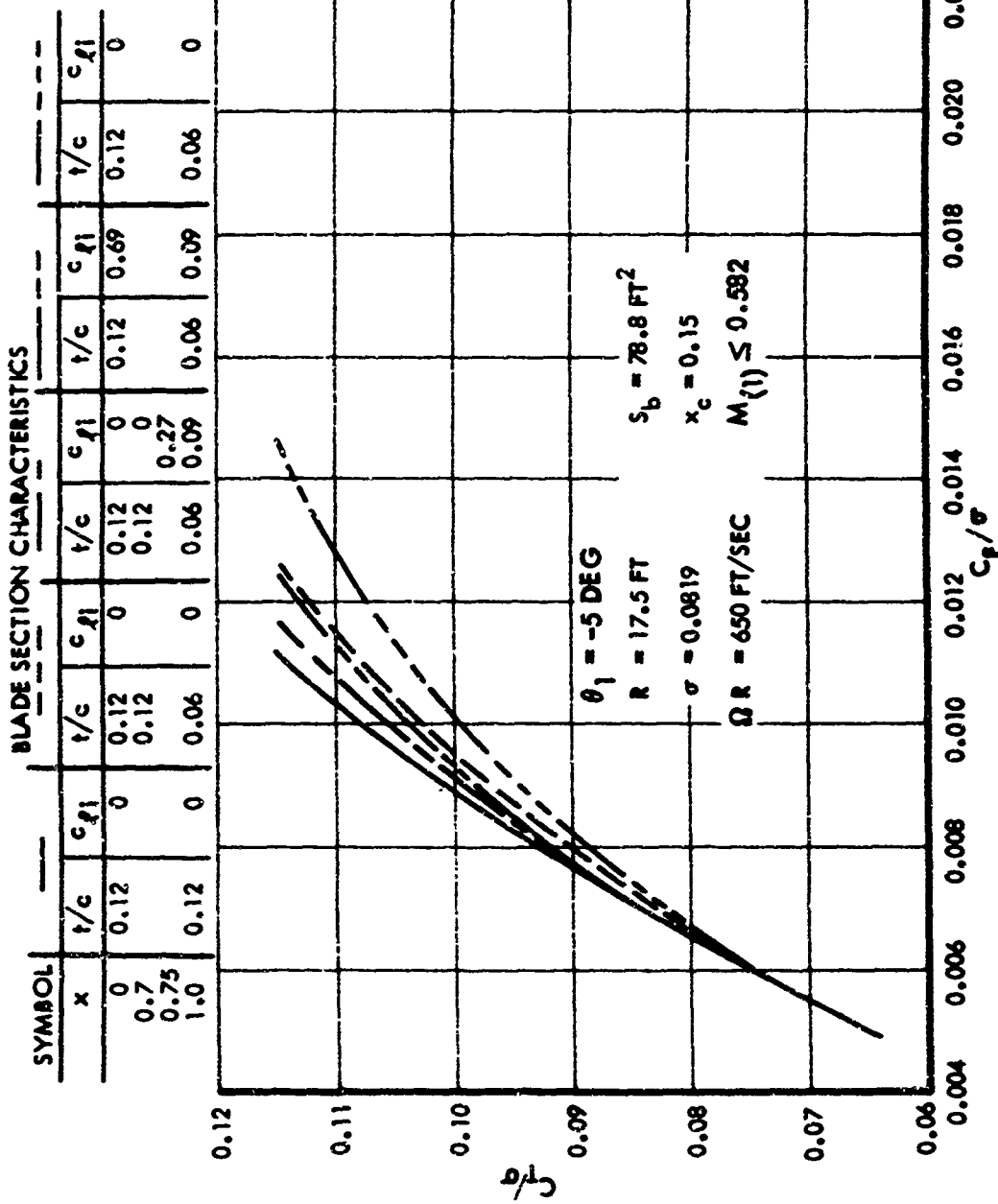


Figure 44. Rotor Hovering Performance, Effect of Airfoil Distribution.

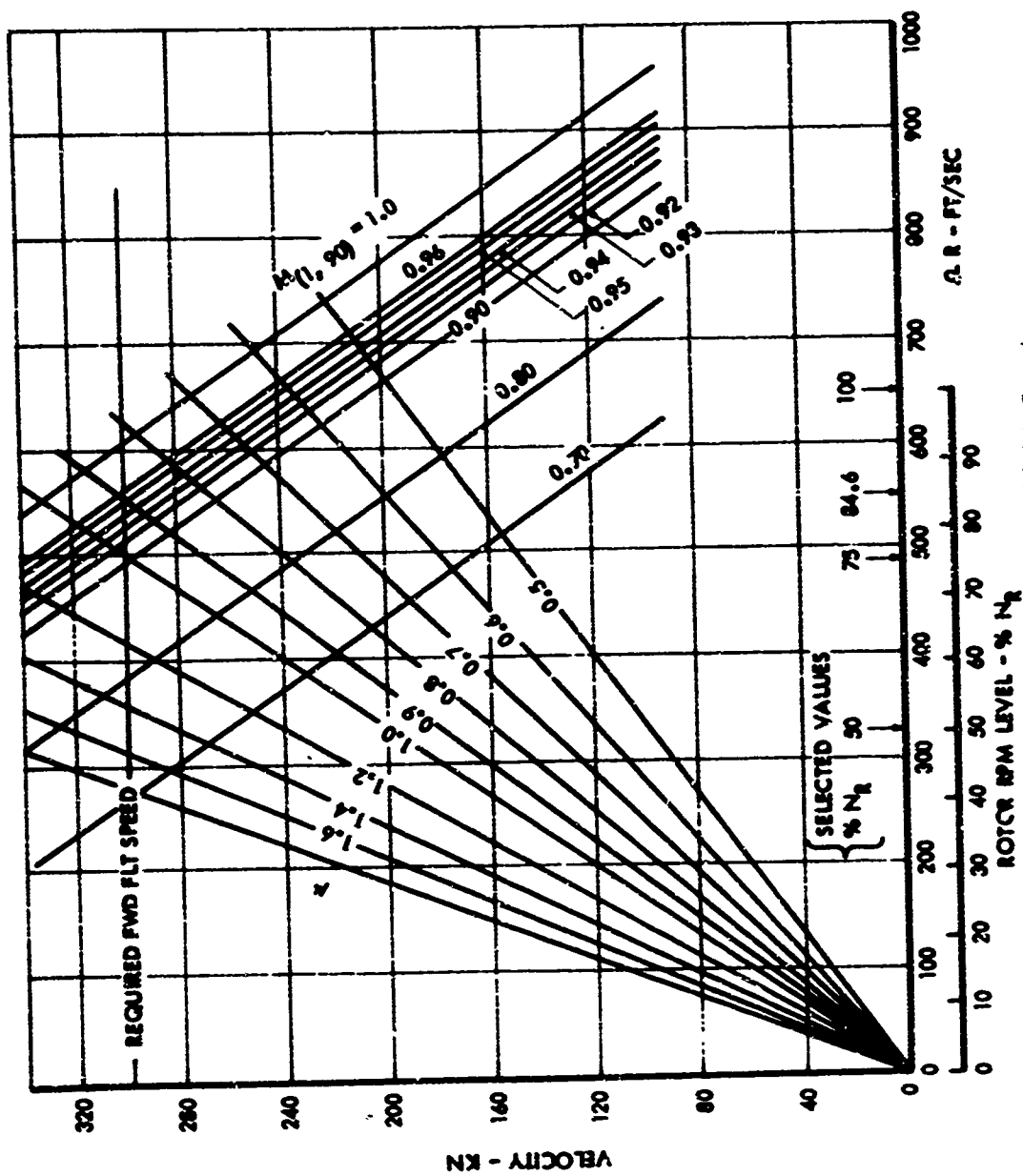


Figure 45. Rotorcraft Flight Spectrum.

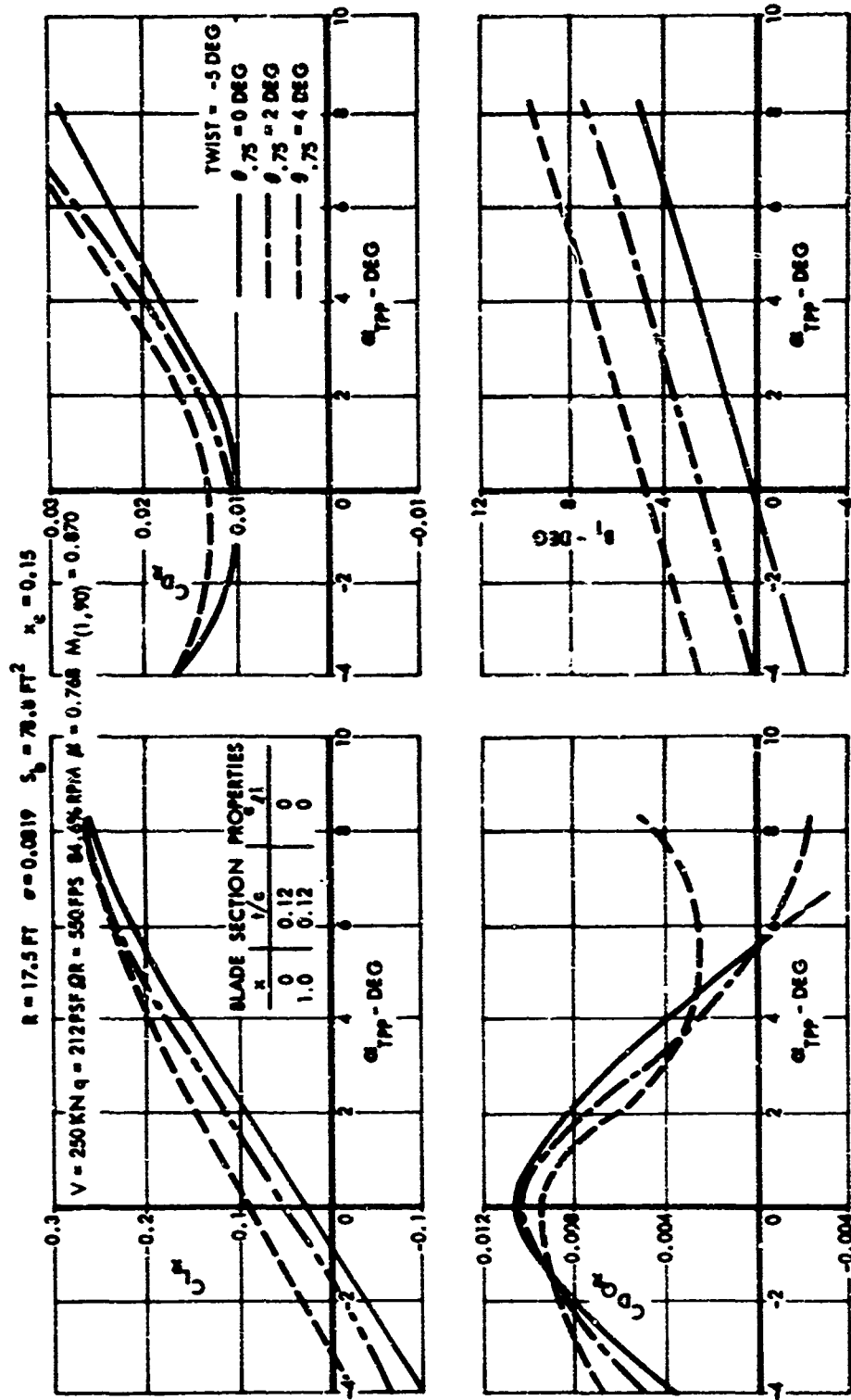


Figure 46. Motor Performance Data for High-Speed Flight, Case 1.

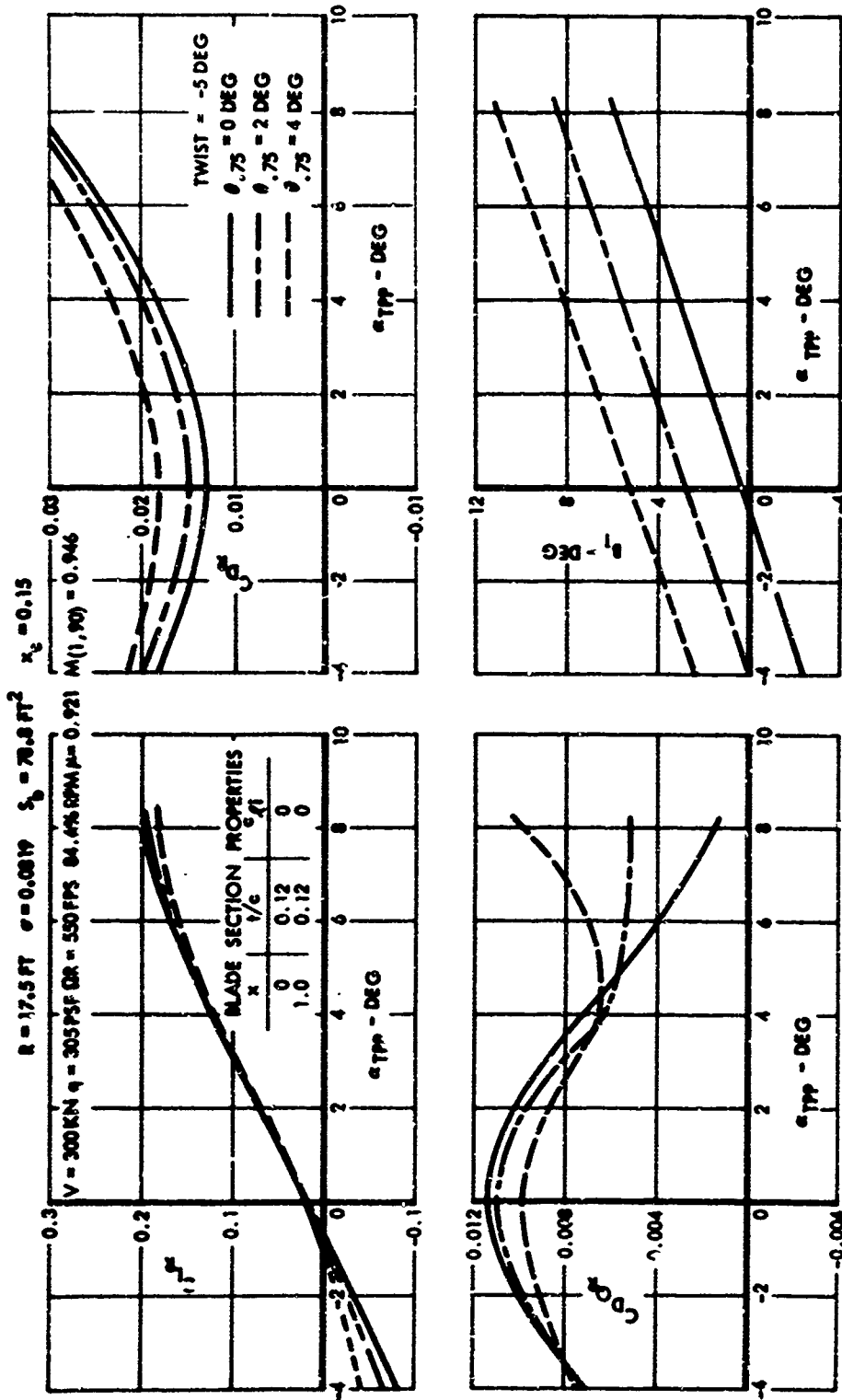


Figure 47. Rotor Performance Data for High-Speed Flight, Case 2.

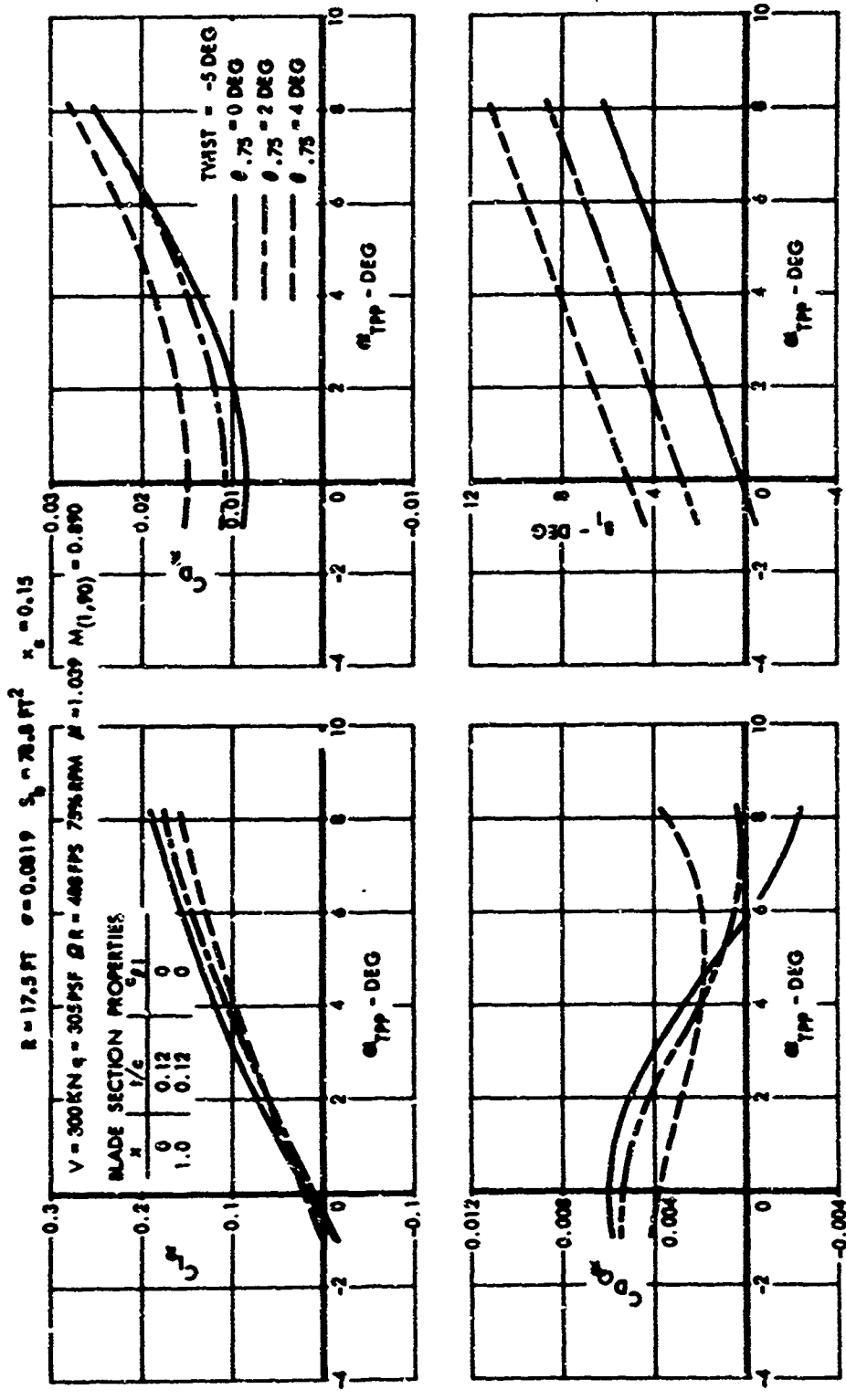


Figure 48. Rotor Performance Data for High-Speed Flight, Case 3.

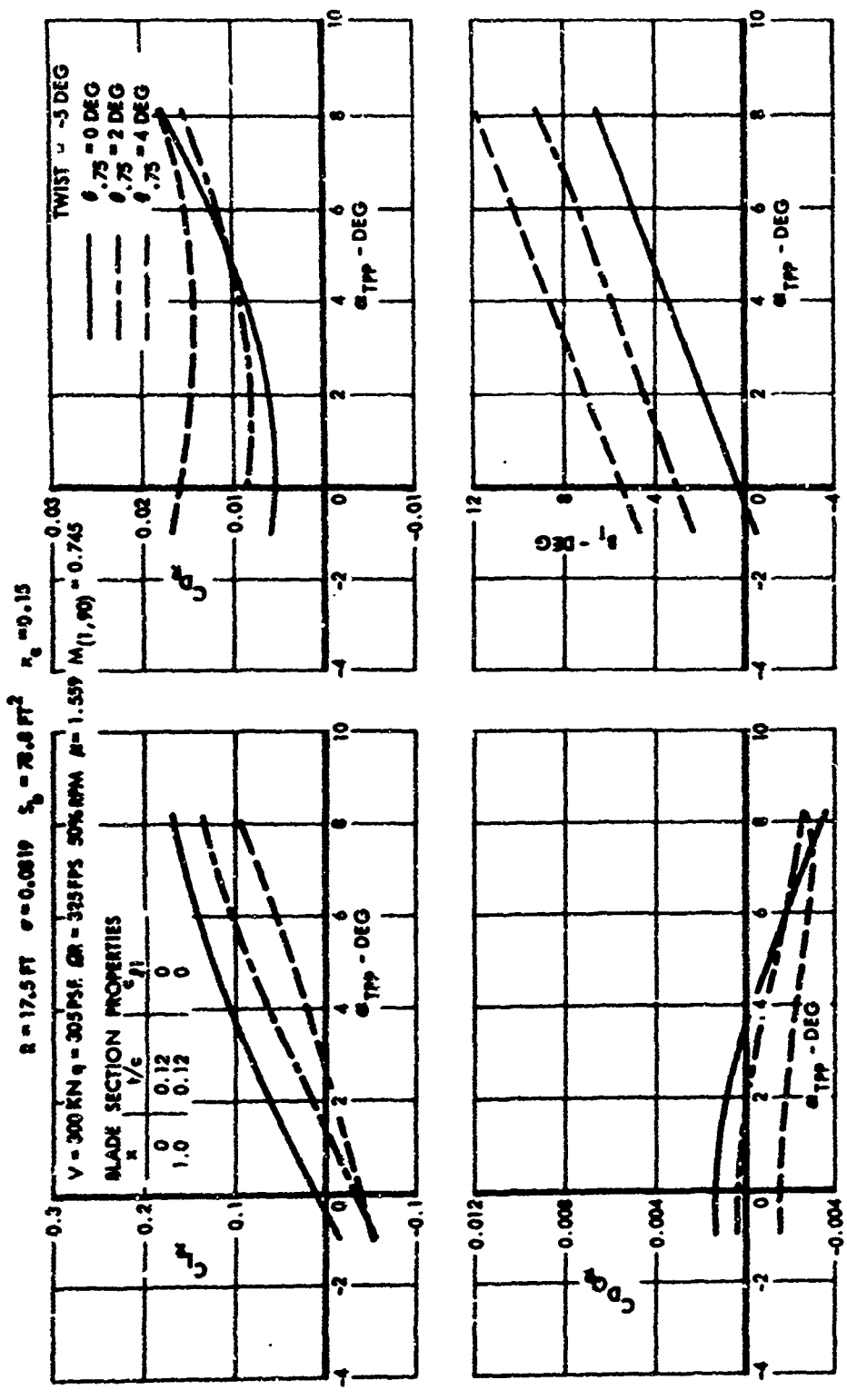


Figure 49. Rotor Performance Data for High-Speed Flight, Case 4.

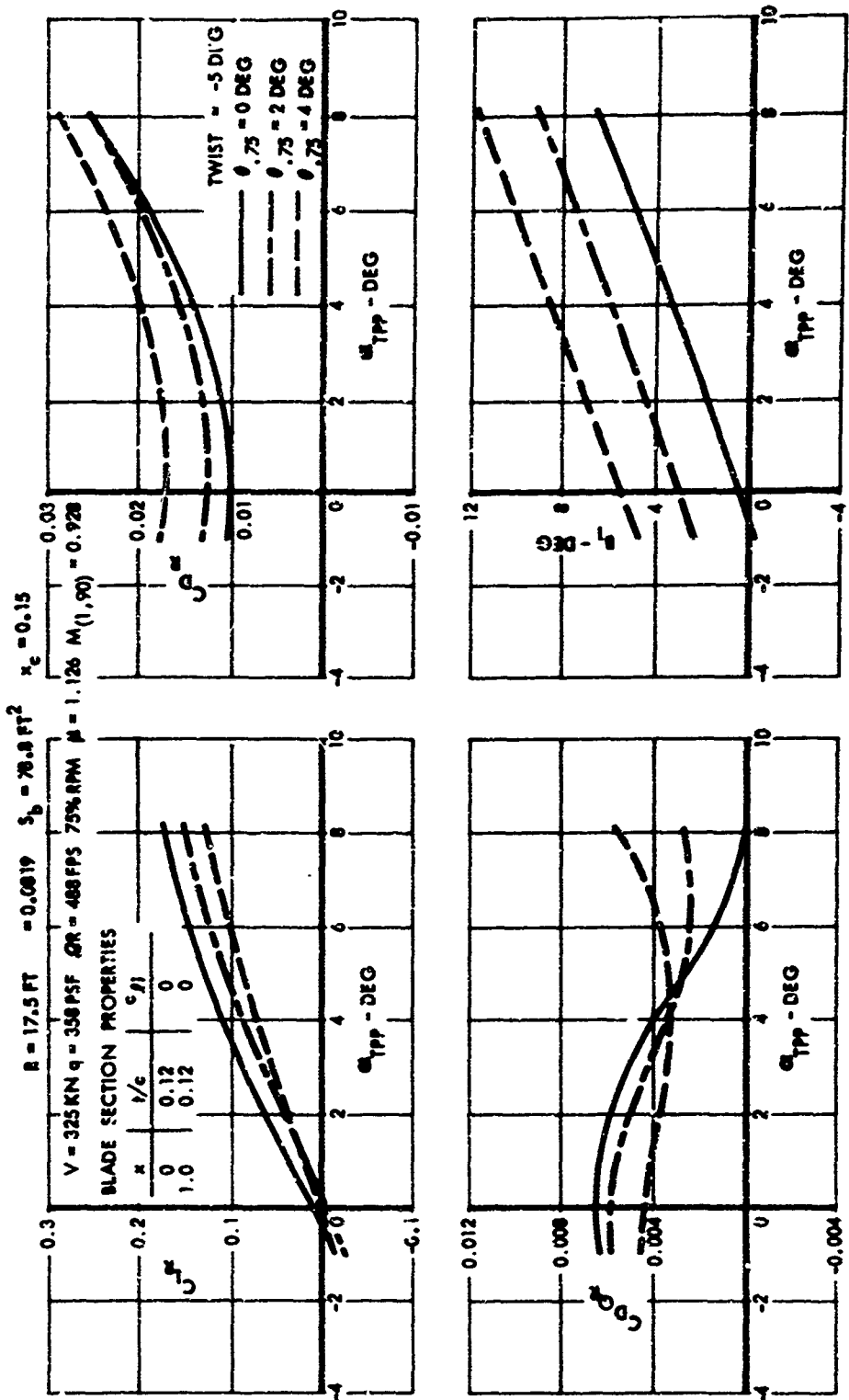


Figure 50. Rotor Performance Data for High-Speed Flight, Case 5.

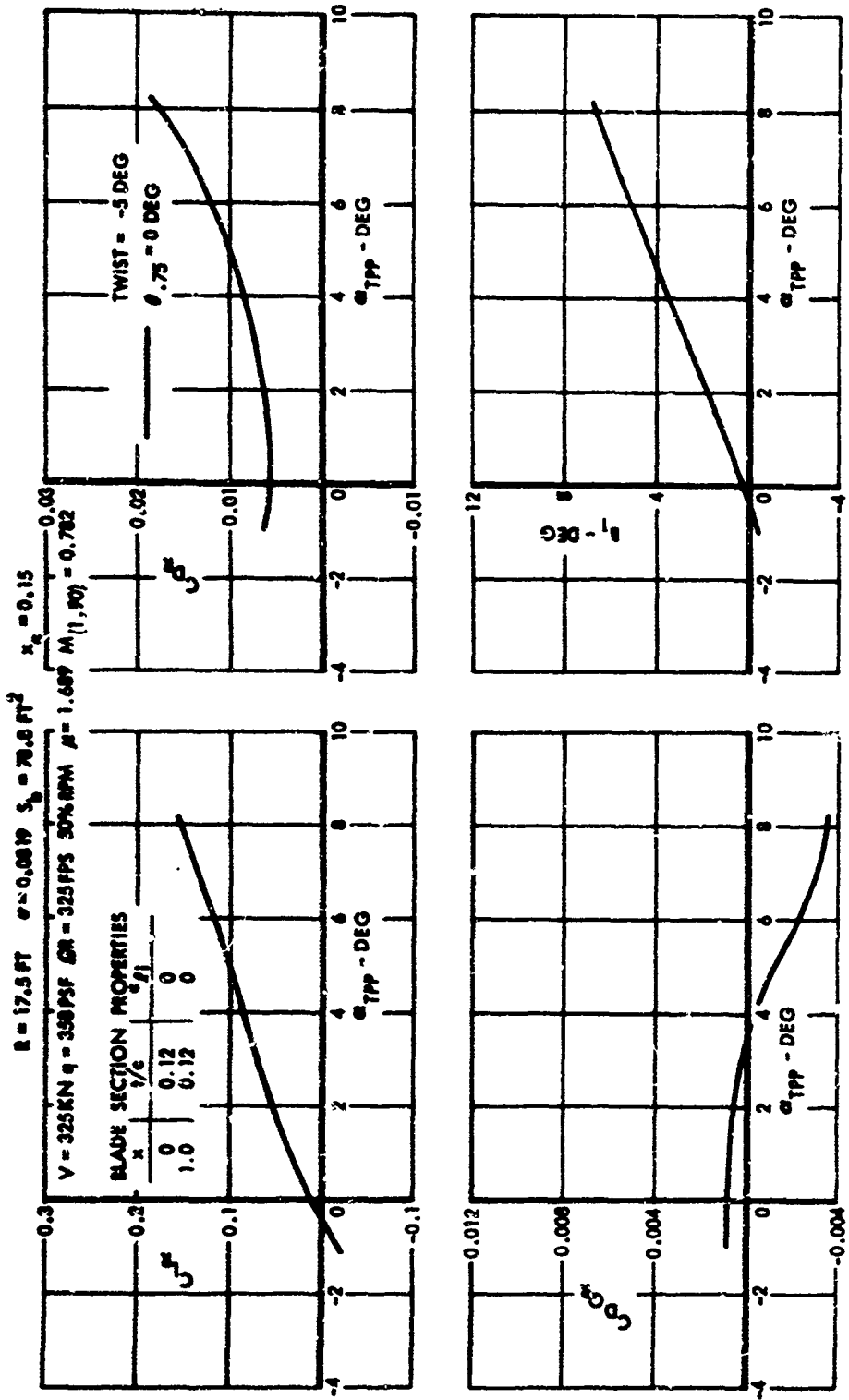


Figure 51. Rotor Performance Data for High-Speed Flight, Case 6.

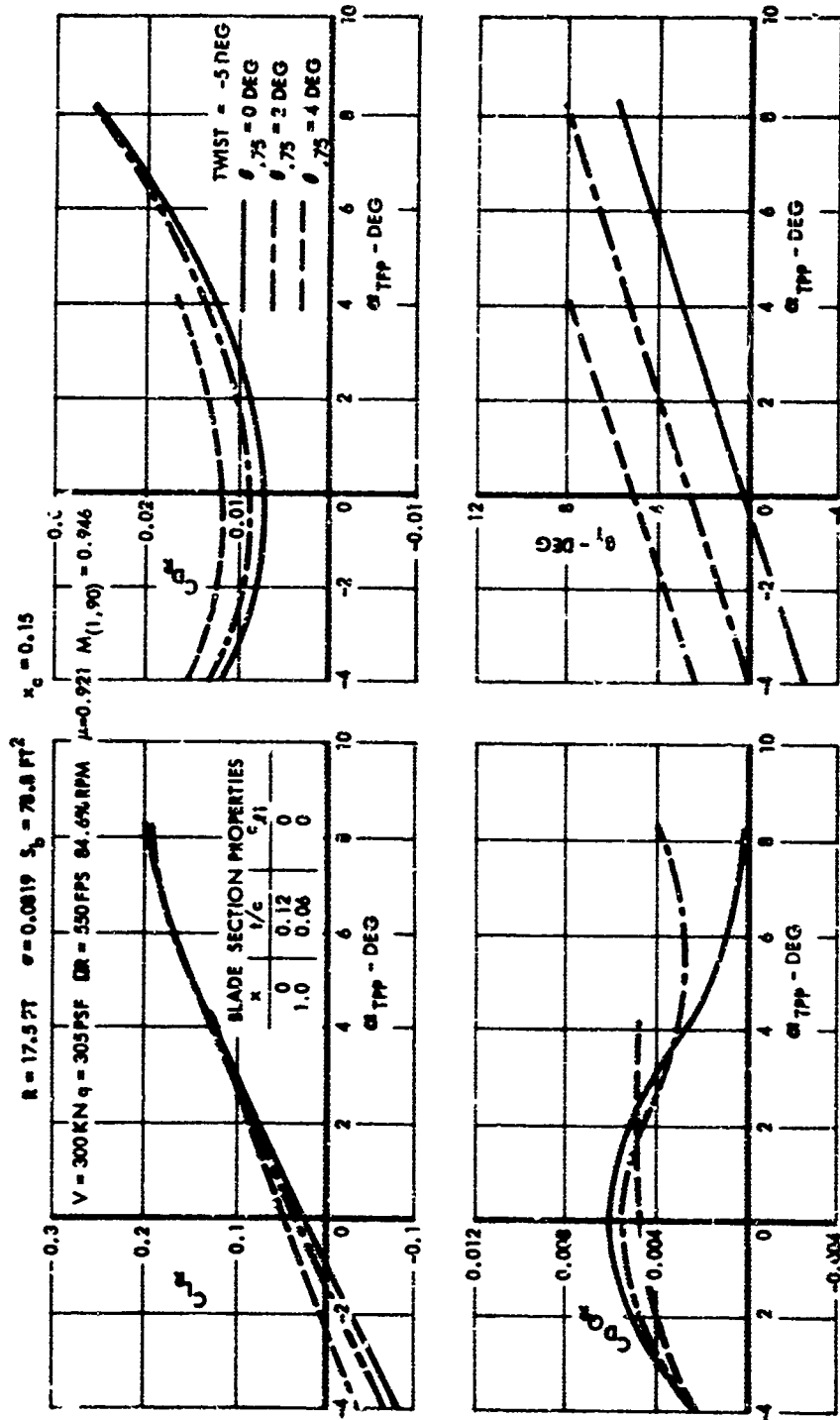


Figure 52. Rotor Performance Data for High-Speed Flight, Case 7.

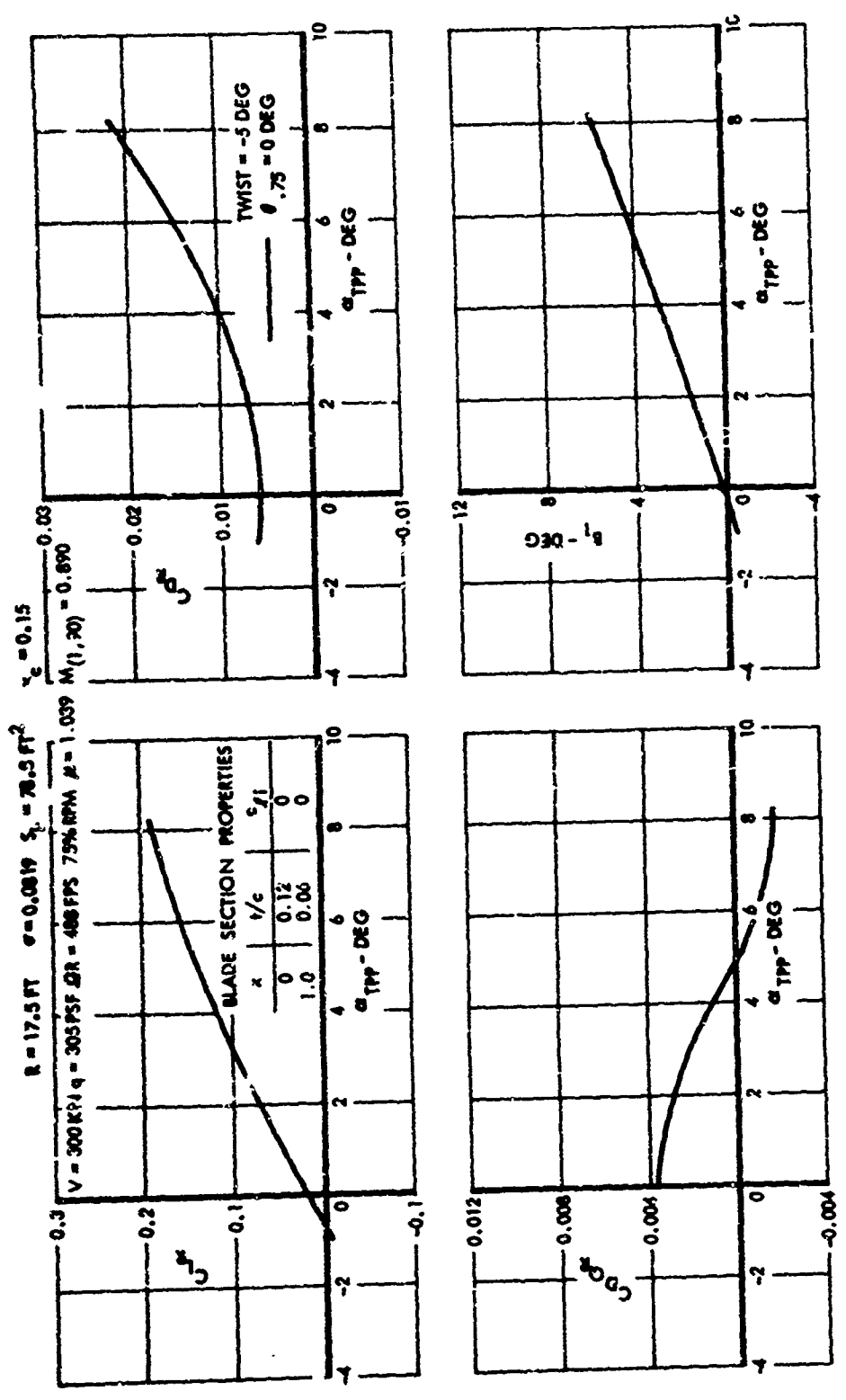


Figure 53. Rotor Performance Data for High-Speed Flight, Case 8.

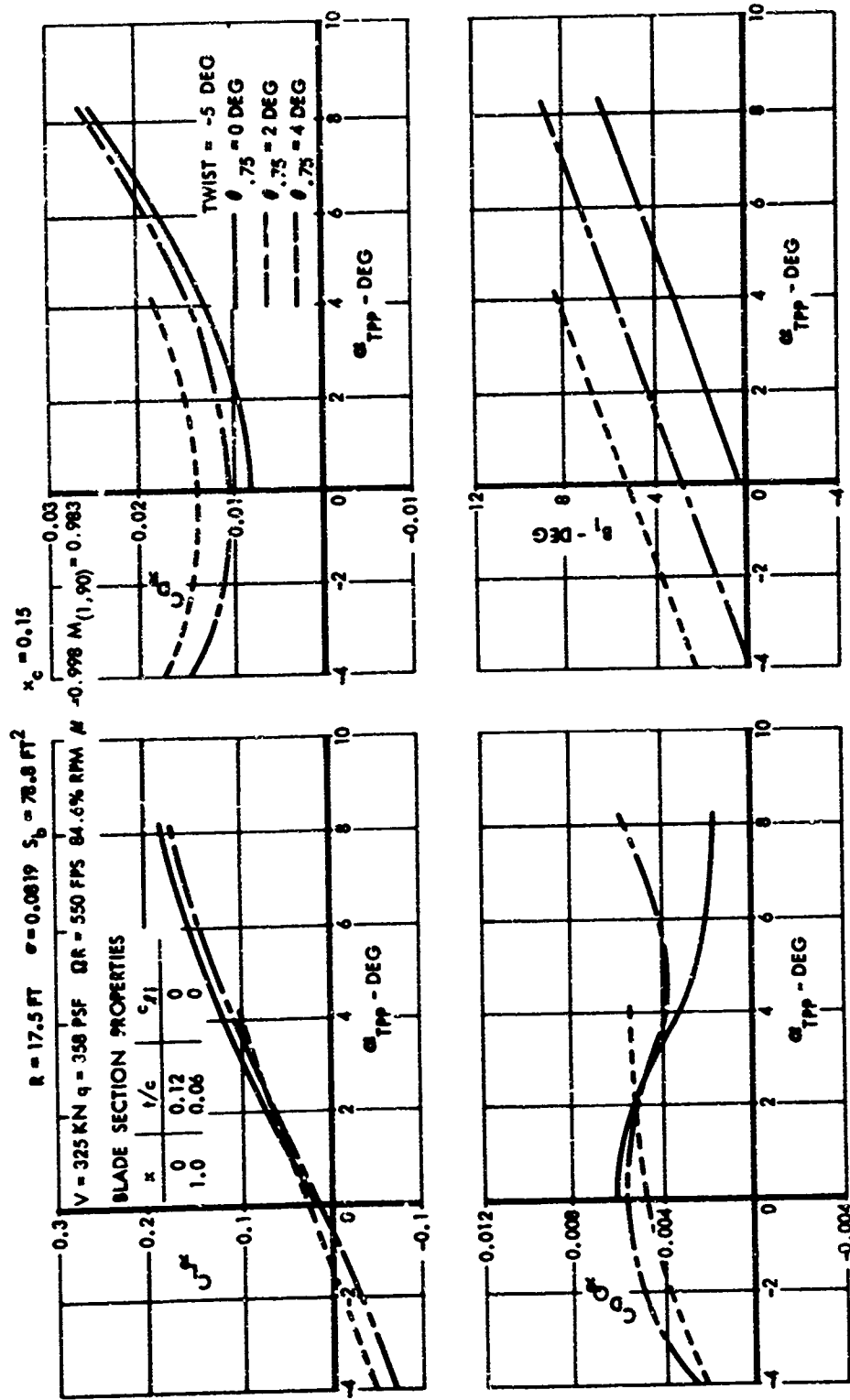


Figure 54. Rotor Performance Data for High-Speed Flight, Case 9.

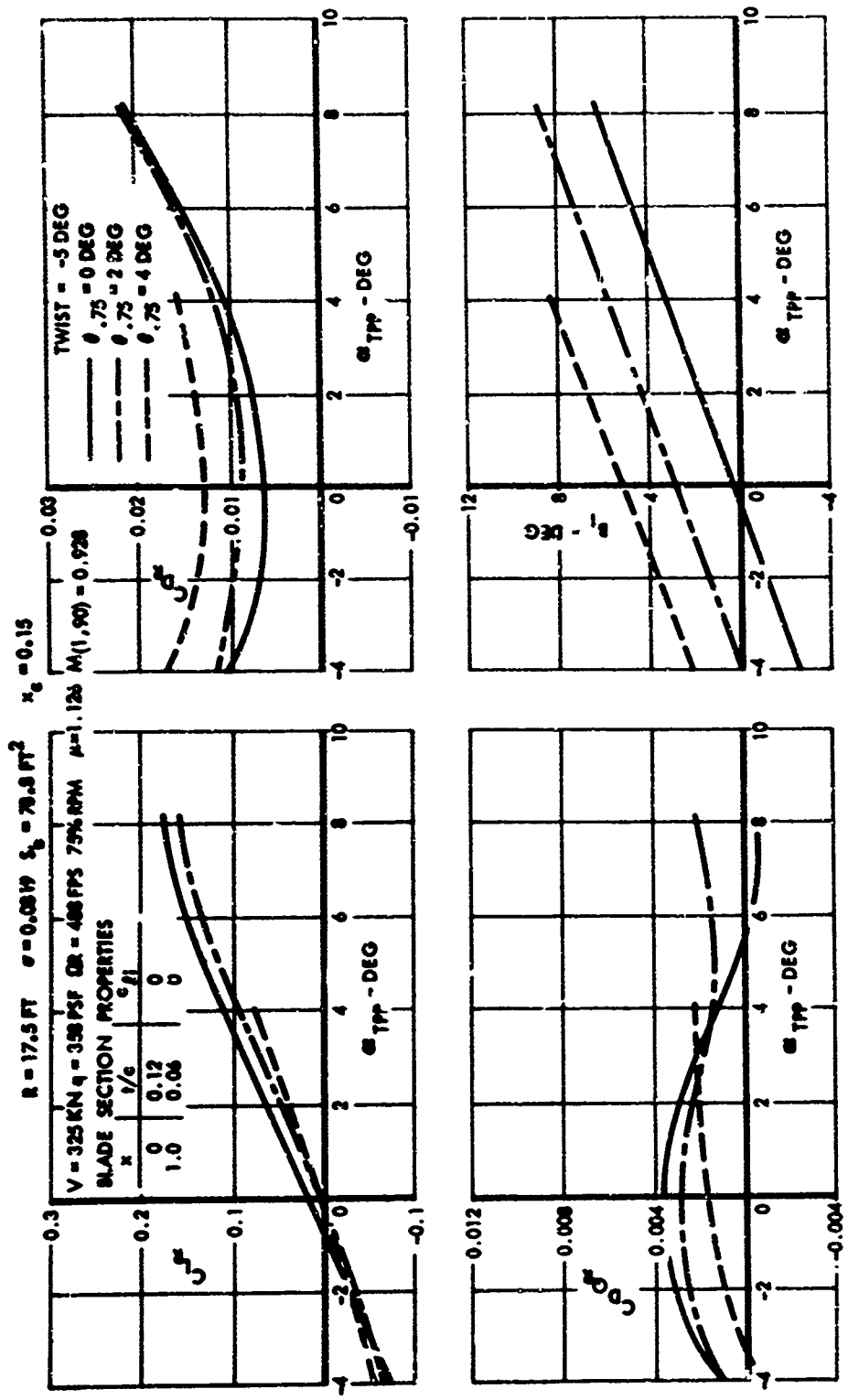


Figure 55. Rotor Performance Data for High-Speed Flight, Case 10.

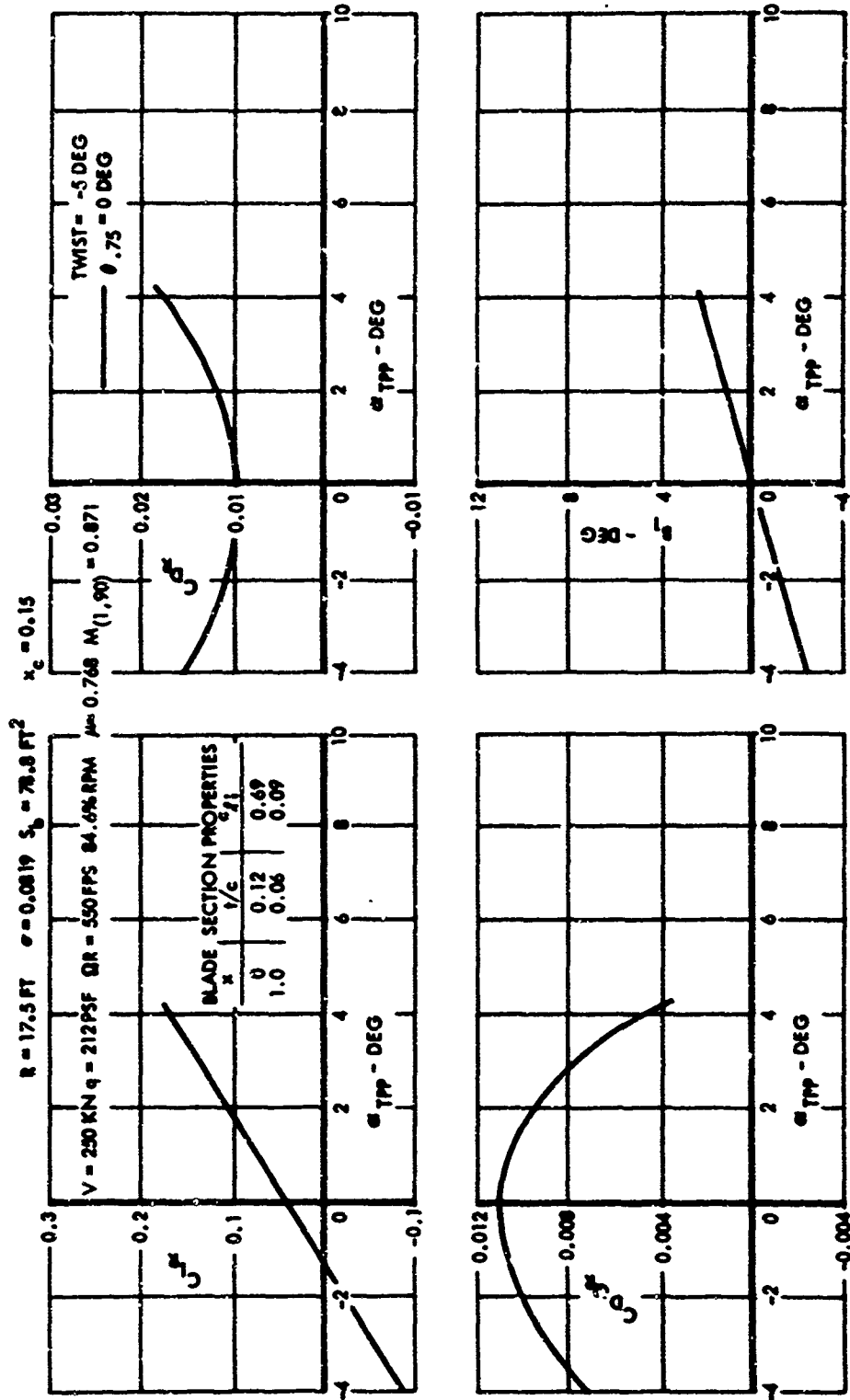


Figure 56. Rotor Performance Data for High-Speed Flight, Case 11.

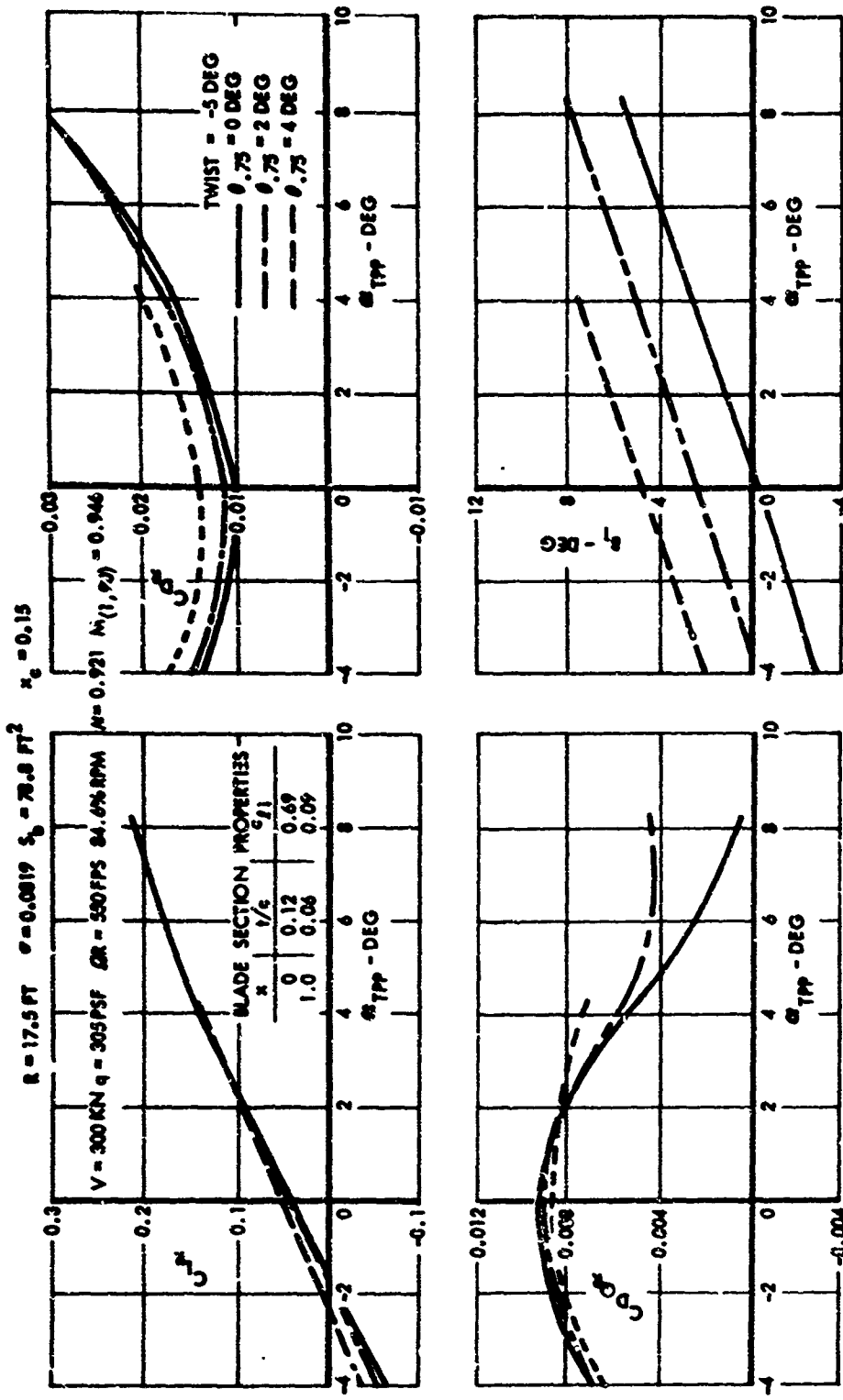


Figure 57. Rotor Performance Data for High-Speed Flight, Case 12.

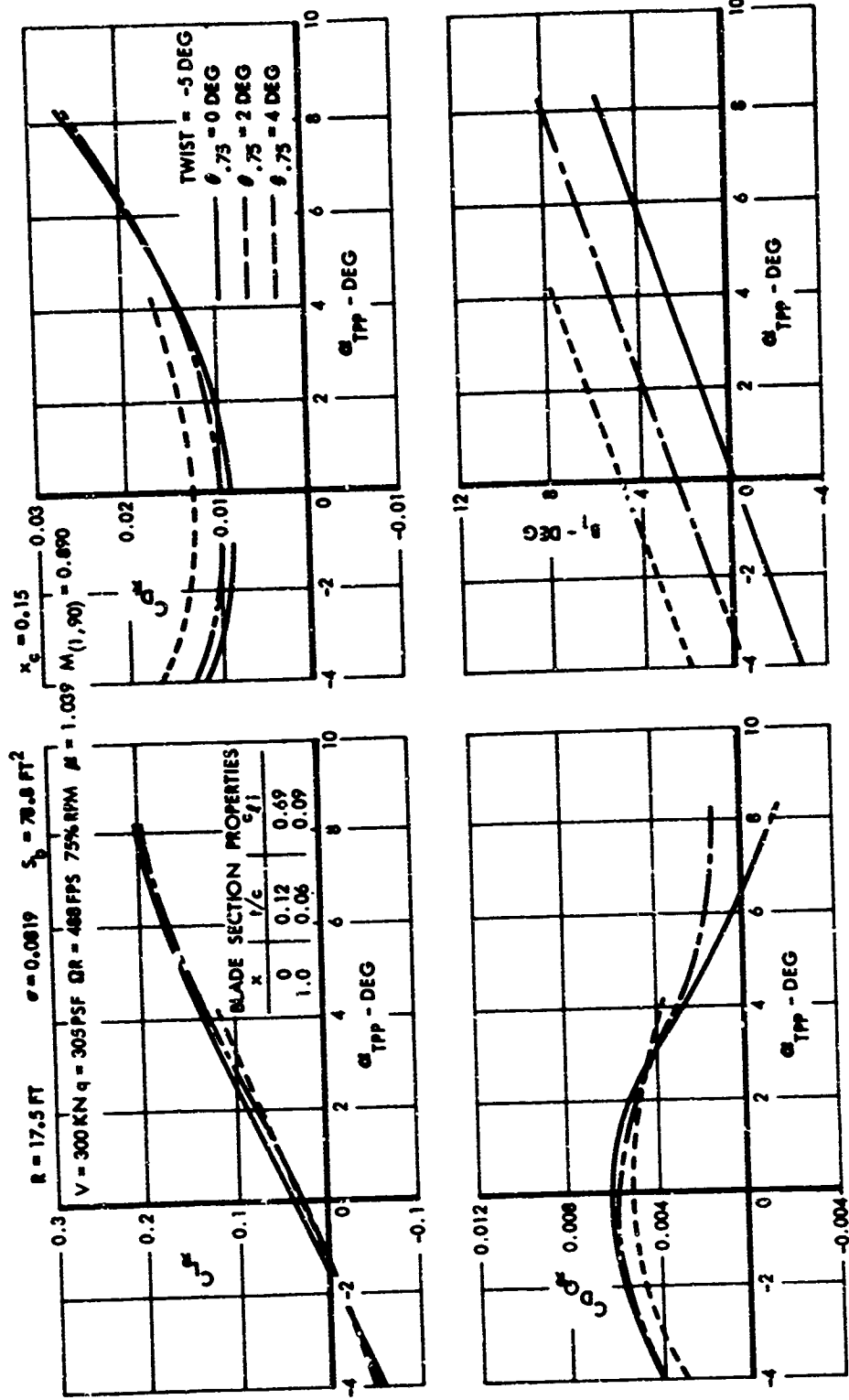


Figure 58. Rotor Performance Data for High-Speed Flight, Case 13.

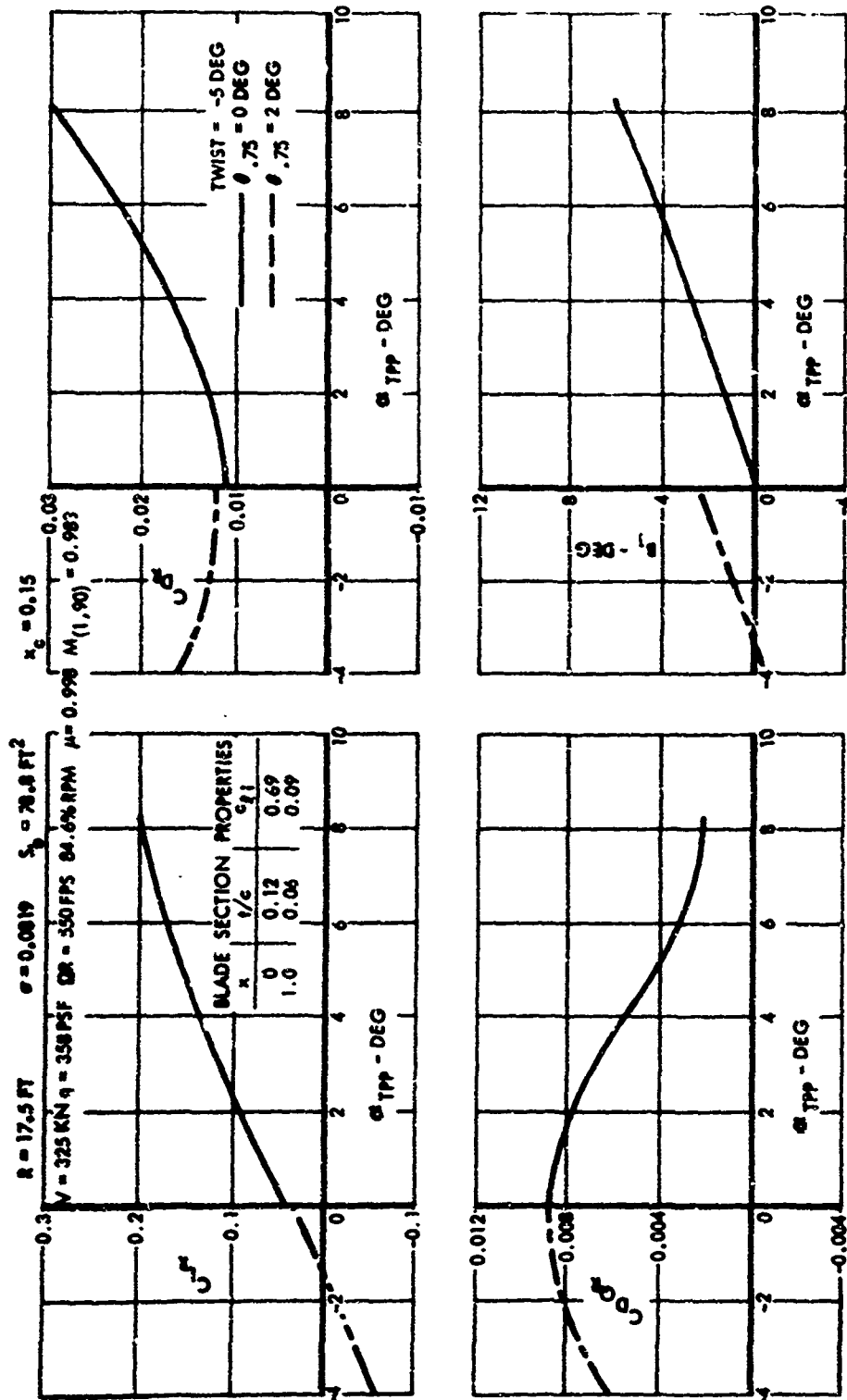


Figure 59. Rotor Performance Data for High-Speed Flight, Case 14.

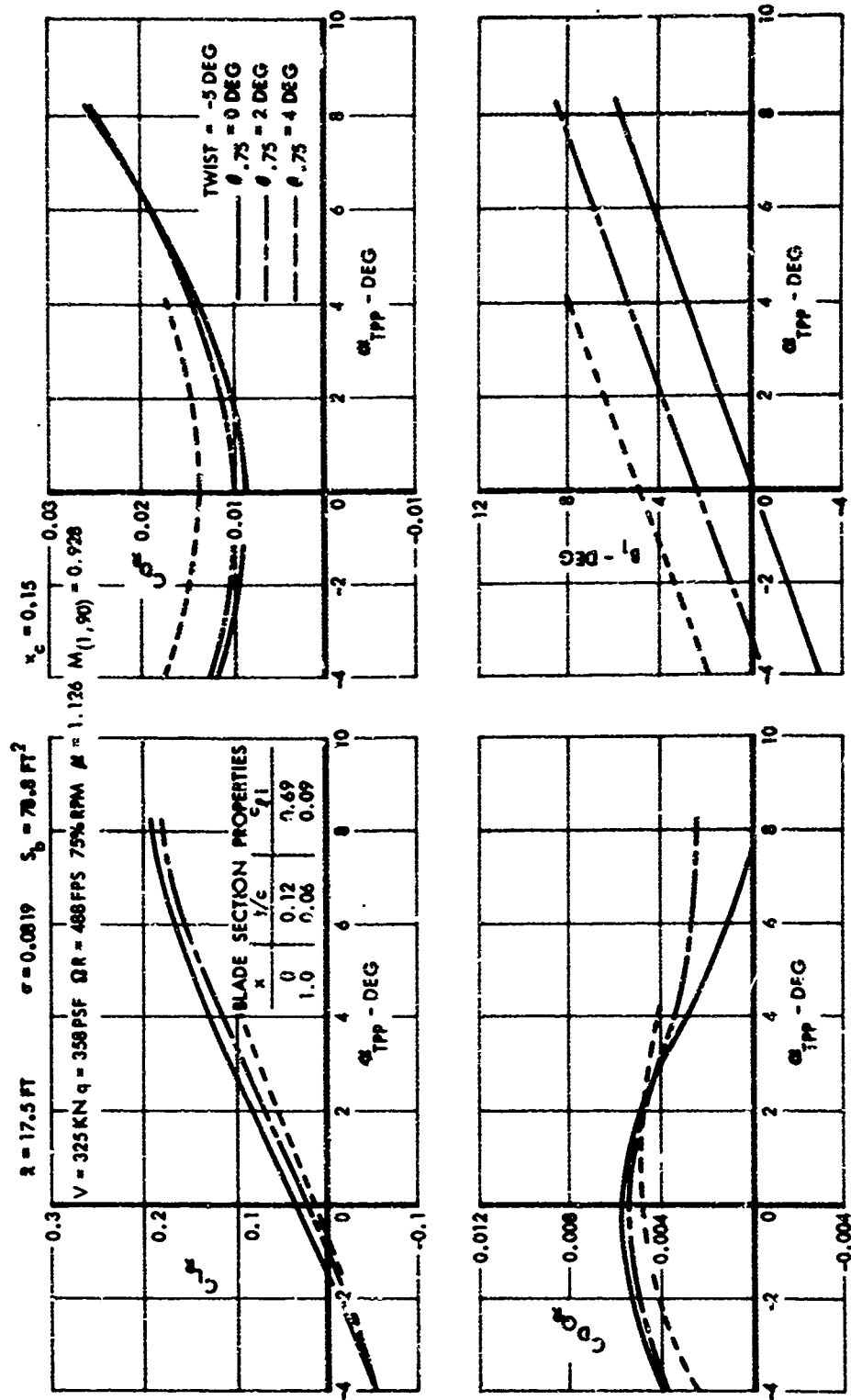


Figure 60. Rotor Performance Data for High-Speed Flight, Case 15.

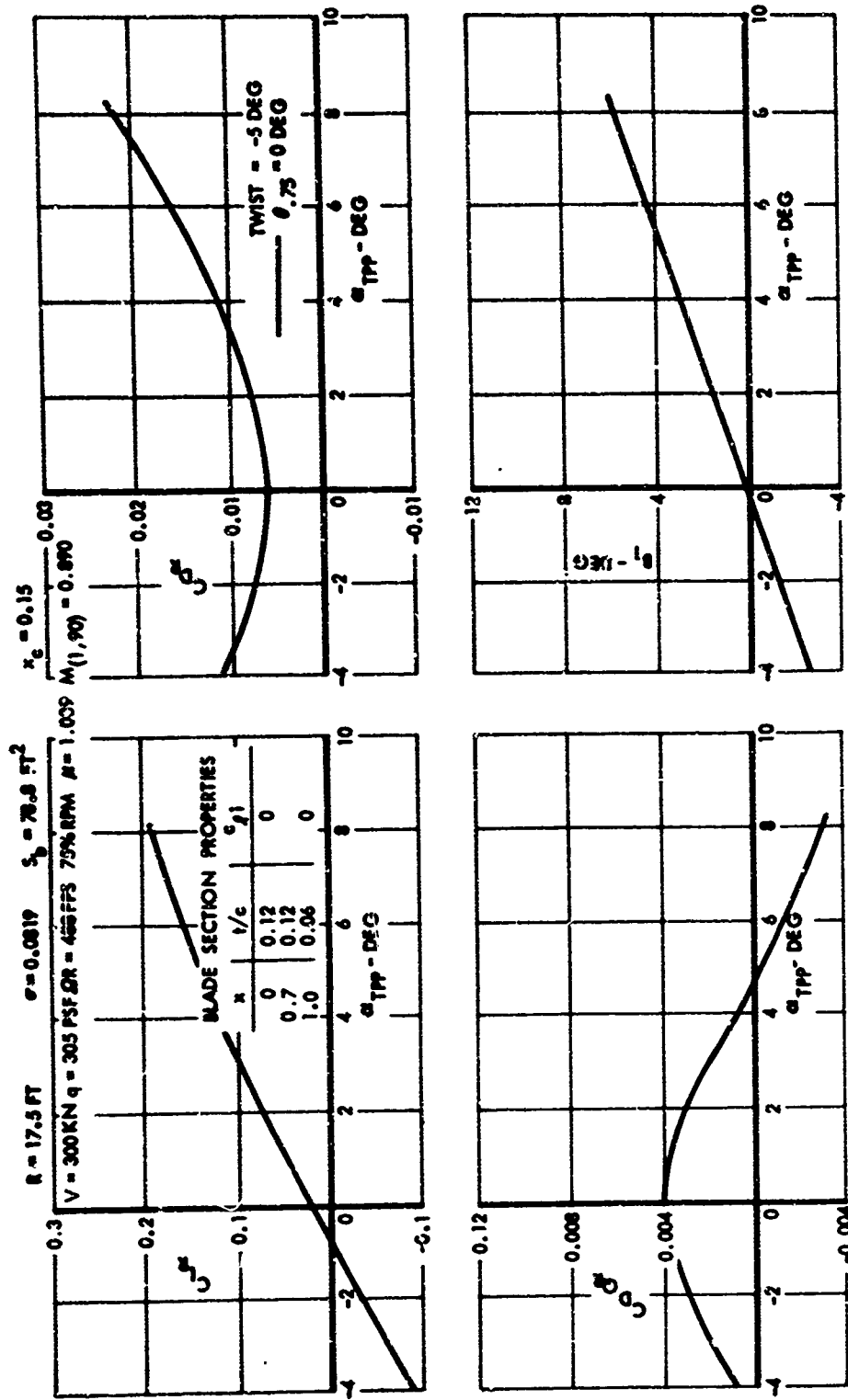


Figure 61. Rotor Performance Data for High-Speed Flight, Case 16.

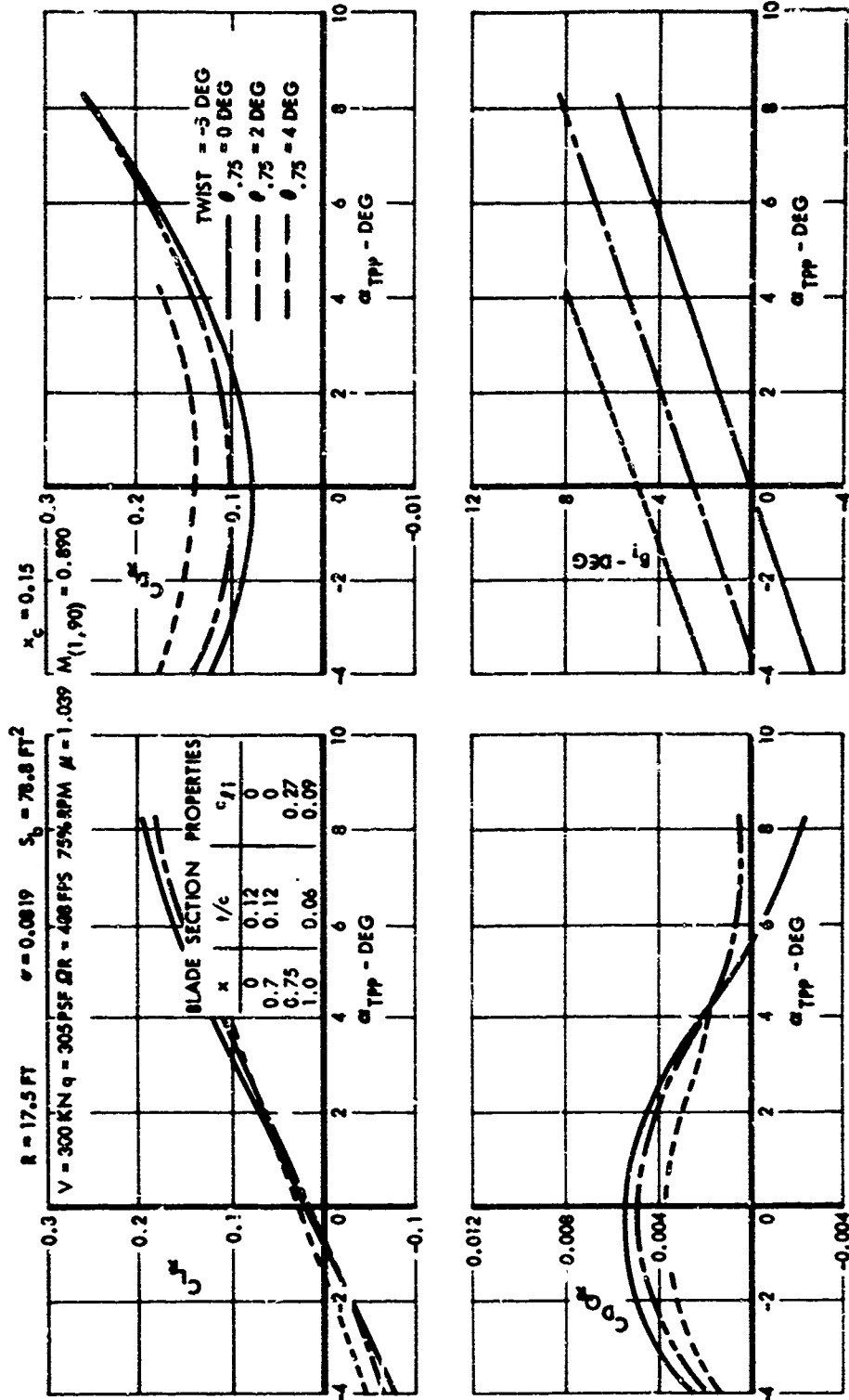


Figure 62. Rotor Performance Data for High-Speed Flight, Case 17.

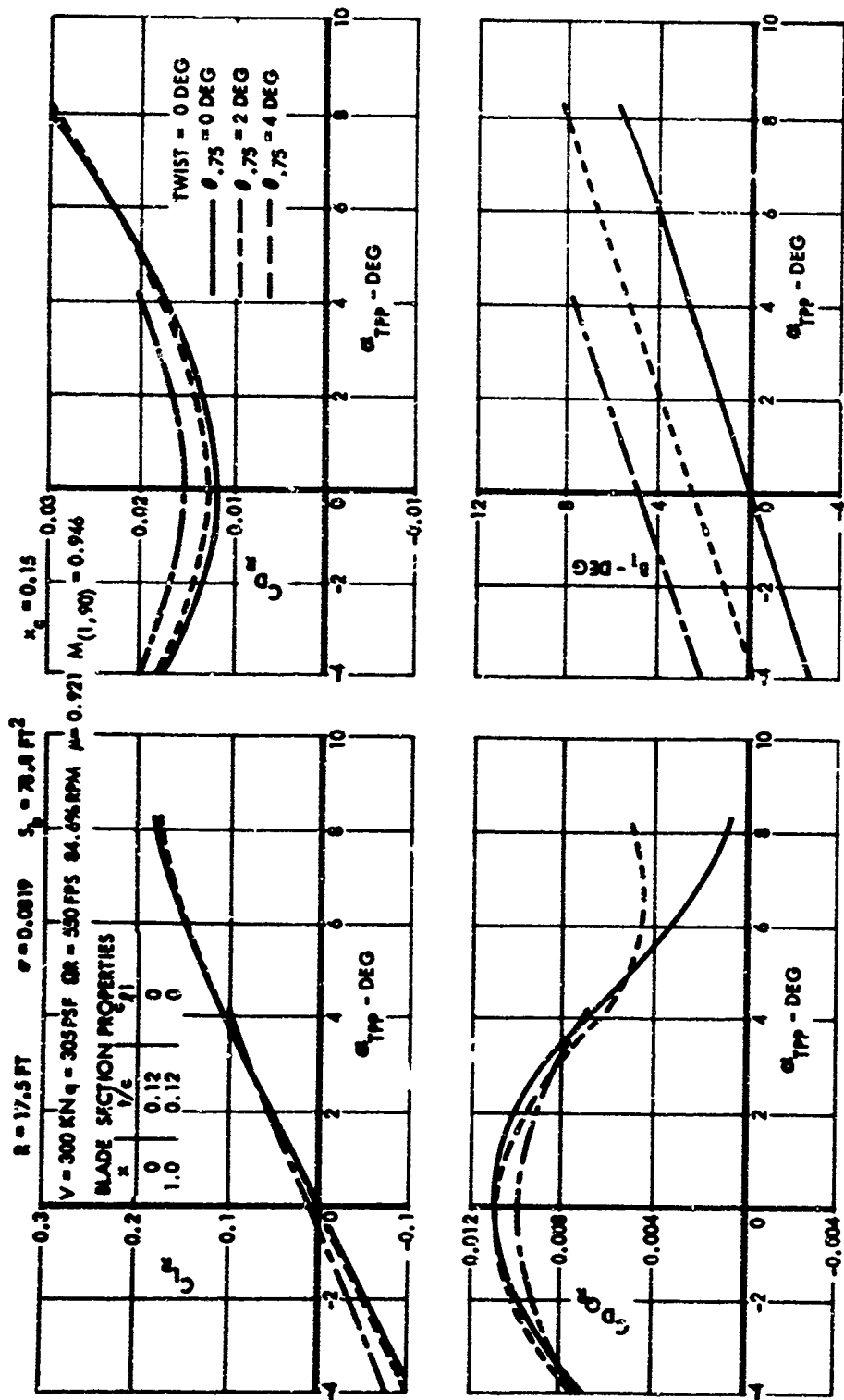


Figure 63. Rotor Performance Data for High-Speed Flight, Case 18.

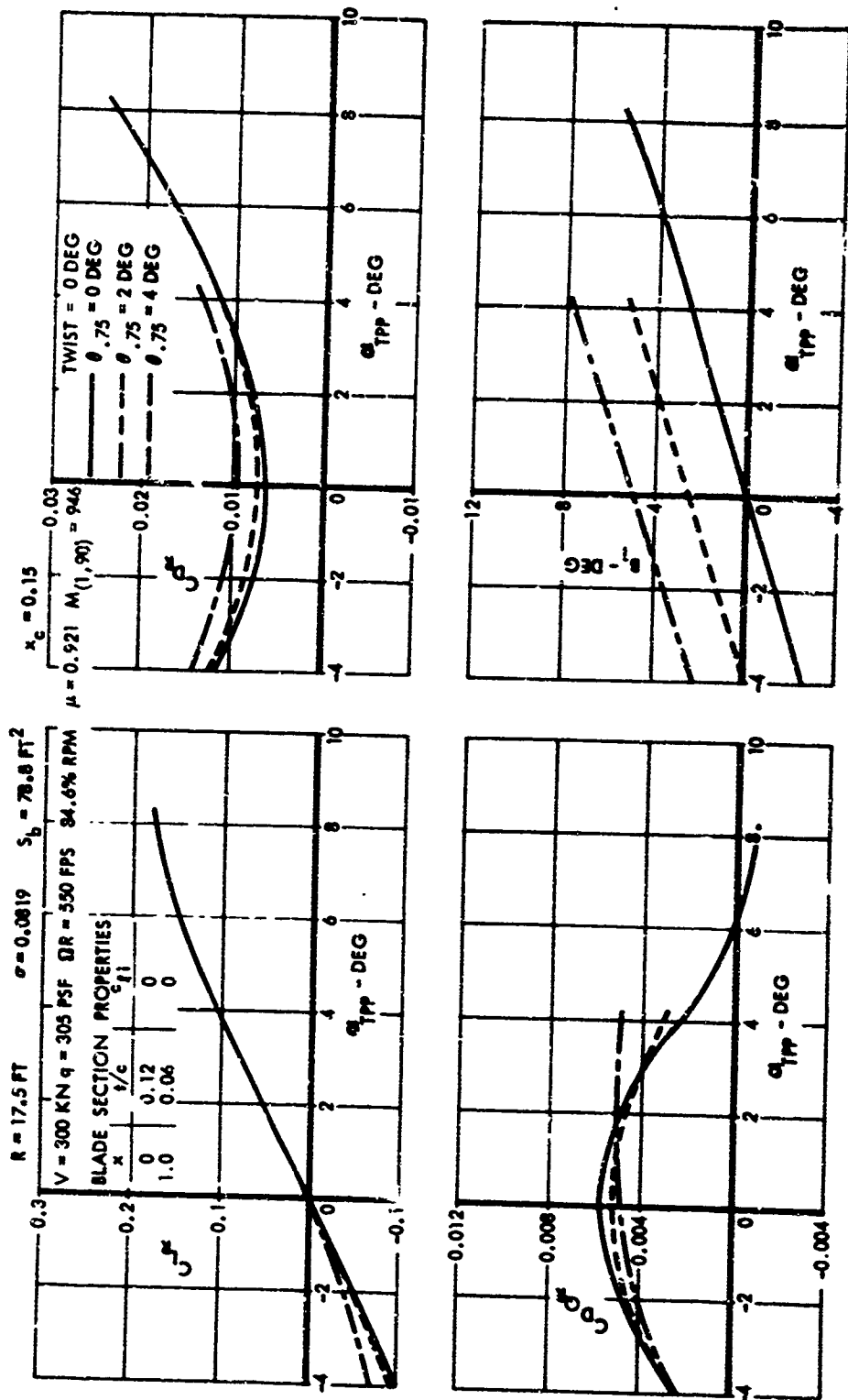


Figure 64. Rotor Performance Data for High-Speed Flight, Case 19.

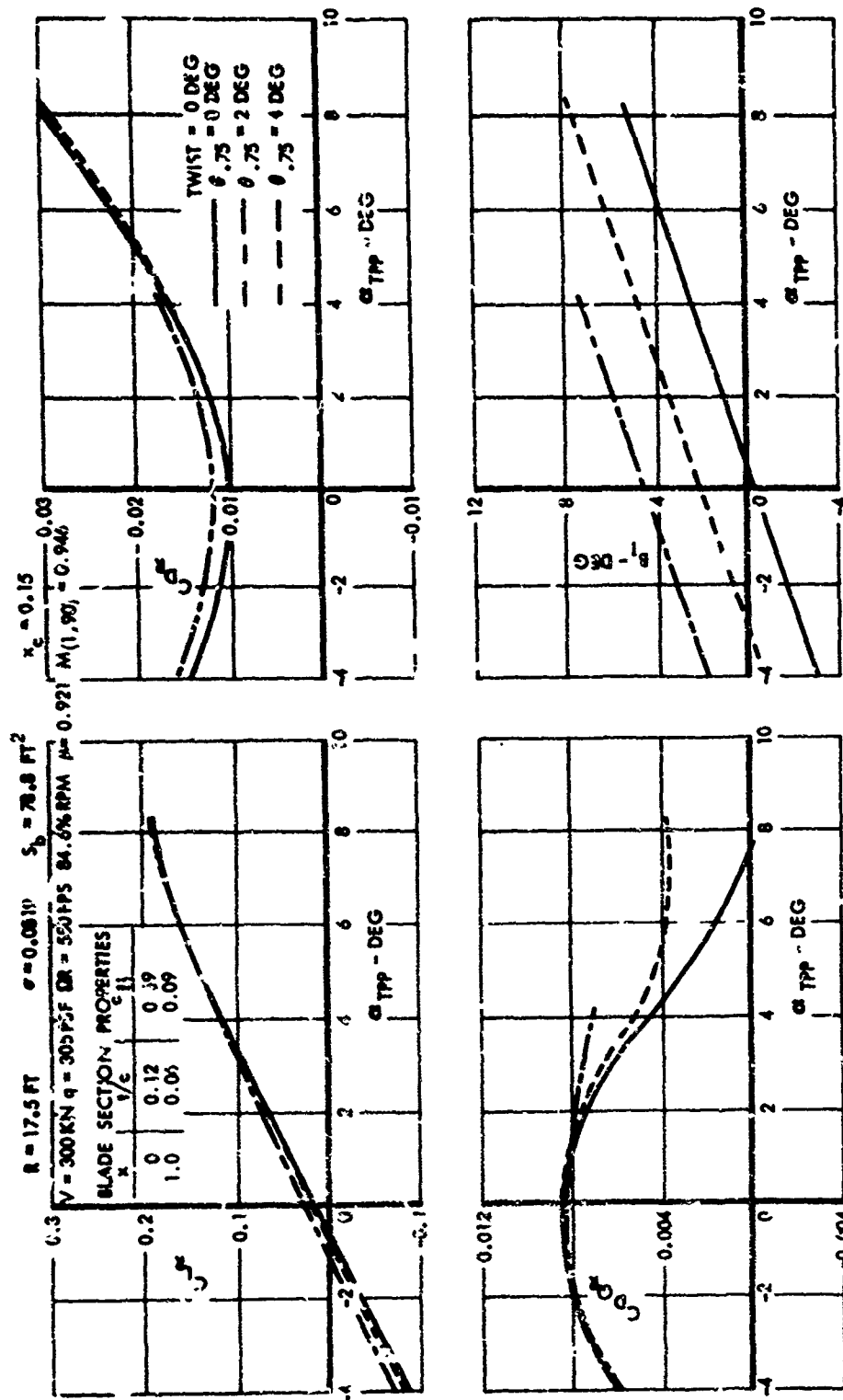


Figure 65. Rotor Performance Data for High-Speed Flight, Case 20.

A number of the performance charts include data in addition to the basic design regime for one or two more collective pitch settings in 2-degree increments. These are included to show the effect of increasing collective pitch as the advance ratio increases and becomes greater than unity. The zero setting, or a near-zero three-quarter-radius collective pitch setting, is used in order to obtain the maximum available range of longitudinal cyclic pitch for maneuvering. (There is no requirement for collective pitch control at high-speed flight, and the collective pitch control is normally set at a detent for this flight condition.)

Reference to the performance charts for a selected blade geometry at successively increasing flight speeds and decreasing rotor rpm (therefore increasing advance ratio) shows a gradual decrease in lift coefficient with increasing collective pitch at each discrete advance ratio. At advance ratios above 1, there is a decrease in lift with increasing collective pitch. It is evident that there is no need to make use of the collective pitch control at high speeds, and the lift reversal makes it undesirable to employ collective pitch control at high advance ratios, especially those above unity.

Figure 66 is included to describe tail rotor operation in high-speed flight. Unlike the main rotor, which is trimmed parallel to the shaft normal plane for zero hub moments and which shows a lift reversal with increasing collective pitch at the advance ratios above unity, a conventional tail rotor is free to teeter with respect to its shaft and does not demonstrate reversal of thrust with increasing collective pitch at the higher advance ratios. The quality of no reversal is, of course, essential to provide yaw control through the tail rotor regardless of flight speed and main rotor rpm.

With allowance for the characteristics noted, the performance data charts show no fundamental rotor limitations through the flight speed of 325 knots covered by these charts. Data developed by the forward flight analysis are compared with flight test data of Reference 3 in Figure 67 and show good correlation. The increments between the analytical and the test curves reflect very small amounts of drag and power, and the analytical results are slightly conservative.

SAMPLE CALCULATION FOR RIGID-ROTOR COMPOUND HELICOPTER AT HIGH SPEED

This sample calculation shows how the rotor is combined with the nonrotating airframe at the high-speed point and how the aircraft designed for that point is flown to a range of lower speeds at the same collective pitch setting.

Assume that a maximum forward speed of 325 knots at sea level on a standard day at a gross weight of 6300 pounds is desired. Such a design point may, in fact, be selected to insure the desired performance at the objective speed of 300 knots. At 325 knots, the rotor lift is zero and the collective

V = 300 KN q = 305 PSF TWIST = 0 DEG $i/c = 0.07$ CONSTANT
 R = 3.25 FT $\sigma = 0.1273$ $S_b = 4.23 \text{ FT}^2$

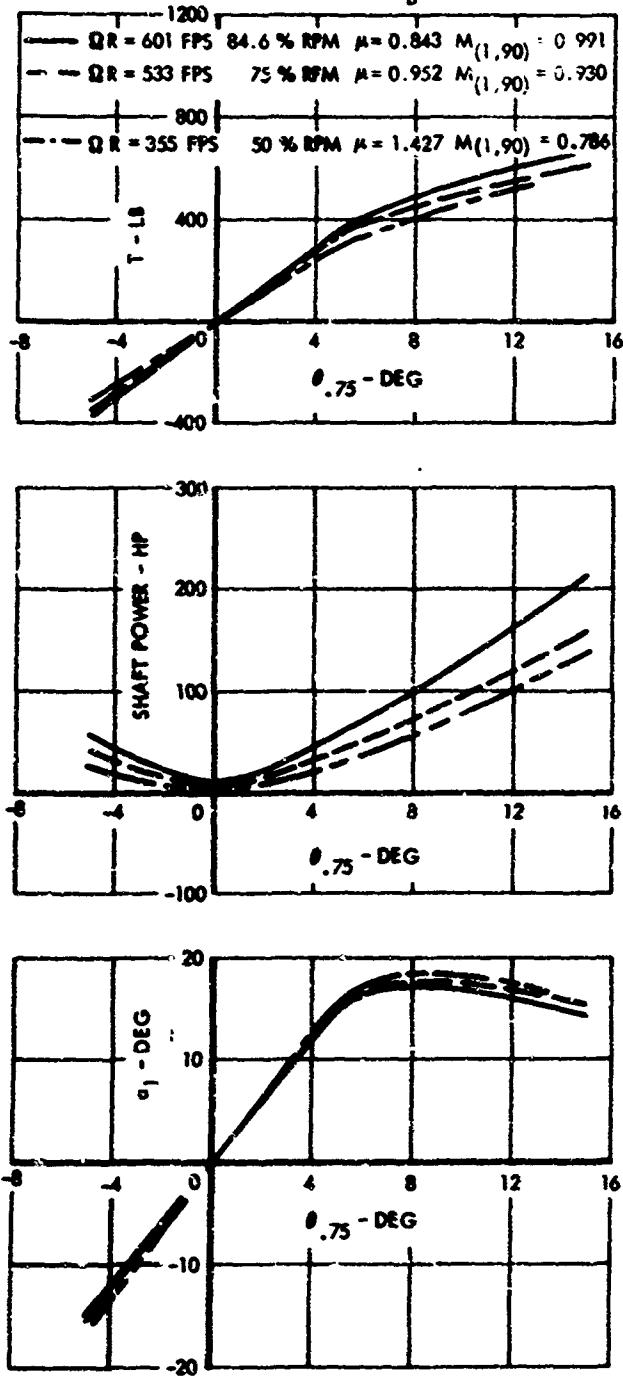


Figure 66. Tail Rotor Performance Data for High-Speed Flight, Case 21.

V = 180-240 KN DR = 650 FPS 100% RPM TWIST = -5 DEG $\gamma/c = 0.12$ CONSTANT
 $\theta = 0.75 = 0$ DEG

— TEST DATA FROM REF 3
 --- ANALYTIC PREDICTION

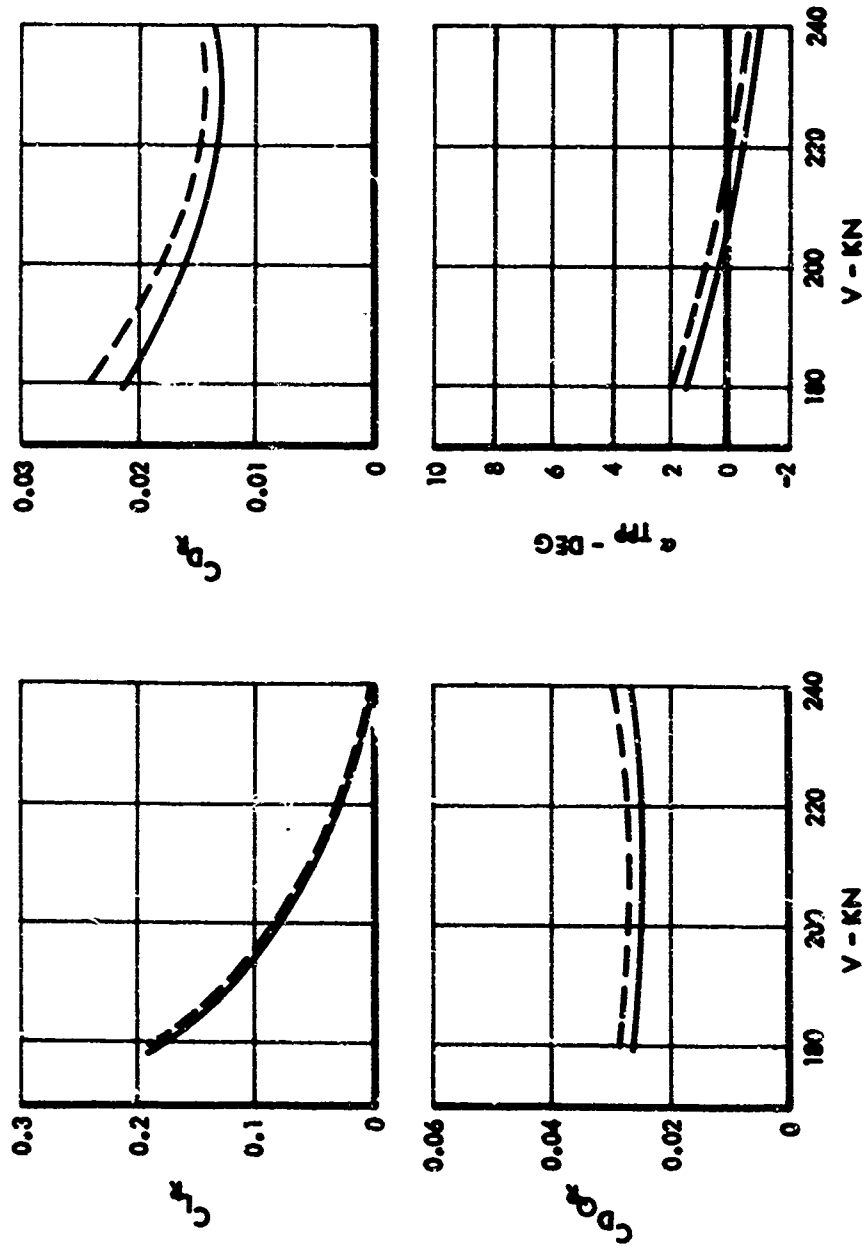


Figure 67. Correlation of Performance Data Theory and Test.

pitch is set at a low value, $\theta_{.75} = 0$ degrees. Referring to Figure 60 for a tapered thickness, cambered, -5 degree twist rotor configuration operating at 75% rpm, it is seen that if

$$\begin{array}{l}
 C_{L_R} \text{ is assumed to be } 0 \text{ and} \\
 \theta_{.75} \text{ is assumed to be } 0 \text{ deg, then}
 \end{array}
 \left\{
 \begin{array}{l}
 \alpha_{TPP} = -1.55 \text{ deg} \\
 C_{D_R} = 0.00915 \\
 C_{D_{QR}} = 0.00542 \\
 R_L = -1.27 \text{ deg}
 \end{array}
 \right.$$

Since $q = 358$ psf and $S_b = 78.8$ ft²,

$$D_R = q S_b C_{D_R} = 258 \text{ lb} \quad (1)$$

$$HP_R = (q V S_b / 550) C_{D_{QR}} = 152 \text{ hp} \quad (2)$$

Wing lift must equal vehicle weight and an operating lift coefficient of 0.35 is chosen. Wing area is found to be

$$S_W = L_W / q C_{L_W} = 50.25 \text{ ft}^2 \quad (3)$$

Selecting the wing span as 16.6 ft and Oswald's airplane efficiency factor as $e = 0.7$, the drag varying with lift is

$$D_L = (L_W / b_W)^2 / q \pi e = 183 \text{ lb} \quad (4)$$

Conventional design practice for a high-speed compound helicopter would result in a near-zero rotor shaft incidence. Since this example is intended to parallel the high-speed XH-51A compound helicopter, which was developed from the XH-51A helicopter, a shaft tilt of 6 degrees forward is used.

Hence, from Figure 68,

$$\alpha_F = \alpha_{IPP} + i_S = 4.45 \text{ deg} \quad (5)$$

Assuming a lift curve slope for the total nonrotating airframe of 0.09 per deg,

$$\alpha_W = \alpha_F + i_W = \frac{C_{L_A}}{0.09} = 3.89 \text{ deg} \quad (6)$$

which gives $i_W = -0.56 \text{ deg}$.

Identifying a minimum drag area for the airframe with interference but minus main rotor blades as equal to 9.55 ft^2 and the tail rotor drag expressed in terms of an equivalent parasite area as 0.05 ft^2 , a subtotal of drag area of 9.60 ft^2 is obtained. Then

$$D_P = qf = 3435 \text{ lb} \quad (7)$$

Finally, the propulsive force requirement is

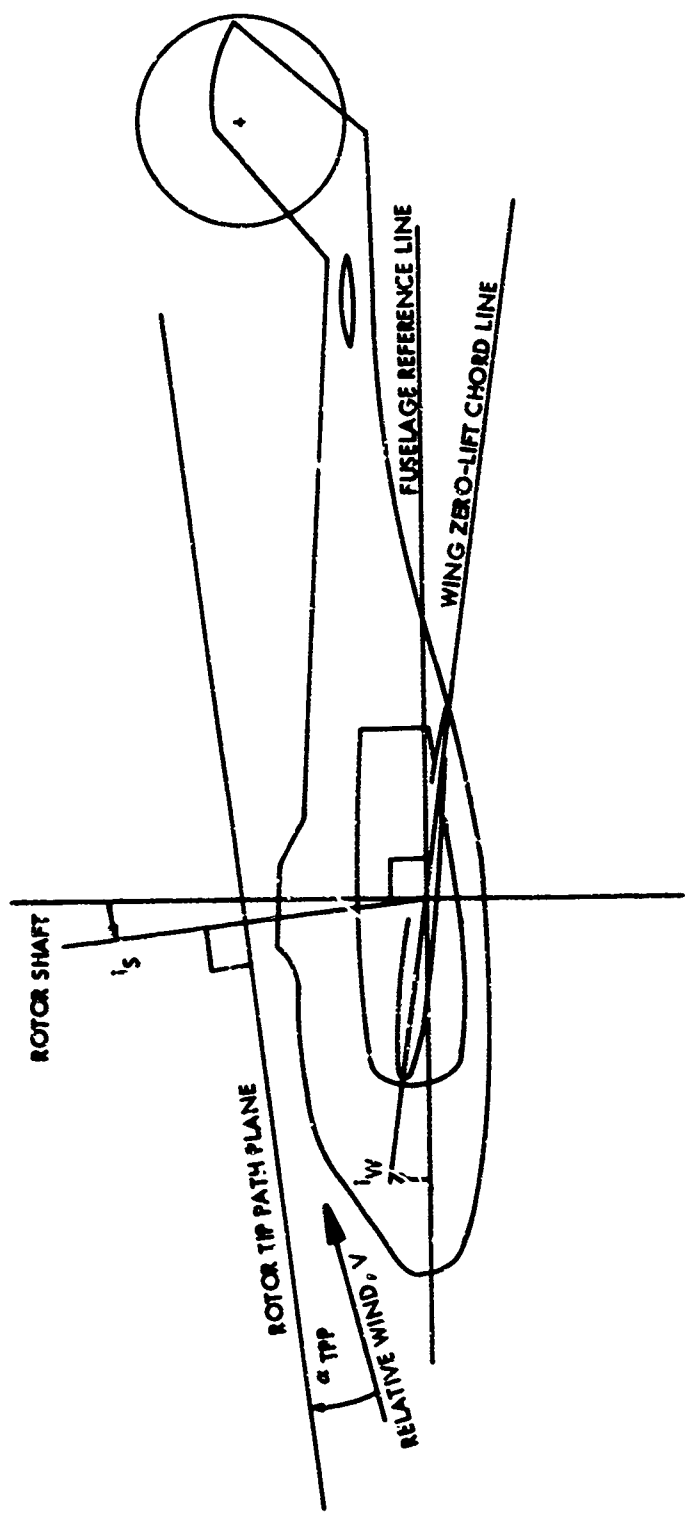
$$F_N = D_P + D_L + D_R = 3876 \text{ lb} \quad (8)$$

Tail rotor power is 10 hp and accessories and losses amount to 6 hp plus 3% of the total shaft power required:

$$HP_{REQD} = 1.03 (HP_R + HP_{TR} + HP_{LOSS}) = 173 \text{ hp} \quad (9)$$

Now consider the effect of reducing speed to 300 knots while holding constant collective. Wing and rotor lift sharing is determined by

$$G\dot{w} = L_R + L_A \quad (10)$$



104

Figure 68. Aircraft Component Angles and Relative Wind.

Nondimensionalizing by qS_b and substituting for $L_W = qSC_{L\alpha}(\alpha_W)$,

$$\frac{GW}{qS_b} = C_{L_R} + \frac{S_w}{S_b} C_{L\alpha_W} (i_S + i_W + \alpha_{TPP} - \epsilon) \quad (11)$$

where ϵ is the rotor downwash angle; in the flight regions covered by this example, ϵ is of negligible magnitude. Rearranging and entering values,

$$C_{L_R} = 0.262 - 0.0573(5.44 + \alpha_{TPP}) \quad (12)$$

Referring to Figure 58, this condition is satisfied when

$$\left. \begin{array}{l} \alpha_{TPP} = -1.05 \text{ deg} \\ C_{L_R} = 0.0104 \\ C_{D_R} = 0.0081 \\ C_{D_{QR}} = 0.0059 \\ B_1 = -0.91 \text{ deg} \end{array} \right\} \begin{array}{l} \theta_{.75} \text{ is assumed to be } 0 \text{ deg; then} \end{array}$$

Since $q = 305 \text{ psf}$,

$$L_R = 250 \text{ lb}$$

$$D_R = 195 \text{ lb}$$

$$HP_R = 130 \text{ hp}$$

Also,

$$\alpha_F = 4.95 \text{ deg}$$

$$\alpha_W = 4.39 \text{ deg}$$

$$C_{L_W} = 0.395$$

$$L_W = 6050 \text{ lb}$$

and

$$D_L = 198 \text{ lb}$$

$$D_P = 2926 \text{ lb}$$

$$F_N = 3319 \text{ lb}$$

$$HP_{REQD} = 150 \text{ hp}$$

As the forward speed is reduced further, it is no longer necessary to maintain the 75% rpm. Selecting 84.6% rpm at 250 knots as shown in Figure 56,

$\epsilon_{.75}$ is assumed to be 0 deg; then

$$\left. \begin{aligned} \alpha_{TPP} &= 0.27 \text{ deg} \\ C_{LR} &= 0.049 \\ C_{DR} &= 0.0097 \\ C_{DGR} &= 0.0109 \\ E_1 &= 0.06 \text{ deg} \end{aligned} \right\}$$

Since $q = 212$ psf,

$L_R = 819$ lb	$\alpha_F = 6.27$ deg	$D_L = 234$ lb
$D_R = 162$ lb	$\alpha_W = 5.71$ deg	$D_P = 2035$ lb
$HP_R = 140$ hp	$C_{LW} = 0.515$	$F_N = 2431$ lb
	$L_W = 5481$ lb	$HP_{REQD} = 161$ hp

The preceding is illustrated in Figure 69.

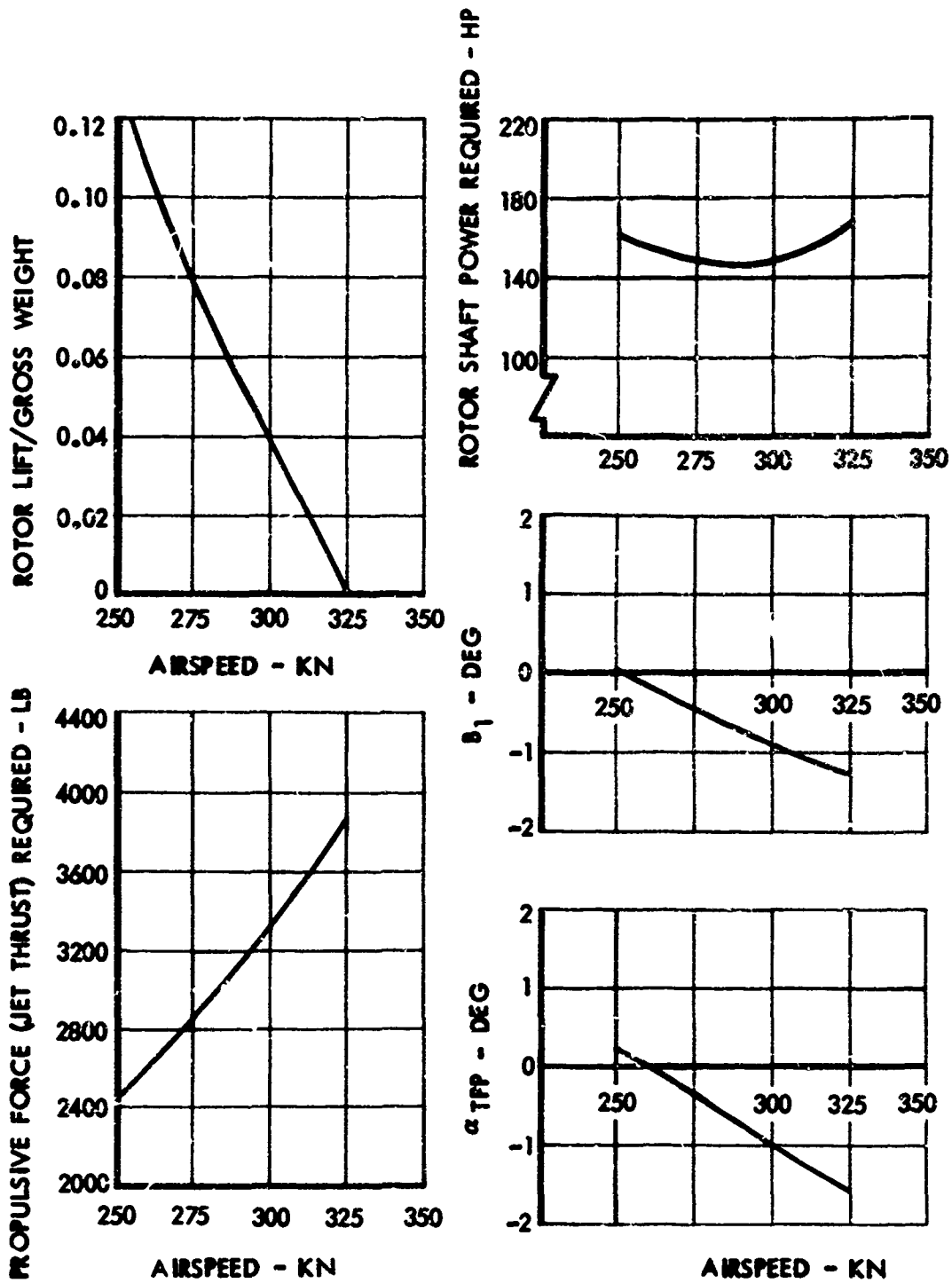


Figure 69. Application of Rotor Performance Data Charts.

UNCLASSIFIED
Security Classification

DOCUMENT CONTROL DATA - R & D

(Security classification of title, body of abstract, and indexing annotation must be entered when the overall report is classified)

1. ORIGINATING ACTIVITY (Corporate author) Lockheed-California Company Burbank, California		3a. REPORT SECURITY CLASSIFICATION Unclassified	
		3b. GROUP	
2. REPORT TITLE A FLIGHT ENVELOPE EXPANSION STUDY FOR THE XH-51A COMPOUND HELICOPTER			
4. DESCRIPTIVE NOTES (Type of report and inclusive dates) Final Technical Report			
5. AUTHOR(S) (Print name, middle initial, last name) E. S. Cruz N. B. Gorenberg A. W. Kerr			
6. REPORT DATE October 1969	7a. TOTAL NO. OF PAGES 125	7b. NO. OF REFS 12	
8a. CONTRACT OR GRANT NO. DAAJ02-68-C-0033	8b. ORIGINATOR'S REPORT NUMBER(S) USAAVLABS Technical Report 69-78		
8c. PROJECT NO. Task 1F162203A14301	8d. OTHER REPORT NUM(S) (Any other numbers that may be assigned this report) LR 21468		
10. DISTRIBUTION STATEMENT This document is subject to special export controls, and each transmittal to foreign governments or foreign nationals may be made only with prior approval of US Army Aviation Materiel Laboratories, Fort Eustis, Virginia 23604			
11. SUPPLEMENTARY NOTES		12. SPONSORING MILITARY ACTIVITY U. S. Army Aviation Materiel Laboratories Fort Eustis, Virginia	
13. ABSTRACT This report describes the results of an analytical study to determine the feasibility of expanding the flight envelope of the XH-51A compound helicopter to include a 300-knot speed objective through substantially slowed-rotor operation in high-speed flight, and to provide data to support preliminary design of such an aircraft. The phenomena associated with the speed limits observed in prior flight programs are identified and analyzed, and methods for their elimination are presented to show that the flight envelope may be expanded. Also, the effects of various rotor system design parameters on both high speed, at a range of tip speeds, and hover operating characteristics are considered to identify those parameters which are most critical to the design, and to provide a basis for the selection of the best rotor design for the slowed-rotor XH-51A compound helicopter. ()			

DD FORM 1473
NOV 68

REPLACES DD FORM 1473, 1 JAN 64, WHICH IS OBSOLETE FOR ARMY USE.

UNCLASSIFIED
Security Classification